A model for deposition
of fibers in the lung
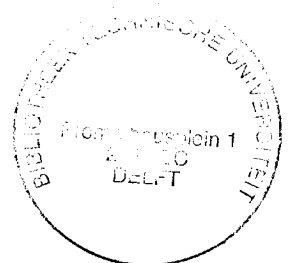
A model for deposition
of fibers in the lung

PROEFSCHRIFT

ter verkrijging van de graad van doctor
aan de Technische Universiteit Delft,
op gezag van de Rector Magnificus Prof.dr.ir. J. Blaauwendraad,
in het openbaar te verdedigen ten overstaan van een commissie,
door het College van Dekanen aangewezen,
op vrijdag 16 mei 1997 te 10:30 uur
door

Yue ZHOU

Master of Science in Environmental Engineering,
Jiao Tong University

Geboren te Hangzhou, Zhejiang Provincie, P.R. China.

To Wen and Moxi
To my parents

Contents

1

Introduction

1.1 Fibers and diseases

Fibrous particles are those with an elongated shape. They include glass fibers and various types of asbestos. Glass fibers have straight needle-type geometry and are resistant to high temperatures and mechanical forces. Asbestos fibers are divided into four main types: chrysotile, amosite, crocidolite and anthophyllite (Michaels and Chissick, 1978). Asbestos fibers have been known and used in small amounts for thousands of years, but were not widely applied until about 1930.

Asbestos has become very widely used because it is a low-cost natural material with highly desirable chemical and physical properties. This unique combination makes the economical replacement of asbestos very difficult in many applications. Heat and fire resistance, the most widely known properties, are actually not as great as is popularly believed. Asbestos cannot be classified as a refractory, but its properties are still sufficient to withstand superheated steam and other high-temperature industrial environments. Whereas major loss of strength can occur at temperatures in the range 300 - 500 °C, useful performance can still be obtained at higher temperatures. Other properties making asbestos a popular industrial material are its resistance to chemical and biological attack. The combination of all these properties allow asbestos to be applied in hostile environments; its durability also gives it a long service life.

The mining and use of asbestos have always been associated with serious occupational diseases. However, because prior to 1900 the number of people involved with asbestos was not large, there was little to draw attention to these hazards. It is now well-established that asbestos fibers can produce a number of serious health effects, such as pleural thickening, asbestosis, mesothelioma, and lung cancer. These asbestos-related diseases can appear from several years to decades after the first exposure to airborne asbestos dust; the recent increasing incidence of cases in many countries can be regarded as a result of past dust exposure, which was obviously too high. The current incidence of asbestos-related diseases is, however, not regarded as a measure of the effects of present asbestos dust levels.

Diseases caused by asbestos fiber inhalation are related to the deposition of those particles in the lung. Deposition of fiber particles in the lung are thought to be determined primarily by their diameter and secondarily by their length-to-diameter (i.e. aspect) ratio (Timbrell, 1965). Due to geometric differences, the deposition pattern of fibrous particles is different

from that of spherical particles. Fibrous particles tend to align themselves parallel to the flow streamlines and are therefore, it was hypothesized, more likely to penetrate deeper into the lung than spherical particles.

However, this hypothesis has never been experimentally validated. Toxicologists had no way of conducting experiments with fibers of well-defined lengths and diameters. Such fiber fractions were simply not available due to the difficulties of separating fibers into various length and diameter fractions.

1.2 Lung structure models

It has been well-recognized that the deposition of inhaled particles in the human lung depends upon the anatomic structure and physical dimensions of the lung airways. Findeisen (1935), Landahl (1950), and Davies (1961) published early representations of the respiratory tract. A classical study on the structure and dimensions of human lung airways was performed by Weibel (1963).

On the basis of detailed measurements of a lung cast, Weibel (1963) proposed a mathematical description of a dichotomous system of airways. He showed that his model 'A' with a symmetrical dichotomy can be characterized by 24 generations of bifurcating cylindrical elements between the trachea (generation 0) and the alveolar ducts (generation 23), and 3×10^8 alveoli. Beginning from the 17th generation, increasing numbers of alveoli are present on the airway walls. The last three generations are completely covered with alveoli. Thus, the alveolar space in Weibel's model consists of all the airways in the last seven generations. This model simulates adult human lungs with a volume of 4.8 litres at about 3/4 maximal inflation.

In recent years, because more accurate and detailed morphological measurements of the airways became available, several new lung models have been proposed. Yeh and Schum (1980) presented a mathematical airway model for each lobe of the lungs. Their model improves on the Weibel model by including branching angles and gravity angles. The calculational model of Yeh and Schum can be physically represented by glass bifurcational models.

1.3 Lung deposition models

Many models for particle deposition in lungs have been published. The Landahl model (1950) is representative of the early predictive models. Landahl defined the mouth, pharynx and second order of alveolar sacs as three additional parts of the model and applied it to various mouth-breathing conditions. Another well-known model which is still referred to by many studies is the ICRP (International Commission on Radiological Protection) model developed by the Task Group (1966). From the 1970s experimental studies of the human lung made great progress, and extensive data relating to total and regional deposition became available. This new knowledge stimulated further theoretical studies. Many new models were developed which took the various particle deposition mechanisms into account (Heyder, 1973, Ferron, 1976, Lippmann and Altschuler, 1976, Taulbee at al., 1978). The Task Group of the ICRP

(1994) published a new model based on experimental data and compared their model with the existing lung deposition models. Recently, the availability of the computer has made it possible to calculate three dimensional particle deposition behaviour in lung tubes. Many models dependent on the computer have been developed, such as the models of Gradon and Orlicki (1990) and Hofmann and Koblinger (1990). In Chapter 2 of the thesis, we discuss these deposition models in detail.

For fibers, however, only a few studies were carried out before computers became widely used. Beeckmans (1970) was the first study to apply Weibel's model A to predict the deposition of asbestos fibers by assuming the fiber orientation to be random. Harris (1972) developed a fiber deposition model by considering the effects of impaction, interception, sedimentation, and diffusion. Because fibers cannot be described by a single size parameter, his calculation is related to the fiber length and aerodynamic diameter. Some 16 years later Asgharian (1988) extended the previous studies by performing a detailed analysis of the fiber orientation in each generation of human lungs. An orientation function related to Eulerian angles was developed in his model. One can use his model to calculate the fiber deposition efficiency in any generation of the human lung in any given fiber orientation.

1.4 Experimental data for particle deposition in lungs

Experimental determination of particle deposition in human lungs have been performed in many studies over the years. Many of these studies were devoted to total deposition. Lippmann et al. (1980) reviewed total deposition data from studies he considered to be reliable and precise. Regional lung deposition can be measured based on the external counting of radioactive particles retained in the lung. The studies of Stahlhofen at al. (1980), Heyder (1986), and Rudolf et al. (1986) were conducted for mouth and nose inhalation of monodisperse spherical particles over a wide size range. These experimental data are still referred to by many studies of particle deposition in lungs. In Chapter 3 of this thesis, the model we developed is also compared with these experimental data to check our model's validity.

In contrast to spherical particle deposition, however, experimental data for fibrous particle deposition in human lungs are not available. The reason for this is the serious health hazard caused by inhaling fibers. Fiber inhalation data are therefore only available from animals.

1.5 Aims of the research

Fibers which deposit in the lower regions of the human lung are removed from the lung only at a very low rate. Such particles are therefore more dangerous than those deposited in the upper parts of the respiratory tract, which are removed much faster. Occupational hygiene standards are usually based on alveolar deposition (generations 17 to 23). From this point of view, it is important to understand and to predict the deposition behaviour of fibers in the lower parts of the human lung as a function of the physical parameters of fibers and breathing conditions. Indeed, this was the goal of the present research. In order to achieve this goal, the research consisted of:

3

1. Building a physical model by means of a granular bed filter to simulate the lower parts of the lung.

2. Testing this physical model with spherical aerosol particles.

3. Producing monodisperse fibers with various size distributions.

4. Dispersing the fibers into the air, without agglomerates, followed by measuring the particle sizes and concentration.

5. Investigating the fiber inhalation behaviour as a function of the physical properties of the fibers, like dimensions, shape, density and electric conductivity.

6. Simulating the behaviour of the fibers in the human inhalation system with a lung model.

1.6   Previous research carried out at Delft University of Technology

In 1989 the sections Chemical Risk Management and Particle Technology started a research project to study the transport and deposition behaviour of fibers in a model of the human respiratory tract as a function of chemical and physical properties of fibers. This research was begun in order to study possible health hazards of newly developed commercial organic fibers whose diameter could be made so small that inhalation was possible.

Van Pinxteren (1989) and Bilius (1989) succeeded in producing fibers with monodisperse lengths. Zeckendorf (1991) started the experimental research on the upper part of the human lung and chose the lung model Yeh and Schum (1980). Stoelinga (1992) constructed experimental apparatus to simulate the upper part of the lung and worked on the generation of fibrous aerosols with the van der Wel aerosol generator and the spinning top aerosol generator. Stoelinga (1992) also applied the method of Prodi (1982) to separate fibers with varying diameters; in this way he obtained monodisperse fibers in terms of both length and diameter which were used for further research. Van der Put (1992) derived a mathematical model for the deposition of fibrous particles in the lower part of the lung.

1.7 This work

The procedure of the study is illustrated in Figure 1.1. As it is impossible to build a model of the lower parts of the respiratory tract using glass bifurcations, it was decided to investigate the possibility of representing these parts by a granular bed filter. Deposition of particles in a lung is often compared with filtration, because it relies on the same basic mechanisms that cause particle collection in a filter. Granular bed filters are used for removing micron and submicron particles from gases. They are especially important in the filtration of hot and corrosive gases for which no other filters can be used.
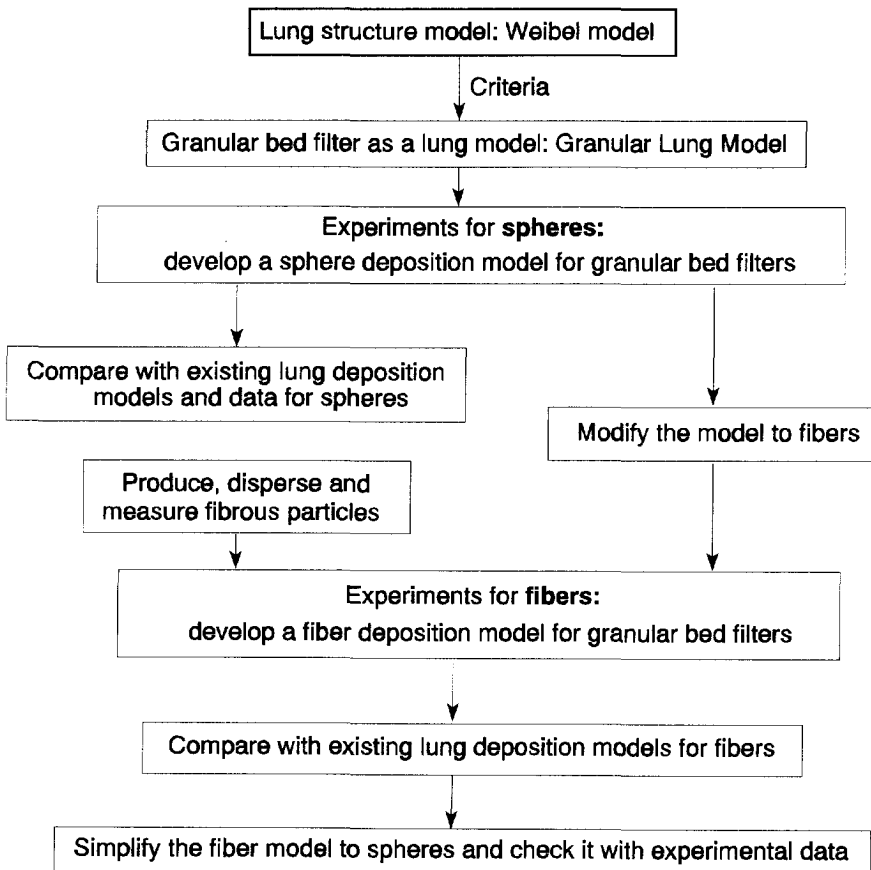
Figure 1.1. *Illustration of the research procedure.*

The specific goal of this project was to compare both the theoretical and experimental fiber deposition in the lower parts of the human lung (8th-23rd generation of Weibel) during inspiration with the deposition of fibers in a granular bed filter with similar dimensions and equal air flow rates.

It is useless to compare deposition in a granular bed filter with deposition in the lower parts of the human lung when it is not known how the different deposition mechanisms contribute to the total deposition in both system. So the intention of the theoretical part of the project was to investigate the differences and similarities between the collection efficiencies of separate deposition mechanisms in both systems and the dimensionless numbers on which they depend. The intention of the experimental part was, firstly, to investigate the validity of the theory of Boulaud (1991) for *spherical* particles in the granular bed filter which was used

5

in the experiments. The second experimental goal was to validate the theory we derived for the collection efficiency of *fibrous* aerosols in a granular bed filter as a function of bed height, glass bead diameter, particle dimensions and flow rate.

Besides the need for information about the fiber collection efficiency of a granular bed filter, it is also necessary to know how fibers behave in the lower parts of the human lung. Unfortunately, experimental and theoretical information on deposition of fibers in the deeper parts of the human lung is scanty. Experimental work on deposition of fibers in hollow casts or tubes only extends to 0.2 cm diameter airways or until the 6th generation of Weibel (1963). As already mentioned, no experiments with fibers have been done in live human beings. Due to this lack of experimental data, our fiber deposition model, based on a granular bed filter, is compared with two representative theoretical models for fiber deposition in lungs: the models of Harris (1972) and Asgharian (1988).

2

Particle deposition in lungs

2.1 Introduction

The deposition of inhaled particles in the respiratory system is the process by which the particles, as far as they are not exhaled, are deposited and redistributed between a great variety of anatomical locations. This process can be simulated by means of kinetic models for specified locations of interest. If the model is suitable, it may be possible to find systematic changes of the numerical transfer rate values resulting from changes of the variables that control the experimental conditions. In the past, this approach led to a number of useful semi-empirical models for selected aspects of particle deposition after inhalation. In some cases, subsequent generalizations and predictions for the same species under modified experimental conditions have been quite successful (Stöber et al., 1993).

The deposition of particles in the lungs relies on the same basic mechanisms that cause collection in a filter, but the relative importance of each mechanism is quite different for the two situations. While filtration occurs in a fixed system at a steady flow rate, respiratory deposition occurs in a system of changing geometry and at a flow rate that changes with time and cycles in direction (Hinds, 1982). This added complexity means that we are unable to predict deposition from basic theory and must rely to a much greater extent on empirically derived equations. In fact, truly predictive mathematical modelling of particle deposition in the lungs is possible only to a limited extent. Lack of mechanistic information about some of the transfer processes requires the return to empirical assessment, which may give characteristic constants in the complex model. In this chapter, we review the basic mechanisms of deposition as they apply to the respiratory system and the characteristics of particle deposition in the lungs. In order to do this, it is necessary to review first the characteristics of the human respiratory system.

2.2 Respiratory system

The human respiratory system can be divided into three regions (Task Group on Lung, 1966), each covering one or more anatomical regions. These regions differ clearly in structure, airflow patterns, function, and sensitivity to deposited particles. The first is the **head region**, which includes the nose, mouth and pharynx. Air inhaled through this region is warmed and humidified. The second is the **tracheobronchial region** (0 to 16th generation in the lung

structure model A of Weibel, 1963), which includes the airways from the larynx to the terminal bronchioles. This region looks like an inverted tree with a single trunk. The trachea subdivides into smaller and smaller branches. Finally, beyond the terminal bronchioles, is the **pulmonary or alveolar region** (17th to 23rd generation connecting with alveolar sacs), in which gas exchange takes place.

The respiratory system (see Figure 2.1) of a normal adult processes 10-20 m^3 of air per day. The gas-exchange area of the lungs is about 30 m^2 and is perfused with over 2000 km of capillaries. At rest, about 700 ml of tidal air (all air during one respiration) is inhaled and exhaled with each breath (Hinds, 1982). During heavy work, tidal volume may be three times this amount. A resting adult breathes about 12 times per minute and this rate will triple during heavy work. About 1100 ml of reserved air is not exhaled during normal breathing but can be exhaled by forced exhalation. Inhaled air follows a flow path through a sequence of 23 branchings from the trachea to the alveolar surfaces. The first 16 branchings take place in the tracheobronchial region and the remainder in the alveolar region.

2.3 Particle transport and deposition mechanisms

Deposition is the process that causes inhaled particles to be caught in the respiratory tract and thus fail to exit with the expired air. Total deposition fraction, DF, is expressed as

$$DF = \frac{amount\ inhaled\ -\ amount\ exhaled}{amount\ inhaled}.$$ (2.1)

It is general accepted that all particles that touch the surface of the respiratory tract are deposited at the site of initial contact. Different physical mechanisms operate on inhaled particles and move them across streamlines of air to the surface of the respiratory tract; these mechanisms are gravitational sedimentation, inertial impaction, Brownian diffusion, interception, and electrostatic force. The mechanisms that contribute to the deposition of a specific particle depend on the particle's aerodynamic behaviour, particle composition, the breathing pattern of the human lung, geometry of the respiratory tract, and the flow and mixing patterns of the aerosol in the respiratory tract.

It is not possible to completely and quantitatively characterize aerosol deposition in the respiratory system; this would require a full solution of the constantly changing hydrodynamic flow field in the respiratory airways and superposition of the independent aerosol particle motion in this field. An understanding of the factors involved can be gained from an examination of the specific mechanisms by the deposition of individual particles at different points in the respiratory system. Understanding these mechanisms permits insight into the complexity of the relationship between respiratory deposition and lung volume, respiration rate, and respiration volume.

2.3.1 Inertial impaction

During inhalation, the inhaled air must pass a series changes in direction as it flows from the
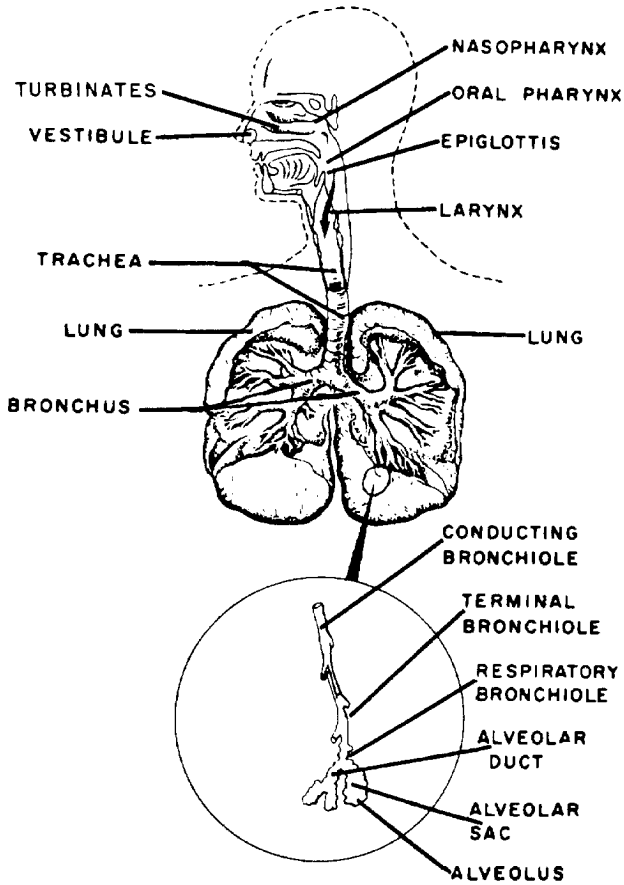
Figure 2.1. *The respiratory system. (Handbook of Air Pollution USPHS 999-AP-44, 1968).*

nose or mouth down through the branching airway system. Each time the air changes direction, the suspended particles tend to continue a short distance in their original direction because of their inertia. This causes some of the particles near the airway surfaces to deposit there by inertial impaction. The deposition by this mechanism depends on the stopping distance of the particle at airway velocity. Consequently, this mechanism is limited to the deposition of large particles which are close to the airway walls. The inertial impaction is important for particles with a diameter larger than about 1 μm. The maximum deposition by impaction occurs at or near the first few generations. This is because the streamlines bend most sharply in these areas and pass close to the bifurcation. The probability of deposition by impaction depends on the ratio of particle stopping distances to airway dimensions and is the highest in the bronchial region.

9

2.3.2 Sedimentation

Whereas impaction is of primary concern in the large airways, sedimentation is most important in the smaller airways and the alveolar region, where flow velocities are low and airway dimensions small. The deposition by sedimentation increases with particle free falling speed and the residence time. Sedimentation has its maximum removal effect in the airways which are oriented horizontally. This mechanism, during inhalation, will be high in the most distal airways, when low respiratory flows occur. Hygroscopic particles grow as they pass through the water-saturated airways, and this increase in size favours deposition by sedimentation in the lower parts of the airways. Sedimentation becomes less effective than diffusion when the terminal settling velocity of a particle falls below about 0.001 cm/s, which means that the aerodynamic diameter of a particle is smaller than about 0.5 μm.

2.3.3 Diffusion

The constant random collision of gas molecules with small aerosol particles pushes the particles about in an irregular fashion called Brownian movement. Thus, even in the absence of gravity, a particle in still air moves as a "random walk". This is a stochastic process that causes motion in 3 dimensions. The force of diffusion results in a net transport of particles from a region of high concentration to one of low concentration. In the lungs, regions of low particle concentration exist near the lung surface since particles are removed from the air when deposited. Deposition by diffusion, which depends on the diffusion coefficient, is affected by particle size, distance of particles from the airway wall, residence time, and for fibers, the fiber orientation in the airstream. The airway and flow conditions that favour sedimentation, long residence time and small airway diameter, also favour diffusion. Particle removal by this mechanism is significant only for particle diameters less than ca. 0.5 μm.

2.3.4 Interception

Interception is the process by which a particle, although it does not deviate from its gas streamline, touches the airway surface because of its physical size. The likelihood of interception depends on the proximity of the particle to the airway surface and on the ratio of particle size to airway diameter, which is usually small even in the smallest airways. Fibers, however, can readily traverse the tortuous path to the small airways. In order to remain suspended in the air, fibers must be separated from all surfaces by distances larger than their projected length. As the angle between the streamlines and the major fiber axis increases, interception deposition becomes an increasingly important mechanism.

2.3.5 Electrostatic forces

·A charged particle may deposit in the respiratory tract by electrical forces. Although the surfaces of the respiratory tract are uncharged, they are electrically conducting. When an electrically charged particle approaches the tract surface, the particle induces an image charge of opposite polarity on the lung surface to attract the particle. This force may cause the particle to deposit in the lung.

In summary, the large particles (diameter larger than ca. 1 µm) will be deposited by impaction and for fibers, also by interception in the nasal passages and in the large airways, particularly at bifurcations. Of the remainder, particles with a diameter down to 1 about µm tend to be deposited by sedimentation and for fibers, by interception in the small airways. The small particles with a diameter less than 1 µm tend to pass through and are deposited in the respiratory bronchioles and alveolar sacs by sedimentation and, in case of the smallest, by diffusion or interception at the entrance of the alveolus. The particles which do not deposit are exhaled. Highly charged particles can deposit on the airway surfaces by the electrostatic image charge. Unipolar charged particles with high number concentrations are deposited because their mutual repulsion drives particles toward the airway walls.

2.4 Lung deposition models

Kinetic models involving complex biological systems always require certain simplifications, and the deposition of inhaled aerosol particles in the lung during the breathing cycle is no exception. In this case, however, the biological aspects influencing the particle deposition patterns do not directly involve any specific biochemical response. Instead, they relate simply to the lung architecture and the dynamics of respiration. Thus, in order to determine the direct variables of initial particle deposition in the lung, it is sufficient to know the morphological features, e.g., sizes, lengths, and configurations of the tubular structures of the tracheobronchial tree and the alveolar dimensions of the pulmonary region, as well as various functional parameters, such as tidal volume and breathing frequency. The needed characteristics of the model are thus physical and physiological, not biochemical. They determine the motion of the airborne particles under the influence of external forces as the particles flow through the respiratory conduits. Thus, fluid dynamics, aerosol physics, gas kinetics, gravity and other forces, the mechanics of respiration, and anatomical structures provide the independent variables for the basically physical models of particulate deposition in the lung. The replacement of individual respiratory architectures and personal breathing patterns by average values in order to describe deposition in a "standard human" may be accomplished by different model approaches. Together with the degree of physical simplification, they account for the variety of accepted deposition models today. In principle, computer-supported solutions could be established at any level of physical, topographical, and individual detail, although some of them may be very demanding on computing time and financial resources (Stöber et al., 1993).

2.4.1 Early predictive models

An anatomical lung model for particle deposition can be developed consisting of two compartments: a schematic tracheobronchial tree and a finite volume of inflated alveoli. Simply assuming laminar flow, particle deposition is then similar in each sub-compartmental generation of tubes and is governed by a number of physical phenomena which depend strongly on particle size. It is therefore not surprising that the first particle deposition model was published by a meteorologist, Findeisen (1935), who was familiar with atmospheric particles with respirable size. The model of Findeisen consists of only several generations. Starting with the trachea, Findeisen subdivided the branching airways and the pulmonary

spaces into nine sections based on a functional concept.

Many years later, Landahl (1950) modified and extended Findeisen's original model trying to interpret his earlier experimental data (Landahl, 1948) with corn oil droplets and methylene blue particles. He defined the mouth, the pharynx and a second order of alveolar ducts as three additional parts of the model and applied it to a variety of mouth-breathing cycles. Agreement was somewhat limited and deviations around 50% deposition occurred in either direction, although particle hygroscopicity may have interfered in some cases. Subsequent experiments by Landahl et at. (1951, 1952) with different exhaled air under various mouth-breathing conditions gave exhaled particle mass concentrations comparable to the data from Davies (1949) and Brown et al. (1950). Some further extension of the Findeisen-Landahl model resulted in a general agreement between theoretical and empirical data, although not all discrepancies were removed. However, the authors thought that the calculation for the deposition in the various parts of the respiratory tract was fairly accurate (Stöber et al, 1993).

At about the same time, Hatch and Hemeon (1948) developed a semi-empirical model from nose breathing data. They described a simple two compartmental approach for respiratory deposition in their model. They concluded that the deposition in the alveolar region could not exceed two thirds to three quarters of the inhaled particles even when the local deposition efficiency were 100%, because no more than this fraction of the inhaled air volume is likely to reach the alveolar region. In their paper, they found that particles above 5 µm diameters are practically completely removed by the nose and for this reason neglected penetration to the alveolar region. Their deposition model for nose breathing featured simply two compartments, an upper one comprising the conducting airways and a lower one representing the alveolar region. They assumed that the deposition in the alveolar region is caused by sedimentation of all particles reaching this compartment. Thus, the particle deposition in the alveolar region was calculated with the tidal fraction actually reaching the alveolar range after simply accounting for the sedimentation losses in the upper respiratory tract. Hatch and Hemeon did not consider the deposition by Brownian diffusion of very small particles.

In 1959 Altshuler et al. (1959a) described more detailed theoretical aspects of respiratory airflow by accounting for intra-pulmonary gas mixing. They tested their theoretical results in human experimental studies of aerosol wash-in and wash-out by sequential breathing of aerosol and clean air. Subsequently, Altshuler (1959b) used an extended tubular filter bed as the simulation of the respiratory tract to calculate the particle deposition. The treatment derived the regional deposition from local removal characteristics and the distribution of aerosol in the exhaled air. The authors concluded that the filter bed model was more accurate and gave higher amounts of deposition in the upper compartment.

2.4.2 Advanced deposition models and the experimental results

After the Second World War, the growing concern about occupational health hazards due to accidental radioactive aerosol inhalation in the atomic energy industry caused very great interest in particle deposition in the lung. Thus, systematic experimental results became increasingly available within a decade. In the mid-sixties, the Task Group on Lung Dynamics
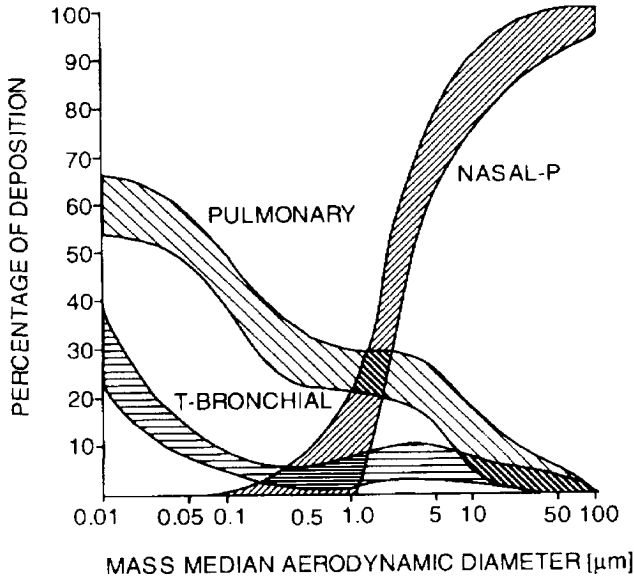
Figure 2.2. *Variability of regional particle deposition in the respiratory tract (ICRP model). Inhalation at 1450 cm³ tidal volume and 15 cycles per minute (Task Group, 1966).*

. (1966) was appointed by the International Commission on Radiological Protection (ICRP) to develop, for safety reasons, a conservative estimate for lung deposition and retention of inhaled radioactive aerosols. After a careful examination, the Task Group used the Findeisen approach to estimate the initial deposition in connection with an empirical equation for nasal deposition reported by Pattle (1961). Furthermore, the calculation of diffusional deposition, which Findeisen accomplished by using a graphical procedure, was simplified by using the equations derived by Gormley and Kennedy (1949). In this way, it was possible, within a certain margin of error, to characterize deposition of the inhaled particles by using a single collective parameter: the mass median aerodynamic diameter of the particle size distribution. For a selected breathing pattern: inhalation at 1450 cm³ tidal volume and 15 cycles per minute. Figure 2.2 shows the average range of deposition variation in the nasopharyngeal, tracheobronchial, and pulmonary compartments when the geometric standard deviation of the mass median aerodynamic diameter of the inhaled particles varies between 1.2 and 4.5.

In the 1970s and 1980s, the progress of experimental data obtained in human studies made an extensive data base on total and regional deposition available, which accelerated further theoretical studies. Heyder et al. (1975) presented data from careful human studies on total lung deposition performed at better controlled conditions than many older investigations. By accounting for the subjects' normal functional residual lung volume capacity, they resolved most of the intersubject variability observed for mouth breathing in other studies. Nose breathing, however, still showed scatter of data between individuals. Heyder et al. also described their low experimental deposition values and gave a semi-empirical analytical explanation for all their particle number deposition data obtained for mouth breathing.

13
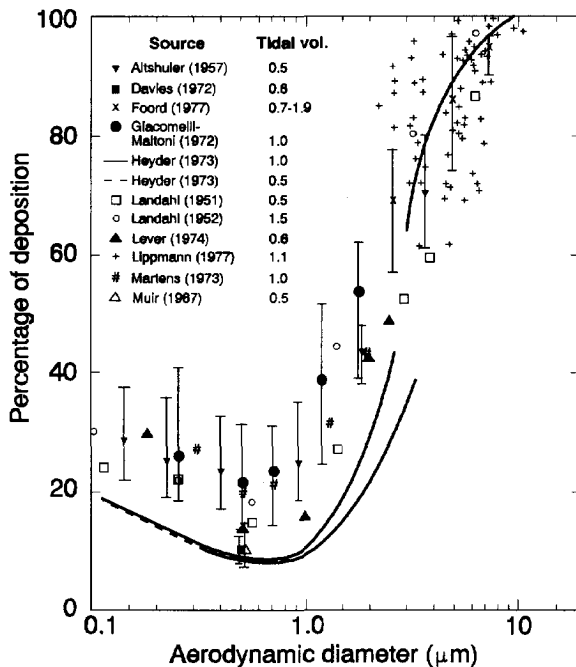
Figure 2.3. *Experimental data on total respiratory tract deposition for mouth breathing (Stöber et al., 1993).*

A few years later, Heyder et al. (1978) harmonized their experimental efforts and data, and Gerrity et al. (1979) predicted deposition of inhaled particles in the airway generations by using Landahl's deposition model and applied it to Weibel's (1966) symmetric anatomical lung model. They neglected aerosol mixing and turbulent deposition and estimated that the error from neglected factors would be no more than 10%. In spite of the simplifications, the calculations were in reasonable agreement with experimental observations and closest to the mouth-breathing data of Heyder et al. (1975). For the largest tested particle size of 3 μm the discrepancy between the calculation and experiments was about 30%; for smaller particles the discrepancy was less. In a detailed review, Lippmann et al. (1980) suggested that the low deposition fractions obtained by Heyder and co-workers in 1975 were most reliable. Figure 2.3 gives an impression of the scatter of empirical mouth-breathing data discussed at the time.

Subsequently, Heyder et al. (1980) reported the total and the alveolar deposition data for mouth breathing for various particle sizes including particles with an aerodynamic diameter larger than 3 μm. That year Stahlhofen et al. (1980) also published additional mouth breathing data on regional deposition. The latter data were simulated by a non-mechanistic semi-empirical model developed by Rudolf et al. (1983). The model considered the respiratory system as a series of aerosol filters. Each filter corresponded to a functional compartment of

the respiratory tract. This semi-empirical model was then extended to cover particle sizes between 0.005 and 10 μm (Rudolf et al., 1986), with the experimental data of mouth and nose breathing and particle size down to 0.005 μm (Heyder et al., 1986; Schiller et al., 1988). For three sets of tidal volume, flow rate, an breathing frequency, the model predicted total deposition values which were in very good agreement with experimental data.

2.4.3 Continuous path airflow deposition models

A new theoretical model for particle deposition in lungs was developed by Taulbee and Yu (1975). They designed a "trumpet" lung model which was originally proposed by Scherer et al.(1972) for gas diffusion studies. This model describes the respiratory tract over the whole path length as a trumpet with continuously increasing cross section (Figure 2.4). With this form, the pathway permitted the application of a continuous partial differential equation with two components accounting for the three deposition mechanisms involved and for mixing between tidal and residual air (Yu, 1978a). Using Weibel's anatomical model A in the numerical computations, Yu and Taulbee (1977) found the finite-difference solutions to be in good agreement with the mouth-breathing data reported by Heyder and co-workers. Neglecting the air mixing effect, it was even possible to obtain an analytical solution by using the method of characteristics (Yu, 1978b). To improve the trumpet lung model, Egan and Nixon (1985) used new expressions for various particle deposition mechanisms and new mouth and nose breathing parameters, and got good agreement with the low values of experimental mouth and nose breathing results for total deposition reported by Heyder et al.(1975). For high ventilation flow rates the quality of their simulation was superior to that of the model by Yu and Taulbee (1977) for high ventilation flow rates. Egan and Nixon reported the regional simulations of tracheobronchial and the pulmonary deposition data obtained in mouth-breathing experiments by Stahlhofen et al. (1980) and by Chen and Lippmann (1980). Predictions were in general in good agreement with the experimental work. When significant differences between model and experiment did occur, they were due to extrapolations involved in the indirect determination of regional data for tracheobronchial deposition. The authors also pointed out that their model requires a larger computational effort than the relatively simple model expressions of particle dynamics and fluid mechanics.

The trumpet lung model was also used by Yu and Diu (1982) to predict the total and regional deposition in the lung by using five different anatomical lung models. The predictions for total deposition were also compared with experimental data of Heyder et al. (1975) and Foord et al. (1978). There was a good agreement on total deposition for all lung models, except for the original Findeisen model. However, the regional deposition values predicted by the different lung models were not compared to experimental data and showed considerable mutual differences. Using Weibel's lung model in their own deposition model and the analytical solution by the method of characteristics, Yu and Diu (1983) obtained good agreement with the regional data of Heyder et al. (1980) and Stahlhofen et al. (1980).

In order to investigate the particle deposition behaviour in mouth breathing, Ferron et al. (1985) compared the experimental data published by Stahlhofen et al. (1980, 1983, 1984) and Heyder (1984) with data obtained with different deposition models. The models used were

15
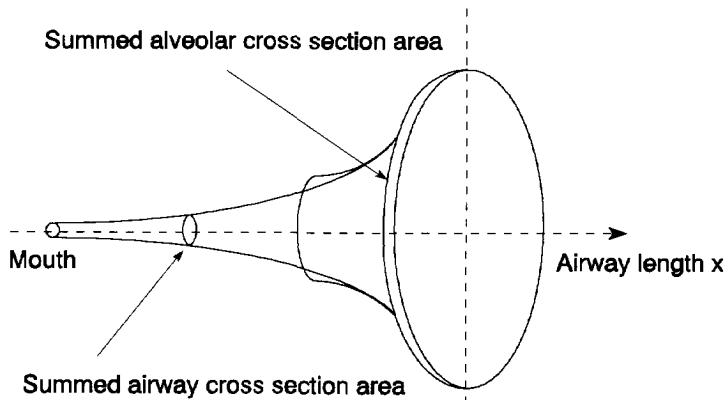
Figure 2.4. *Increase of the summed cross-sectional area of the airways with length in the "trumpet" lung model (Taulbee and Yu, 1975).*

combined from four different lung structure models, two sets of deposition equations for impaction, sedimentation and diffusion, and three different methods of compartmental computation. Again, the calculated total deposition values were mostly in good agreement with experimental data. All models, except one, were also suitable for calculating the regional deposition. However, the calculated bronchial depositions tended in general to be greater than the measured values. The predicted pulmonary deposition was mostly less than the experimental values.

Recently, a new deposition model was developed by the Task Group of ICRP (1994). The model is based on the experimental data and the theoretical studies in the literature. In this model, each region of the respiratory tract is represented by an equivalent particle filter which acts in series. The approach was to compare the theoretical model's simulations with the available experimental information. It is found that the model can predict accurately the experimental data relating total deposition to particle size and breathing behaviour. This model can also simulate the variation of regional deposition with particle size and breathing pattern inferred by Stahlhofen et al. (1980) from their measurements of thoracic deposition and retention.

2.4.4 Computer simulation models

The computed deposition fraction in a mathematical lung model are converted to the surface doses (i.e. deposition per unit surface area) by implicitly assuming that particles are uniformly distributed along human airway surfaces. In the study of Gradon and Orlicki (1990), the equations for the diffusion and convection of aerosol particles in the three-dimensional space of the tracheobronchial tree bifurcation were solved. They used a geometric model of a bifurcation of the tracheobronchial tree and the results of computations of the stationary air velocity field in such a system. From their calculation, they reported that an increase in the

volumetric flow rate causes an increase of large particle deposition, and is insensitive to particle size at locations in the lung where the diffusional mechanism dominates. When the particle size decreases and when the contribution of the diffusional mechanism in the overall transfer increases, the effect of the flow character declines.

In the same year, Koblinger and Hofmann (1990) developed a stochastic model for calculating particle deposition in human lungs. In their model, the geometry of the airways along the path of an inhaled particle is selected randomly, whereas deposition probabilities are computed by deterministic formulae. Their stochastic model is based on two sources of the randomness, the selection of the actual paths of individual particles and the physical nature of a particle walk.

By using their Monte Carlo program, the calculation of the deposition pattern throughout the tracheobronchial and pulmonary regions of the lung can be performed. They also compared their calculation results with other lung deposition models (Hofmann and Koblinger, 1990). The results obtained by their model showed satisfactory agreement with experimental data for total deposition over a wide range of aerosol particles diameters.

2.4.5 Fibrous particle deposition models

In a theoretical study with no experimental data available for comparison, Beeckmans (1970) used Weibel's anatomical model to calculate the deposition of asbestos fibers by treating them as randomly oriented prolate spheroids. It was known at that time, however, that random orientation of fibers in a laminar shear flow is not a realistic assumption. Beeckmans also assumed that the interception of the particle could be neglected, although it should be important for rotating fibrous particles. The published analysis was not very detailed and did not include the particle deposition in the head region. In the small particle size range, below about 0.2 μm, which is controlled by diffusion mechanism, Beeckmans' results showed that for constant diameters deposition decreased with increasing fiber length. This appears credible as extended dimensions should reduce diffusional mobility. In the size range where sedimentation and impaction are the controlling mechanisms, his results showed that an increase in the fiber length for constant diameter is equivalent to an appropriate increase in its weight.

Two years later Harris (1972) used the Task Group model (1966) together with the anatomical model of Weibel in order to derive a deposition model for asbestos fibers. The fibers were again treated as stretched spheroids. However, for the calculations in the sedimentation regime, Harris assumed that the orientation of the fibers is parallel to the streamlines of the laminar shear flow in the bronchial tree. The effects of interception, impaction, sedimentation, and diffusion mechanisms were predicted separately by specific fiber-related expressions. Since fibrous particles cannot be described by a single size parameter, the calculations were related to the actual fiber length as well as to the specific aerodynamic diameter of fibers settling parallel to the boundary surface. Then, for each aerodynamic diameter, the relative deposition is not a unique value like the case of spherical particles, but depends on the actual fiber length. Figure 2.5 shows a typical example of results for fibers of 50 μm length in
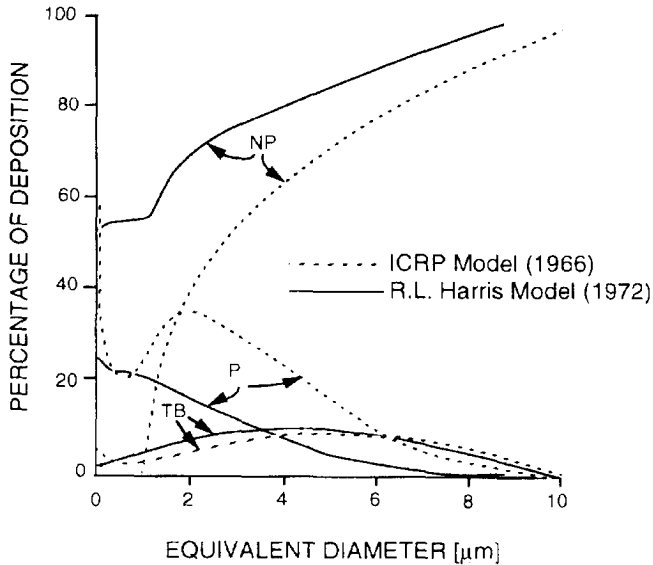
Figure 2.5. *Comparison of regional deposition between the Harris' model and the ICRP model (Stöber et al., 1993) with a fiber length of 50 µm. NP: nasopharyngeal; P, pulmonary; TB, tracheobronchial.*

comparison with the Task Group model (ICRP) for the equivalent volume diameter of spherical particles. The fiber model curves for the three respiratory compartments will approach the curves of the Task Group model. However, for an airborne particle to be classified as a fiber, the aspect ratio (the ratio of fiber length to diameter) should exceed 3.

16 years after Harris, Asgharian and Yu (1988) extended the previous approaches by a detailed analysis of the fiber orientation in each generation of the lung. Fiber rotation by the velocity gradient of the shear flow and by Brownian diffusion was accounted for. They devised a smooth transition along the airways from the region where rotation was primarily controlled by shear flow to the area where the motion was totally controlled by Brownian diffusion. Their results showed again that impaction and interception are the predominant deposition mechanisms in the upper airways, while interception, diffusion, and sedimentation play an important role in the deeper regions of the lung. They also developed expressions for fiber deposition in the head region. To verify the theoretical data, they used the bivariate relative asbestos retention data by fiber diameter and fiber length reported by Timbrell (1982). Comparison of the Timbrell data with the theoretical fiber deposition values gave a reasonable agreement. However, it should be noted that the Timbrell data were the result of both deposition and clearance and therefore cannot be used to support a model simulating strictly deposition behaviour.

Unfortunately, there are still no experimental data available to assess the validity of the

theoretical models. Due to the potential carcinogenicity of fibrous particles, experimental deposition data would have to come from animal experiments, where breathing parameters cannot be as tightly controlled as in human studies. Margan et al. (1977) reported the experimental data of fiber deposition in the lungs of rats using various fibrous materials in 30-minutes exposures. They observed a linear relationship between the fiber mass respired and the total fiber mass deposited in the airways. A relatively constant amount was found in the lower respiratory tract. They reported that the alveolar deposition in rat lungs is lower than for human lungs, but the maximum in alveolar deposition appears to occur at a similar aerodynamic diameter. Later, Hammad et al. (1982) exposed rats for 6 hours per day for 6 days to man-made mineral fibers at about 300 fibers/cm^3 concentration with varying fiber size. The lungs were analyzed for alveolar fiber retention as a function of length, diameter, and equivalent aerodynamic diameter of the fibers. The retention of fibers less than 0.5 µm in diameter with the different length is significantly higher than for large diameters, which indicates that the fiber retention in the alveolar region increases with the increase of the fiber aspect ratio. For the fiber aerodynamic diameter, fiber retention is associated with a maximum volume at 1 µm and decreases rapidly between 1.5 to 2.5 µm. Subsequently, the retention decreases at a faster rate about 4 µm.

Similar to their human deposition model, Asgharian and Yu (1989) also developed a corresponding model for the rat lung. In their study, the fiber deposition calculations were made according to the model of Yu and Diu (1983). The anatomical rat lung model was taken from Yeh (1980), but the distribution of alveoli was assumed according to Weibel's human lung model. The authors found that their calculated results compared favorably with the experimental data of Morgan et al. (1977) and Hammad et al. (1982) especially in the alveolar region. Considering the uncertainties of the animal data, however, the agreement could not be considered to be conclusive.

As it is impossible to build a physical model of lower parts of the respiratory tract with glass bifurcations or a lung cast, a granular bed filter was used at the Delft University of Technology (van der Put, 1992 and Zhou et al., 1993) to investigate the possibility of representing the lower parts of human lungs. The idea of using a granular bed filter to represent the human lung was introduced by Gebhart and Heyder (1985). They determined the deposition of monodisperse droplets after inhalation by a human being as a function of a breath-holding period and compared this with diffusional and sedimentational deposition in a granular bed filter.

The object of the Delft project was to compare fiber deposition in the lower parts of the human lung during inspiration, both theoretically and experimentally, with the deposition of fibers in a granular bed filter with similar dimensions and equal air flow rates. Based on calculations, a trumpet-shaped granular bed filter model with dimensions similar to those of the lower parts of the human lung was developed as shown in Figure 2.6. This, however, is a simulation model for estimating the particle deposition in human lungs. In the experimental work a granular bed filter with a constant bed diameter and constant bead diameter was used. We will discuss the details of the granular lung model in the next chapter.
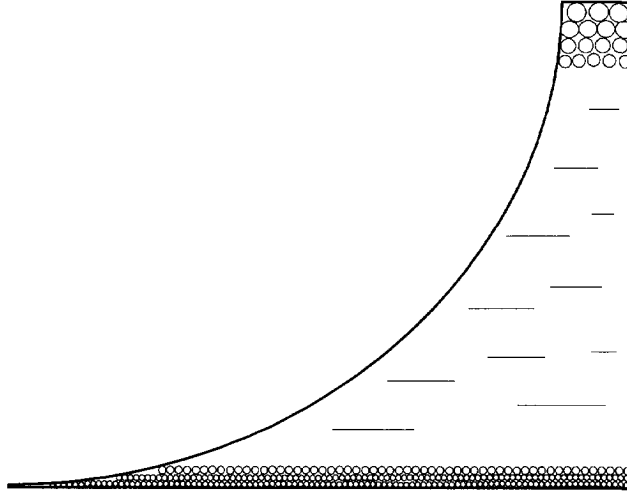
Figure 2.6. *The trumpet-shaped granular bed filter as a model of human lungs.*

In summary, we can conclude that the deposition of inhaled particles and fibers in the respiratory tract and the human body is a multifaceted dynamic process. In general, comprehensive descriptions of the deposition by means of semi-empirical and mechanistic models are useful for integrating existing knowledge, providing a structured approach to applying this knowledge to real situations, gaining insight into the mechanistic aspects of the deposition, and identifying gaps in existing knowledge that can be addressed in future research.

3

The granular bed filter as a model
for the human lung

3.1 Introduction

The term "granular bed filter" describes a device in which particles are removed from a fluid by passage through a bed of an unbounded granular filter medium. Where granular bed filters are currently used for filtration of gases, they are applied to remove particles which are too small, typically less than 5 µm in diameter, to be collected by other kinds of devices. As they are in the lung tract, aerosol particles are captured in a granular bed mainly by mechanical collection mechanisms, such as inertial impaction, interception, sedimentation, and Brownian diffusion. A large number of theoretical and experimental investigations of particle deposition in granular bed filters exist. However, few studies have been conducted focusing on all collection mechanisms, as did Otani et al. (1989) and Boulaud (1990).

Gebhart and Heyder (1985) first introduced the idea of using a granular bed filter as a representation of the human respiratory system. They determined the deposition of aerosol particles from stationary air within a granular bed filter as a function of a breath-holding period, including the effect of diffusion and sedimentation mechanisms. The results were compared with deposition data from lung investigations. In their study, however, the granular bed filter is considered as a macroview of the pulmonary airway of the human respiratory system, and attention is paid only to the pause period of the respiration.

In our study, each generation of the human lung in the lower parts is represented by a layer of the granular bed filters (Zhou et al., 1993). Special attention is paid to the inhalation period because particle deposition in lungs during inhalation is much higher than that during pause and exhalation stages, as is shown later in this Chapter. This Chapter also presents the structure of the granular bed filters, discusses and compares the particle deposition models in the bed, and shows our own experimental results. After that, we compare the dimensions, fluid dynamics, and particle deposition in granular bed filters and those in the lower parts of human respiratory system.

3.2 The granular bed filter

3.2.1 Packing structures of equal spheres

Packings are regular or random. When spheres are packed regularly in space (Figure 3.1), six possible arrays with corresponding elementary orientations exist (Sherrington and Oliver, 1981).

When monosize spheres are poured into a container and allowed to attain a stable arrangement corresponding to a minimum potential energy, the voidage of the random assembly is usually between the two characteristic values for "loose" and "dense" random packings, which is called randomness of the material. Scott et al. (1964) determined the porosity of a bed associated with loose and dense packing and obtained the following values:

Loose packing: 0.3990
Dense packing: 0.3634
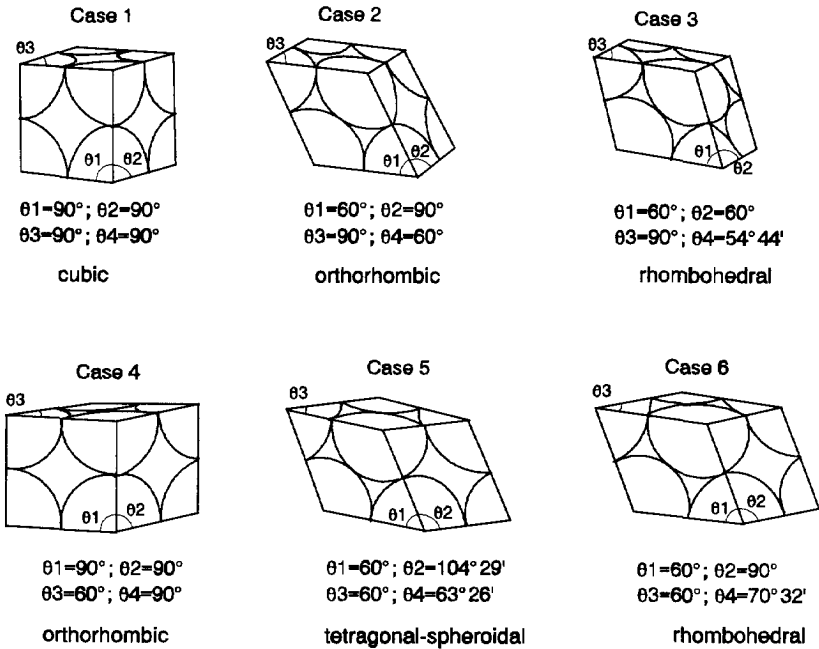
Figure 3.1. *Unit cells of regular packing of equal spheres, θ_4 indicates inclination angle of right side plane to horizontal one (Sherrington and Oliver, 1981).*

It should be noted that the porosity of the dense random packing is stated as 0.3634. Many other researchers have obtained similar values to those of Scott for a wide range of absolute particle size and densities (Gray, 1968). McGeary (1961) studied the packing characteristics of several solids including sand, glass balls, and steel spheres in order to examine the nature of the packing structures. He observed that the structural arrangement within a random packing was basically of two types, i.e. orthorhombic and tetragonal-spheroidal linked within a loose cubic arrangement. Others also obtained similar findings concerning packing structure. The major point to be emphasized is that for spherical, monosize particles within a random array, there is a network of more or less regular packing domains. Given this relatively complex geometrical arrangement, the porosity of particles poured into a container is nearly always within a narrow range of values: $0.3634 < \varepsilon < 0.4$.

3.2.2 Void shape and size

The problem of determining void shape and size in regular packings of identical beads has been discussed by numerous investigators. No one has yet been able to give a unique definition of 'pore diameter' or 'pore size'. The void space in a regular packed bed is a network of a multitude of conduits. Each conduit consists of an alternating sequence of 'voids' and 'windows' (access openings or necks, separating adjacent voids). The channel cross sections in packings are regular and irregular and never circular. There is thus a periodic variation in the cross section of the channels traversing the packing, which simply means that the channel cross section increases (from window to void) to a maximum value and then decreases to a minimum value. Subsequently it increases to another maximum value, and so forth. In random packings there are no repeating unit cells; nevertheless there is always a network that can be divided into 'voids' and 'windows'. Windows and voids are generally distributed over a range of sizes. Various measurements for void size in packed beds have been recommended.

3.2.2.1 The equivalent spherical void diameter
An equivalent spherical void diameter, d_e, may be defined as the size of a spherical void of volume equal to the mean pore volume associated with a bead in the bed (or the pore volume per unit-cell), so that

$$\frac{1}{6}\pi d_e^3 = \frac{\varepsilon}{1-\varepsilon}\frac{1}{6}\pi d_g^3; \quad d_e = (\frac{\varepsilon}{1-\varepsilon})^{\frac{1}{3}} d_g, \tag{3.1}$$

where d_g is the diameter of packed beads. The void fraction or porosity of particle packing, ε, is a basic parameter in packed beds:

$$\varepsilon = \frac{volume \ of \ voids \ in \ packing}{bulk \ volume \ of \ packing}. \tag{3.2}$$

In this case it is difficult to decide whether the length or the diameter of an airway channel should be equalled to d_e.

3.2.2.2 The hydraulic diameter

The simplest approximation is the use of an equivalent (hydraulic) circular tube diameter d_h as four times the ratio of the pore volume to the wetted surface area associated with a given bead; thus:

$$d_h = \frac{4}{\pi d_g^2} \frac{\pi}{6} d_g^3 (\frac{\varepsilon}{1-\varepsilon}) = \frac{2}{3}(\frac{\varepsilon}{1-\varepsilon}) d_g.$$
(3.3)

3.2.2.3 The maximum and minimum tube diameters of the PCT model

In the periodically constricted tube (PCT) model, the airspaces in a granular bed filter are described as sinusoidal, hyperbolic and parabolic tubes. In the sinusoidal and parabolic PCT model of Pendse and Tien (1982), the maximum tube diameter is calculated as $d_{max} = 0.795d_g$, the minimum tube diameter is given by $d_{min}=0.352d_g$.

3.2.3 Model representation of granular media

A fundamental study of a granular bed filter requires granular media to be considered as assemblies of collectors. The specifications of the collectors' structure, geometry, and the flow fields around them must then be considered. A fundamental approach to predict granular bed performance must therefore focus on the following three points (Tien, 1989):

-   The understanding of the processes involving the flow of fluid suspensions through granular media.
-   The nature and mechanisms of the transport and subsequent deposition of particles from the suspension to the individual granules from which the media are comprised.
-   The effect of particle deposition on the suspension flow, transport, adhesion, and re-entrainment.

In the literature a variety of porous media models have been proposed for studying the various physical or chemical phenomena which take place in granular media, such as fluid flow, heat and mass transfer, chemical reaction, etc. Using fluid mechanical considerations as the principle base, Scheidegger (1957) classified these porous media models into four categories: capillaric models, hydraulic radius theory models, drag theory models, and statistical models. For the purpose of filtration studies, Rajagopalan and Tien (1979) grouped porous media models into two kinds: internal flow and external flow, as shown in Figure 3.2.

The external "sphere-in-cell" model (A) proposed by Happel (1958) describes the filter grains themselves. Most known external solutions for velocity profiles in a granular bed filter assume the bed to be a homogeneous swarm of spherical granules of uniform size. No sphere touches another. Significant differences exist between the velocity profile in reality and the one obtained from the model. The existence of contact points between spheres can not be ignored when calculating aerosol particle trajectories, and this factor increases the tortuosity of the
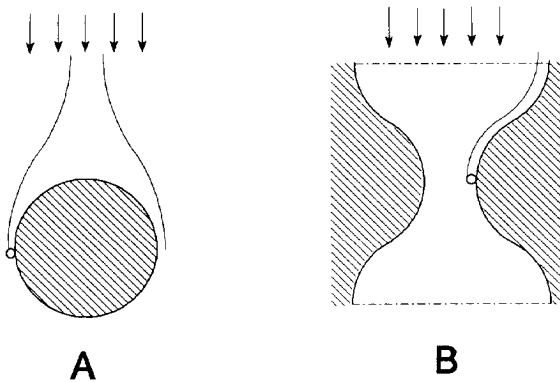
Figure 3.2. *External (A) and internal (B) flow models for granular bed filters.*

streamlines which, in turn. strongly affects the motion of an aerosol particles flowing through the bed. The internal "constricted tube" model (B) of Payatakes et al. (1973), on the other hand, describes the pore spaces of porous media, with the filter grains creating the boundaries of the pore spaces. The granular bed filter is regarded as a bundle of tangled tubes of weird cross sections with diameters at entrance and exit larger than at their centres. The pore is regarded as a parabolic, sinusoidal or hyperbolic tube or as a combination of these three. The unit cell is characterized by the maximum and minimum diameter of the constricted tube and its height. The filtration of aerosol particles is accomplished by the deposition of aerosol particles on the surface of the tube. Aerosol particle trajectories are calculated numerically. Predictions from the "constricted tube" model are sensitive to the assumed tube shape and to the method used to calculate the flow field.

In principle, any porous media model can be used in filtration studies. In practice, however, we are limited to a few relatively simple models in order that the subsequent computational work remains manageable. For the purpose of this project, the widely employed "constricted tube" model was used.

3.3 Particle deposition behaviour in a granular bed filter

Generally speaking, deposition of particles from the stream suspension to the surface of a collector may be described in two steps: the transport of the particle from the suspension to the proximity of the collector's surface and the subsequent surface adhesion between the particle and collector. Although several factors are responsible for particle deposition, and in most cases they are operating simultaneously, it is convenient and useful to examine these factors individually at first. This approach provides a better focus on their meanings and physical significance. Also a sum of the collection efficiencies based on the individual factors often closely approximates the collection efficiency where all these factors are operating simultaneously. This approach is therefore used for many semi-empirical deposition models.

25

3.3.1 Deposition mechanisms

The five most common particle transport mechanisms found in granular bed filters are *inertial impaction*, *interception*, *sedimentation*, *diffusion*, and transport effected by *electrostatic forces*. Some researchers, however, consider interception not to be a separate mechanism, but a part of impaction. Because the interception mechanism affects fiber deposition more than that of spheres, we nevertheless analyze it as an individual mechanism in our study. Because air in the human lung is completely saturated with water vapor, electrostatic forces play a less important role than other factors for particle deposition in human lungs, therefore, we neglect this factor in our discussion. Furthermore, if the collector-particle interaction is favorable in the area near the collector surface, the flux of the particle transport and that of the deposition are the same. This section will discuss these mechanisms and their effective parameters for particle deposition in granular bed filters.

For particles with diameter greater than 1 μm, inertial impaction is one of the major mechanisms for aerosol collection in granular filtration. The mechanism of particle impaction is shown in Fig. 3.3a. When changes occur in streamline trajectory, particles, because of their inertia, tend to continue in a straight(er) line. In this way particles can impact with a collector surface. The parameter that characterizes the importance of inertial impaction as a mechanism for particle deposition is the Stokes number, *Stk*, defined as

$$Stk = \frac{d_p^2 \rho_p C_p U}{18 \mu d_g},$$

(3.4)

where d_p, ρ_p, and C_p are the particle diameter, density, and slip correction factor, U is the stream velocity in the bed, and μ is fluid dynamic viscosity.

Particle deposition by interception occurs specifically because particles are finite in size. Consider the case in which all the forces acting on a particle in a fluid stream are negligible. The particle therefore completely follows the streamlines, as shown in Figure 3.3b. If any particle which touches the surface of the collector is indeed collected, then particles within one particle radius from the tube wall will be deposited. The significant parameter of the single sphere collection efficiency for interception is thus R_i ($=d_p/d_g$).

When particle density is greater than that of the fluid, particles will tend to settle out in the direction of the gravitational force. The single sphere collection efficiency attributable to sedimentation depends on the gravity number, *Grv*

$$Grv = \frac{(\rho_p - \rho_g) d_p^2 g}{18 \mu U}.$$

(3.5)
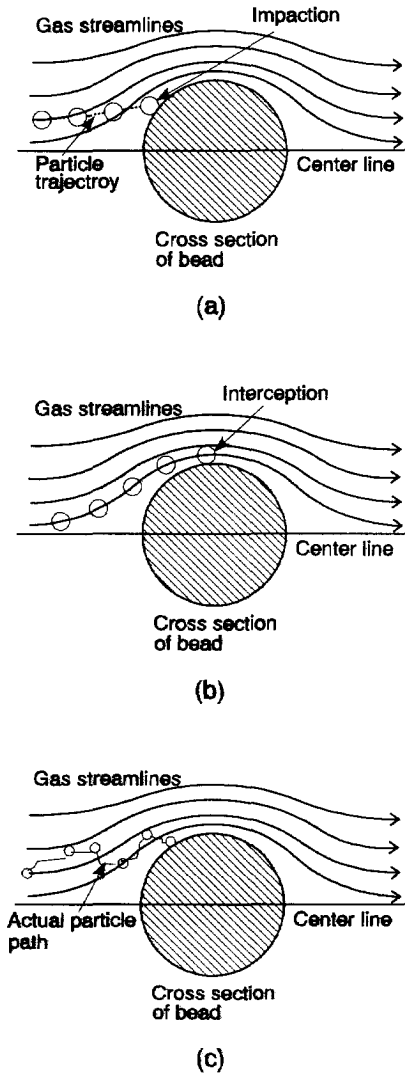
Figure 3.3. *Particle deposition caused by (a) impaction, (b) interception, and (c) diffusion (Hinds, 1982).*

27

For particles of submicron size, the Brownian diffusion force is the dominant factor in determining deposition rate, as shown in Figure 3.3c. In the absence of surface interaction forces, deposition of Brownian particles in granular bed filters may be considered to be a pure mass-transfer process, with the diffusion coefficient, D_i,

$$D_i = \frac{kTC_p}{3\pi\mu d_p},$$ (3.6)

where k is the Boltzmann constant and T is the absolute temperature of the fluid.

3.3.2 Trajectory analysis of particle deposition

The term trajectory analysis refers to a methodology which can be applied to determine the filtration rate from particle trajectories. The trajectory of a particle, which describes the particle's path as it moves past a collector, is dictated by the forces acting on the particle. Thus, when the various forces acting on the particle in the suspension and the magnitudes and the directions of these forces are known, one may determine the trajectories of the particle. The basic premise of trajectory analysis is that by knowing the trajectories and what happens when particles impact on a collector, one may estimate the rate of particle deposition.

The derivation of the basic equations describing the motion of a spherical particle in a flowing fluid began with the work of Tchen (1947) and was further clarified by Hinze (1975), Corrsin and Lumley (1956), and Soo (1967). The general equation for forces acting on a particle is:

$$F_I = F_D + F_P + F_V + F_B + F_e + F_s,$$ (3.7)

where F_I, F_D, F_P, F_V, F_B, F_e, and F_s represent respectively the inertial force, the drag force imparted by fluid, the pressure gradient force, the virtual mass force, the Basset force, the external force, and stochastic forces. For particle deposition studies in granular bed filter, we can ignore the pressure gradient force, virtual mass force, and Basset force, because these forces are much smaller than the drag force. The stochastic forces can be determined by using a Monte Carlo method. Such simulations are extremely time-consuming even for spherical particles; for non-spherical particles they would seem to still be impossible. Because stochastic forces are responsible for Brownian motion, theoretical work only focuses on large particles, for which the Brownian motion can be ignored. Furthermore, the drag force can be assumed to be given by Stokes law, although under certain conditions corrections for the hydrodynamic retardation effect may become necessary. In any case, Equation 3.7 may be replaced by the simple force balance equation:

$$F_I = F_D + F_e.$$ (3.8)

When the hydrodynamic retardation effect is considered in estimating the fluid drag force, particle motion is both translational and rotational. In the constricted tube model, which assumes that inertial, drag, and gravitational forces are occurring and which also assume that

28

the gravitational force acts along the tube's axial direction, x, the trajectory equations are (Pendse, 1979):

$$\frac{Stk}{2}\frac{d^2x^*}{dt^{*2}} = u_x^* - \frac{dx^*}{dt^*} + Grv, \tag{3.9}$$

$$\frac{Stk}{2}\frac{d^2r^*}{dt^{*2}} = u_r^* - \frac{dr^*}{dt^*}. \tag{3.10}$$

The dimensionless variables, r^*, x^*, t^*, u_r^*, and u_x^*, are defined as:

$$r^* = \frac{r}{h}, \quad x^* = \frac{x}{h}, \quad t^* = \frac{tu_0}{h}, \quad u_x^* = \frac{u_x}{u_0}, \quad u_r^* = \frac{u_r^*}{u_0}, \tag{3.11}$$

where h and r are, respectively, the height and radius of the tube, and u_0 is the average velocity at the tube's constriction. The details of the theoretical model for fiber deposition in a granular bed will be discussed in Chapter 5.

3.3.3 Particle deposition models

Assuming that all filter elements in a granular bed experience similar filtration phenomena, the total bed penetration, P_T, can be obtained by assuming that identical unit cells occur in series (Pendse and Tien, 1982):

$$P_T = (1 - \eta')^{n'} \quad or \quad \ln P_T = n' \ln(1-\eta'). \tag{3.12}$$

For $\eta' \ll 1$, the first-order approximation of $ln(1$-$\eta')$ using a Taylor series is:

$$\ln(1-\eta') \approx -\eta' - \frac{1}{2}\eta'^2 \approx -\eta', \tag{3.13}$$

where η' is the efficiency of a unit cell, defined as the ratio of the number of aerosol particles captured by the sphere to the total number of particles flowing toward it in a square duct of cross-sectional area l^2, where l is a characteristic length of the unit cell. The number of unit cells or layers, n', is related to l by:

$$n' = \frac{L}{l}, \qquad l = (\frac{\pi}{6(1-\varepsilon)})^{1/3} d_g. \tag{3.14}$$

It was shown by Clift et al. (1981) that for small values of the single sphere collection efficiency, η_T, the ratio η'/η_T is not always unity, but is given by the expression:

$$\eta'/\eta_T = \pi^{1/3}[0.75(1-\varepsilon)]^{2/3}. \tag{3.15}$$

By combining the above four equations, one deduce the overall penetration of a granular bed filter:

$$P_T = \exp(-K_1 \frac{(1-\varepsilon)L\eta_T}{d_g}).$$
(3.16)

From the previous equations, the value of the constant K_1 can be calculated as *1.5*. Otani et al. (1989) used this value in the case that the superficial velocity is taken as a representative velocity. When the interstitial velocity is used, K_1 is suggested as *1.5/ε* by Paretsky et al. (1971) and Tardos et al. (1974). There are also several other values given for this constant, such as, *1.5f*, where *f* is a collision factor (Patterson and Jackson, 1977) and *1.875*, which is an empirical constant (Schmidt et al., 1978).

It can be seen that penetration through a granular bed is only related to the single-grain collection efficiency by geometric parameters (i.e. porosity, bed depth, grain size). Therefore, thermal-hydraulic variations of the fluid vector will only influence the overall penetration through the bed via η_T. Collection of particles by a single grain of a granular bed involves various mechanisms (discussed in 3.3.1), which transport the particles to the surface of the grain where they can bind. When more than one capture mechanism occurs, the single sphere collection efficiency can be calculated in principle from:

$$1-\eta_T = (1-\eta_i)(1-\eta_j)(1-\eta_k)...(1-\eta_n),$$
(3.17)

where $\eta_i ... \eta_n$ are single sphere collection efficiencies for various mechanisms.

It is, however, commonly assumed that the efficiencies of the component mechanisms are additive when investigating particle deposition in a granular bed filter. This is not an oversimplification, but represents a reasonable approximation, if the individual efficiencies are all small or if one mechanism is dominant. The efficiencies of the four component mechanisms discussed in 3.3.1 can be described as:

$$\eta_T = \eta_I + \eta_R + \eta_S + \eta_D.$$
(3.18)

Many studies of particle deposition mechanisms in granular beds exist. Most of these, however, only concern one individual deposition mechanism. Only two research groups (Otani et al., 1989 and Boulaud, 1991) studied combined deposition mechanisms. Thus Otani and his co-workers studied the single-grain efficiencies separately in the predominant regions of each collection mechanism. On the basis of experimental data they derived expressions for each mechanism. Boulaud included all existing expressions for his granular impactor and compared his experimental data with predictions from his model. The expressions for each mechanism in these two models will be discussed in the following sections.

Impaction
As already discussed, impaction is the dominant mechanism when large particles move in the stream at high velocity. The significance of impaction increases with the Stokes number and Reynolds number. D'Ottavio and Goren (1983) introduced the important idea of the effective

Stokes number (Stk_{eff}), which relates single-grain collection efficiency to the inertial parameters, Stk, Re, and the ε, of the particles. Their empirical equation was adapted in the Boulaud model:

$$\eta_I = \frac{Stk_{eff}^{3.55}}{1.67 + Stk_{eff}^{3.55}}; \quad \text{with } Stk_{eff} = A(\varepsilon, Re)Stk, \quad (3.19)$$

where $A(\varepsilon, Re)$ is a function of the granular bed porosity and the Reynolds number of the flow around a grain:

$$A(\varepsilon, Re) = \frac{(2 - 2(1-\varepsilon)^{\frac{5}{3}})}{(2 - 3(1-\varepsilon)^{\frac{1}{3}} + 3(1-\varepsilon)^{\frac{5}{3}} - 2(1-\varepsilon)^2)} + 1.14 Re^{\frac{1}{2}} \varepsilon^{-\frac{3}{2}}. \quad (3.20)$$

Likewise, Otani et al. (1989) concluded that the expression of D'Otavio and Goren (1983) is not directly applicable to their experimental results. They suggest the use of a different correlation with an effective Stokes number introduced by Gal et al. (1985), based on Ergun's equation (Ergun, 1952):

$$Stk_{eff} = A_1(\varepsilon, Re)Stk; \quad A_1(\varepsilon, Re) = 1 + \frac{1.75 Re\varepsilon}{150(1-\varepsilon)}, \quad (3.21)$$

$$\eta_I = \frac{Stk_{eff}^3}{0.014 + Stk_{eff}^3}. \quad (3.22)$$

Interception
The effect of interception in a granular bed is usually small compared to other mechanisms for spherical aerosol particles. Interception becomes relatively important only in the transitional regions of the other mechanical collection mechanisms. Thus, Otani et al. obtained the interception efficiency from the experimental data of the particles for their model in the transitional regions:

$$\eta_R = 16 R_i^Y \quad \text{with} \quad Y = 2 - \frac{Re}{(Re^{1/3} + 1)^3}. \quad (3.23)$$

In the Boulaud model, Paretsky's (1972) equation was used to describe this mechanism:

$$\eta_R = 6.3 \varepsilon^{-2.4} R_i^2. \quad (3.24)$$

31

Sedimentation

For aerosol particles at low velocities, sedimentation becomes the predominant collection mechanism. The single-grain efficiency due to sedimentation has been theoretically derived by Tardos et al. (1978) and Lee (1980). After comparison with the experimental data, Otani et al. use the following equation in their model:

$$\eta_S = Grv/(1+Grv). \tag{3.25}$$

In the Boulaud model, on the other hand, a semi-empirical equation developed by Paretsky (1972) was used for the sedimentation mechanism. This Paretsky equation distinguishes two cases:

$$upward\ flow: \quad \eta_S = 0.0375\ (Grv)^{0.5}, \tag{3.26}$$

$$downward\ flow: \quad \eta_S = 0.0375\ (Grv)^{0.5} + 0.21\ (Grv)^{0.78}. \tag{3.27}$$

Brownian diffusion

The motion of fine particles with diameters smaller than several tenths of a micrometer is governed by Brownian diffusion. On the basis of their experimental results, Otani et al. express the functional dependence of η on both the Reynolds number, Re, and the Schmidt number, Sc. These expressions are also adopted by the Boulaud model:

$$\eta_D = B(Re)Sc^{f_1(Re)}Re^{f_2(Re)}. \tag{3.28}$$

The parameters of the equation are expressed by:

$$f_1(Re) = -\frac{2}{3} + \frac{Re^3}{6(Re^3 + 2 \times 10^5)}, \tag{3.29}$$

$$\begin{aligned} B(Re) &= 8; \quad f_2(Re) = -2/3 \quad for\ Re<30, \\ B(Re) &= 40; \quad f_2(Re) = -1.15 \quad for\ 30 \le Re<100, \\ B(Re) &= 2.1; \quad f_2(Re) = -0.5 \quad for\ Re \ge 100. \end{aligned} \tag{3.30}$$

To summarize the above discussion, the model of Otani et al and the Boulaud model are presented in Table 3.1:

Table 3.1. *Expressions of models of Boulaud and Otani et al.*

$$\eta = \eta_S + \eta_D + \eta_I + \eta_R$$

	Boulaud (1991)	Otani et al. (1989)
η_S	$0.0375(Grv)^{0.5} + 0.21(Grv)^{0.78}$	$Grv/(1+Grv)$
η_D	$B(Re)Sc^{f_1(Re)}Re^{f_2(Re)}$	$B(Re)Sc^{f_1(Re)}Re^{f_2(Re)}$
η_I	$\dfrac{(A(\varepsilon,Re)Stk)^{3.55}}{1.67+(A(\varepsilon,Re)Stk)^{3.55}}$	$\dfrac{(A_1(\varepsilon,Re)Stk)^3}{0.014+(A_1(\varepsilon,Re)Stk)^3}$
η_R	$6.3\varepsilon^{-2.4}R_i^2$	$16R_i^Y \quad with \quad Y = 2-\dfrac{Re}{(Re^{1/3}+1)^3}$

3.4 Experiments for particle deposition in a granular bed

The purpose of the experimental work is to investigate particle deposition models in granular bed filters. We vary the operating conditions and particle size to determine which of the four important mechanisms are dominant. This section describes the spherical particle dispersion and measurements, the experimental set-up, and the results.

3.4.1 Particle dispersion and measurement

Two different types of aerosol generators were used to spray a salt solution, jet nebulizers and the Spinning Top Aerosol Generator (STAG).

For small particles, the DeVilbiss 45 nebulizer (DeVilbiss Health Inc. USA) and the Mollinger nebulizer (1994) were used (Zhou et al., 1995a), as shown in Figure 3.4. The operation principle of these two nebulizers is similar. Compressed air exits from a small tube or orifice at high velocity. The low pressure, created in the exit region as a result of the Bernoulli effect, causes the particle solution to be drawn from a reservoir into the airstream through a second tube. The solution exits the tube as a thin filament that is stretched out as it is accelerated in the airstream until it breaks up into droplets. The spray stream is directed on to an impaction surface, where large droplets are deposited and drain back to the reservoir. The smaller droplets and the air exit the nebulizer as the aerosol. Most nebulizers produce a maximum droplet number concentration of 10^6-10^7 / cm^3 with the mass median diameter (MMD) of about 5 μm. In our study, the salt concentration of the liquid was changed from 0.2 g/l to 2 g/l in order to obtain various sizes of particles.

The STAG (Figure 3.5) is used to disperse aerosol droplets larger than 0.5 μm. The liquid to be dispersed is delivered through a needle to the surface of the rotor disc. This needle is
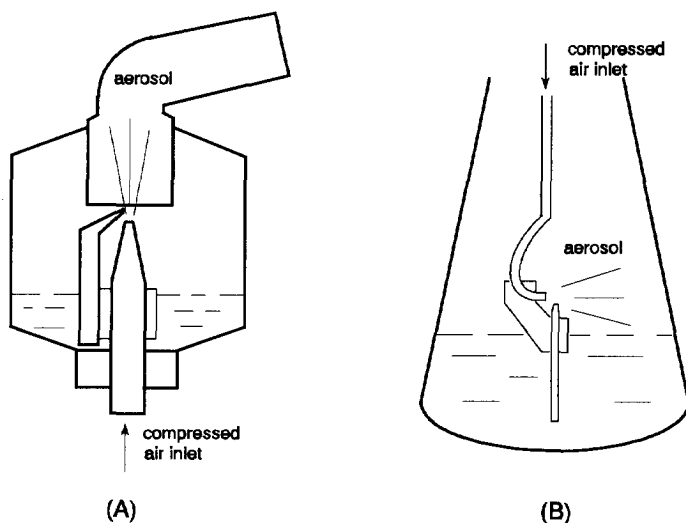
Figure 3.4. *The DeVilbiss 45 nebulizer (A) and the Mollinger nebulizer (B).*

attached to the support spider which enables the needle height and position to be precisely adjusted. The liquid breaks into droplets at the rotor rim after traversing the rotor surface as a thin film. Great care must be taken to position the needle above the center of the disc, in which a small hole is drilled to facilitate the positioning of the needle. With the needle in the center of the disc, the needle height can be changed, in accordance with the operational pressure, by turning the adjustment screws attached to the support spider. A clearance below 0.5 mm between needle tip and rotor disc has been used in this research. It is also important to ensure a constant liquid feed rate: if the feed rate is too high, the large number of outgoing droplets begin to entrain satellites. If it is too low, the film on the rotor surface becomes discontinuous and thus exerts an influence on the size distribution of the primary droplets. In this research, we chose a flow of about 0.4 ml/min and varied the solution concentrations between 0.045 and 0.45 vol./%. A housing and ducting system has been designed (Mori et al., 1990) in order to enhance the separation of primary particles and satellites and to direct the particles to the required areas.

Particle distribution and concentration were measured by two particle counters: the ASASP (Active Scattering Spectrometer Probe, Model X, PMS Inc. Colorado, USA) and the CLIMET particle analyzer (Model CI-226M, Climet instruments Co., CA, USA). They were calibrated using latex particles.

The ASASP is a single particle counting system which is designed with four overlapping size ranges; each size range is divided into fifteen linear size intervals providing up to 60 channels. The spectrometer probe is capable of sizing particles in the range of 0.09 μm to 3 μm. This particle counter operates on the principle that the light scattered by a particle within an active He-Ne laser cavity is directly a function of its size. Particles produce pulses of
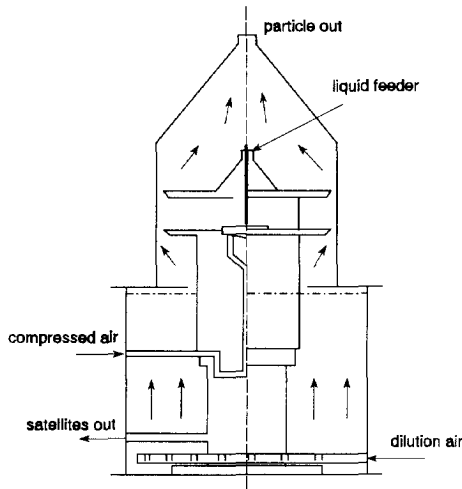
Figure 3.5. *Schematic representation of the spinning top aerosol generator.*

radiant energy during transit through the laser beam. These light pulses are sensed by a detector and measured with a 16 channel pulse height analyzer. The method of particle input is through an aerodynamically focused jet which constrains particle flow to a 200 μm diameter stream surrounded by a filtered sheath flow.

The CLIMET particle analyzer is used to measure the particle concentration and size distribution in gases. Each time a sample is taken, the instrument counts and stores in its memory the number of particles within 2750 different size (pulse height) ranges. Up to six of the size ranges may be selected for display and printout. These ranges are determined by voltage thresholds that define six regions of interest. In order to display and print more size ranges beyond the first set of six, the voltage thresholds may be adjusted to show new regions of interest without the need to run another sample. The data in all 2750 channels can be transmitted for evaluation to an external computer.

3.4.2 Experimental set-up

The experimental work was done in order to investigate the existing particle deposition models in a granular bed filter. In the experimental set-up shown in Figure 3.6, salt (NaCl) solution was dispersed by aerosol generators which were discussed above. After being formed, the salt solution particles flowed into a heating chamber and a diffusion dryer in order to evaporate water. The dried particles were neutralized by a radioactive source (Kr 85) before being introduced into the granular bed filter; this was done in order to avoid electrostatic effects on the particle collection. There are two sampling probes, one at the inlet and another at the outlet of the filter. The ASASP and the CLIMET particle analyzer were used to

35

Kr 85 → measurement

diffusion dryer

diluting air

↖7°

granular bed

heating chamber

measurement

aerosol generator (nebulizers and STAG)

filter

granular medium:
  glass beads with the diameter of 1.04, 1.28, and 2.0 mm

aerosol particles:
  polydisperse NaCl particles with the diameter from 0.1 to 3 μm

measurements:
  ASASP, Climet

total flowrate:
  23, 30 and 50 l/min

bed height:
  7, 12, and 17 cm

Figure 3.6. *Schematic drawing of the measurement system for particle deposition in a granular bed filter and the operation conditions.*

measure the particle concentration and distribution at the inlet and outlet of the granular bed in the particle diameter rage of 0.1 μm to 3 μm.

The granular bed filter used in the experiments consisted of a cylindrical vessel with a diameter of 9 cm. The cylinder could be filled with glass beads to a maximum height of 18 cm. The bottom of the vessel was formed by fine wire gauze which prevented the beads from falling out. The inlet and outlet on either end of the cylinder were funnel-shaped to provide a homogeneous distribution of the aerosol flow inside the filter medium. The angle over which the cross section enlarges from the supply tube is 7°. This angle prevents the formation of turbulent eddies in the filter, which could influence the results. The granular bed filter can easily be disconnected. It has been designed in three pieces so that it can be easily filled and emptied.

The mean diameters of the glass beads used for the experiments were 1.04, 1.28, and 2.0 mm. The porosity of the granular bed filters was determined by two methods:

1.   A measuring-glass of 0.5 litre was filled with glass beads. The total pore volume in this 0.5 litre of beads was replaced by a known volume of water.
2.   A known volume of beads was weighed and the porosity was calculated by the following equation:

$$\varepsilon = 1 - \frac{W}{\rho_b V_b},$$

(3.31)

where W is the total weight of the beads, V_b is the volume of the beads, and ρ_b is the density

of the beads. Table 3.2 shows the experimental results of the two methods for the determination of the bed porosity. From these two methods, we found that the average porosity in our case to be 0.38.

Table 3.2. *Measured porosity of the granular bed filter.*

Diameter of the glass beads (mm)	1.04	1.28	2.0
Volume of water needed to fill up 0.5 l filter volume (l)	0.185	0.190	0.195
Porosity from volume (-)	0.37	0.38	0.39
Weight of 0.5 l filter (g)	885.4	898.4	901.5
Porosity from weight (-)	0.39	0.38	0.38

3.4.3 Experimental results

Experimental data for total particle penetration in the granular bed filter were compared with the models of Boulaud (1991) and Otani et al. (1989). Special attention was also paid to various particle size ranges in order to investigate the equations for the four mechanisms of these two models. When particle size and experimental conditions are limited to a suitable range, deposition may occur largely through only one predominant mechanism. Thus from Equation 3.16, one can get the relation between the overall particle penetration (P_T) and the single collection efficiency for the predominant mechanism (η_p):

$$\eta_p \approx \eta_T = -\frac{d_g \ln P_T}{K_1 L (1-\varepsilon)}. \tag{3.32}$$

All experimental data are listed in Appendix 3A.

The motion of fine particles with diameters smaller than tenths of a micrometer is governed by Brownian diffusion. Figure 3.7 shows the comparison of experimental data and the equations from Otani et al. for diffusion. The spherical particle diameter changes from 0.1 to 0.3 μm with the change of the Reynolds number from 10 to 30. As seen in the figure, the predicted lines describe all our data quite well.

For large particles at low velocity, sedimentation becomes a predominant collection mechanism. The gravity number, *Grv*, is the important parameter in this case. The single sphere collection efficiency as a function of the gravity number is shown in Figure 3.8 with a superficial velocity of 6 cm/s. It can be seen from this figure that the experimental data are in good agreement with the equation from Paresky (1972) in the Boulaud model.
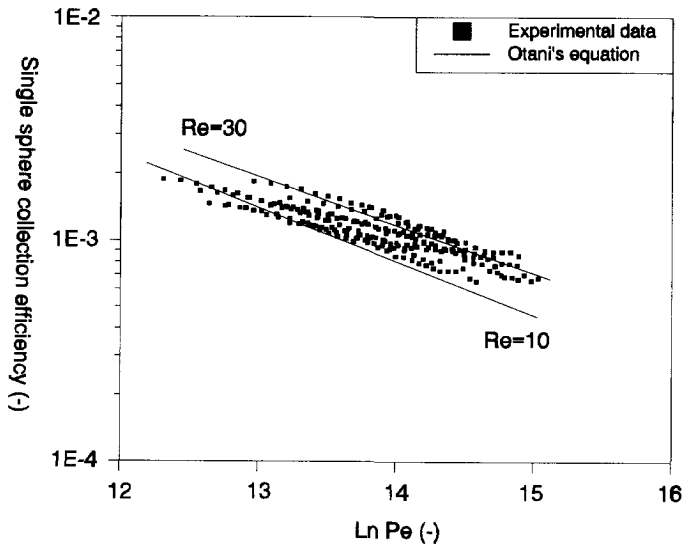
Figure 3.7. *Comparison of experimental data and Otani's model for the diffusion region with the particle diameter from 0.1 to 0.3 μm.*
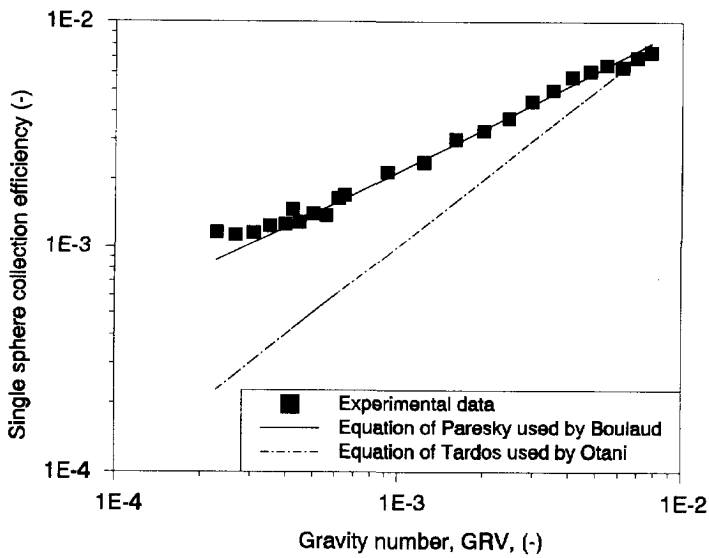
Figure 3.8. *Comparison of experimental data and existing equations for sedimentation with a superficial velocity of 6 cm/s.*
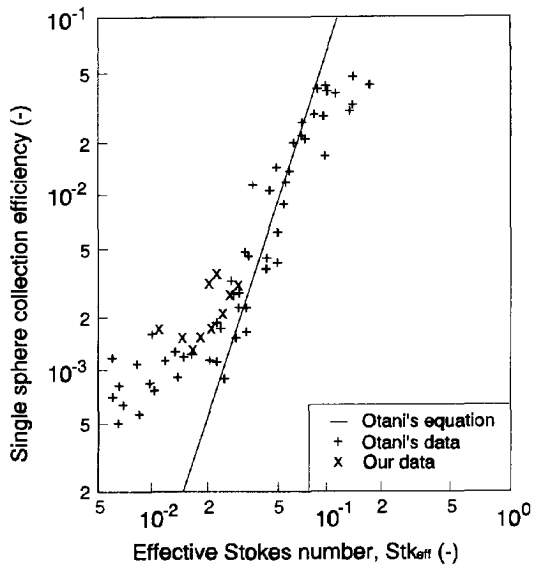
Figure 3.9. *Experimental data of Otani et al. and our study compared with the existing equation for impaction.*

Impaction is a very important mechanism for particle removal from a granular bed filter. In this project, however, it is not important because we are interested in low gas velocities. We got the same results as Otani's experimental data in the range of Stokes numbers from 0.01 to 0.03. Otani also did experiments for high Stokes numbers to test his equation. Figure 3.9 shows the comparison between the experimental data both from our experiments and Otani et al. and the model of Otani et al. as a function of effective Stokes number.

In granular beds, the effect of interception is usually small compared with the other mechanisms. Interception becomes relatively important only in the transitional regions of the other mechanical collection mechanisms. On the basis of a literature study, we decided to use the equation in the Boulaud model (Equation 3.24) as the interception equation of our model.

After comparison of the experimental data with the models of Boulaud and Otani et al. for the individual mechanism, a new semi-empirical model for spherical particle deposition in a granular bed was developed by combining the equations of the two models. Table 3.3 shows the expressions for the single collection efficiencies for various mechanisms of the model.

39

Table 3.3. *Expressions of the new spherical particle deposition model.*

η_S	$0.0375(Grv)^{0.5}+0.21(Grv)^{0.78}$
η_D	$B(Re)Sc^{f_1(Re)}Re^{f_2(Re)}$
η_I	$\dfrac{(A_1(\varepsilon,Re)Stk)^3}{0.014+(A_1(\varepsilon,Re)Stk)^3}$
η_R	$6.3\varepsilon^{-2.4}R_i^2$

Figures 3.10 shows the comparison of the experimental data with the results of different models, namely Otani et al., Boulaud, and our new model, for the total particle penetrations at different conditions. From Fig. 3.10 it is seen that the Boulaud model accurately predicts particle deposition in a granular bed for particle diameters smaller than 1 μm. For particle diameters larger than 1 μm, however, the reliability of the Boulaud model drops sharply. On the other hand, the predictions of the Otani et al. model are in reasonably good agreement with measurements for particles larger than 1 micrometer. In contrast to the models of Otani et al. and Boulaud, our new semi-empirical model is in good agreement with the data over the entire particle size range.

The following sections discuss the simulation of human lungs with the granular bed filter. The use of this new deposition model to predict particle deposition in lungs is also discussed.

3.5 Representation of human respiratory system

The idea of using a granular bed filter as a representation of the human lung is not new. Gebhart and Heyder (1985) determined deposition of monodisperse droplets after inhalation by a human as a function of breath holding period. They compared these results with diffusional and sedimentational deposition in a granular bed filter that was filled with aerosols and emptied after a certain pause. However, their study focused on particle removal from a stationary air flow. In our project, attention was paid to dimensional comparison between the granular bed filter and the human lung systems as well as aerodynamic behaviour (Zhou et al., 1994). We also compared the particle deposition model in a granular bed filter with that in the human lung.

3.5.1 Dimensional comparison

On the basis of detailed measurements of a lung cast, Weibel (1963) proposed a mathematical description of a dichotomous system of airways. He showed that the human respiratory tract can be characterized by 24 generations of cylindrical elements between the trachea (generation 0) and the alveolar sacs (generation 23), and 3×10^8 alveoli. Beginning from the 17th generation, increasing numbers of alveoli are present on the airway walls. The last three
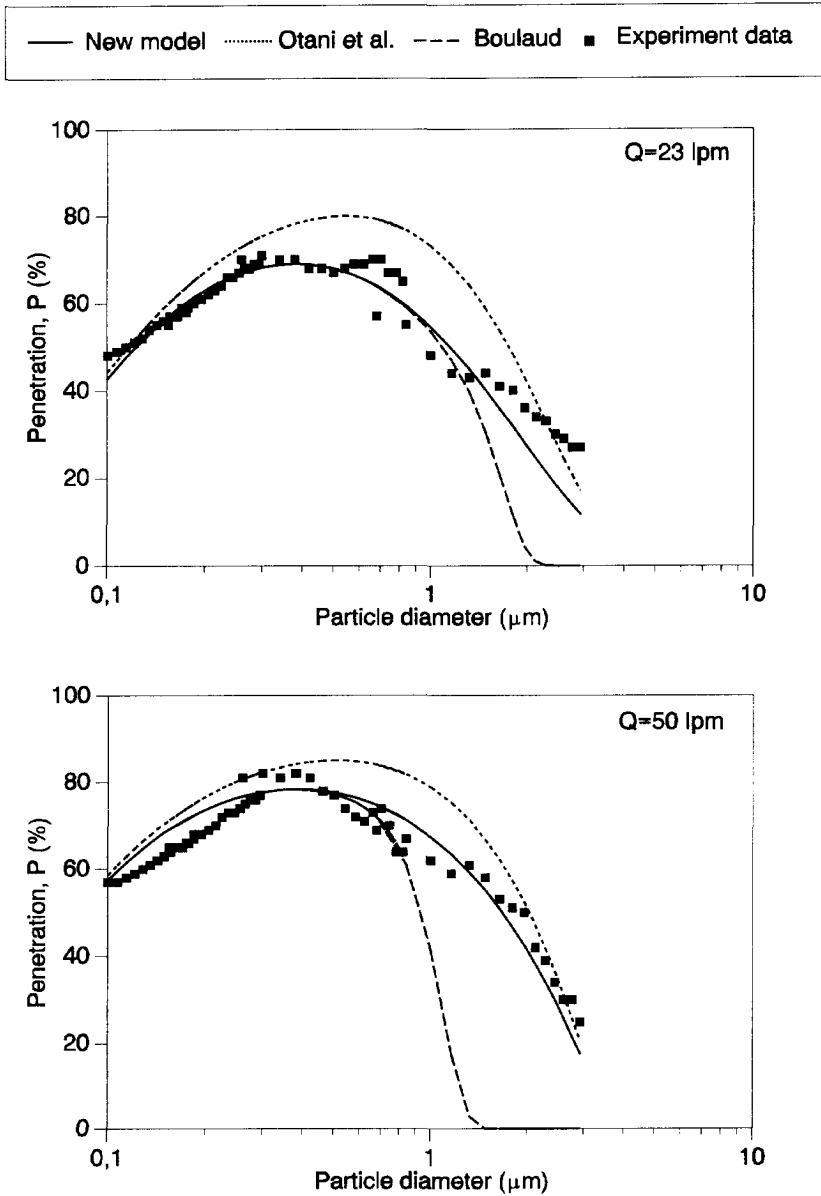
Figure 3.10(a). *Total particle penetration as a function of particle diameter for a bead diameter of 1.04 mm and a bed height of 17 cm at different flowrates.*
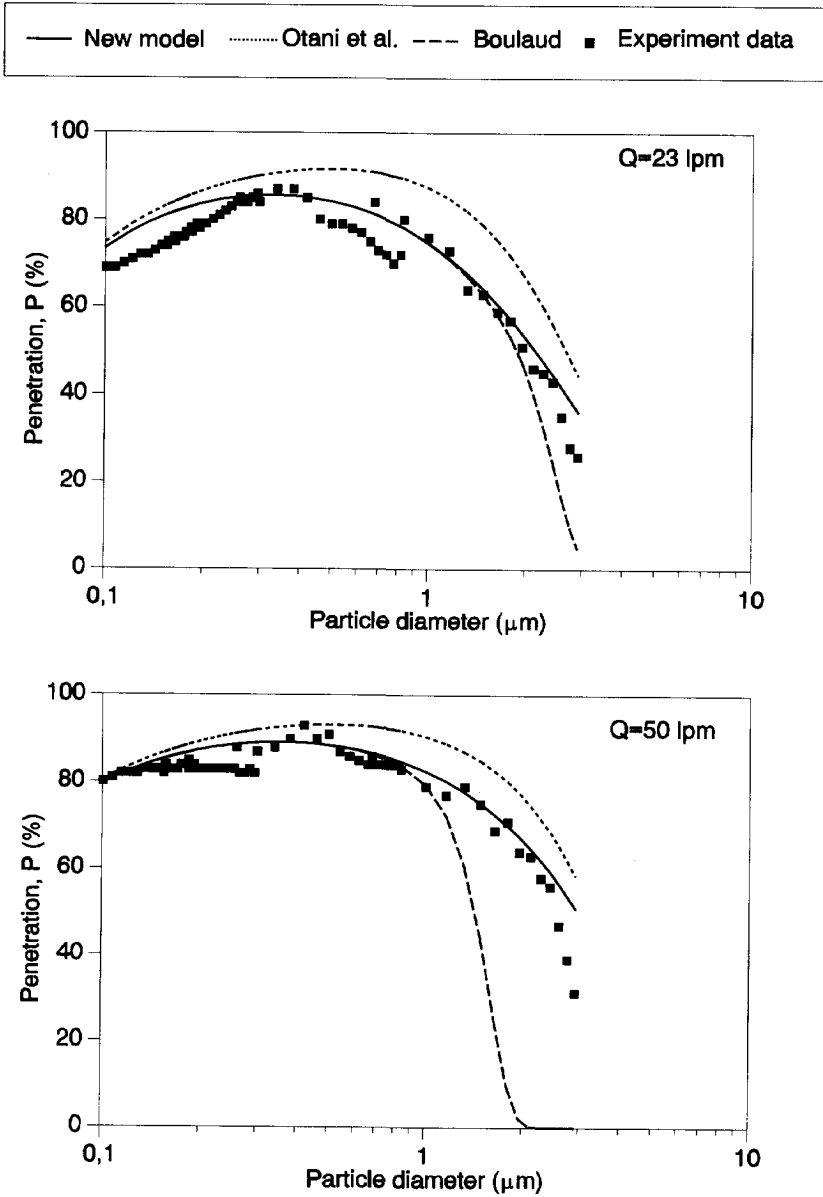
Figure 3.10(b). *Total particle penetration as a function of particle diameter for a bead diameter of 2.0 mm and a bed height of 17 cm at different flowrates.*

generations are completely covered with alveoli. The alveolar space in his model thus consists of all the airways in the last seven generations. In his model, Weibel simulated adult human lungs with a volume of 4.8 litre at about 3/4 maximal inflation.
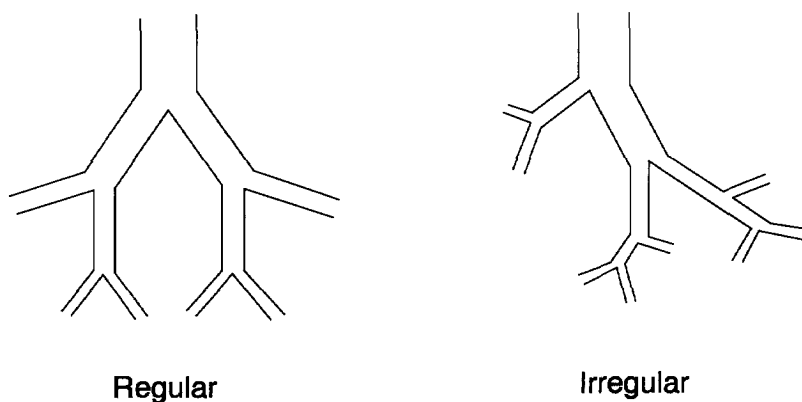
Regular   Irregular

Figure 3.11. *Representation of dichotomous branching of airways.*

Weibel described two types of dichotomies, regular (model A) and irregular (model B), as shown in Figure 3.11. Irregular dichotomy is the type actually observed in the human lung. It is, however, more difficult for theoretical study. In order to simplify the simulation and to make it comparable with other models, the Weibel regular model (A) has been used as a representation of the human respiratory tract. By doing this, one has to account for a number of simplifications that may cause errors in calculating the particle deposition according to van de Put (1991):

-       The concept of specified airway generation dimensions defined by Weibel's model A is an abstraction. Airways of, for example, 2 mm diameter may be found at 4-13 branchings away from the trachea.
-       The branching pattern of human airways is usually asymmetric. Ferron (1976) observed significant differences in deposition patterns between symmetric and asymmetric glass models. The more complex flow patterns which develop in the asymmetric model enhance deposition at the bifurcations.
-       Weibel did not actually measure generations 11 through 16, but inferred their dimensions from the patterns of dichotomous branching and the dimensions of elements of earlier and later generations.
-       Because bifurcating and gravity angles are not included in Weibel's model, the fact that part of the airway flow is directed upwards is neglected. This affects deposition by sedimentation.
-       In Weibel's model it is assumed that the tubes have fixed dimensions from the start to the end of the inspiration. Only the alveolar ducts and sacs change volume during respiration. The assumption is correct for low tidal volumes, but probably breaks down at large ones.
-       The diameters of the airways in the alveolar region used in the calculations are wrong.

The walls of most alveolar space have been replaced by alveoli. An aerosol particle in an airway must be transported over a larger distance to reach the wall of the alveoli than to reach the wall of the airway. It is expected that this factor decreases calculated deposition of small particles.

Airway geometry affects particle deposition in a number of ways: the diameter of the airway determines the displacement required before the particle contacts the airway surface, the cross section of the airway determines the air velocity for a given flowrate, the airway volume and surface area in the alveolar region affects the Brownian motion and the sedimentation deposition, and the bifurcating and gravity angles influence the inertial and sedimentation deposition. It is, however, for two reasons impossible to incorporate all of these factors into a lung model:

(1) To accurately describe the anatomic system, we need to know the angles of branching at a bifurcation, the sharpness of the carina, the way in which the parent branch changes shape to accommodate the two daughters, the radius of the curvature of the tube walls at the junction, whether the bronchi themselves are curved or straight and the nature of the bronchial walls (smooth or irregular). Such detailed anatomic data is unavailable in the literature.
(2) The second problem is caused by intersubject variability and changes in lung structure induced by lung diseases. Heyder et al. (1978) confirmed that variations in the anatomical geometry of the respiratory tract can lead to different deposition patterns within the lungs. Increases in tracheobronchial deposition by a factor of three or four in bronchitic patients due to clogging of the bronchi were demonstrated to be fairly common. Variety in deposition is also caused by the position of the person (standing, lying, sitting or bending). It is therefore impossible to derive a perfect general description of the lung, even if it is much more detailed than those of today, which represents more than one person. For that reason, a lung model will always be a simplification of the human respiratory tract.

Weibel's model A was chosen, in spite of its deficiencies, as a description of the lower parts of the respiratory tract because, (1) it is the most widely used model for studying lungs, (2) it gives a median deposition of particles among existing models (Yu and Dui, 1982), and (3) comparing the lower parts of the human lung with a granular bed filter, it is not possible to account for unequal lengths, diameters, branching and gravity angles of the airway channels. It is therefore not useful to choose a model that includes information about these matters, such as the Weibel model B or model of Yeh and Schum (1980).

The main parameters of a lung structure are length (L_z) and diameter (D_z) of an airway and the number of airways in a generation (N_z). The lengths and diameters of the conjugate daughters in regular dichotomy (Weibel model A) are expressed mathematically by the following empirical equations:

$$L_z = 12\exp(-0.92z); \qquad D_z = 1.8\exp(-0.388z), \qquad (3.33)$$

for generation 0 to 3, and

$$L_z = 2.5\exp(-0.17z); \qquad D_z = 1.3\exp(-(0.293-0.0062z)z), \qquad (3.34)$$

for generation 4 to 23. And the number of airways in a generation is expressed by:

$$N_z = 2^z. \tag{3.35}$$

About $300*10^6$ alveoli as spheres with diameters of 0.028 cm appear from generation 17. This fact should be included in calculating the structure of human lungs. The model does not include bifurcating and gravity angles. Table 3.4 shows the dimensions and the flow conditions of the Weibel A model with a tidal volume of 1450 cm^3.

Table 3.4. *Dimensions and average inspiratory flow conditions for the Weibel A lung model.*

z	N_z	D_z	L_z	S_z	V_z	$A_{s,z}$	U_z	$t_{r,z}$
(-)	(-)	(cm)	(cm)	(cm^2)	(cm^3)	(cm^2)	(cm/s)	(s)
8	256	0.186	0.64	7.0	4.5	95.7	120	0.005
9	512	0.154	0.54	9.5	5.1	134	87.3	0.006
10	1024	0.130	0.46	13.5	6.2	192	61.5	0.007
11	2048	0.109	0.39	19.1	7.5	274	43.5	0.009
12	4096	0.095	0.33	29.1	9.6	403	28.7	0.012
13	8192	0.082	0.27	43.3	11.7	570	19.3	0.014
14	16.4e3	0.074	0.23	70.5	16.2	876	11.8	0.020
15	32.8e3	0.066	0.20	112	22.4	1359	7.42	0.027
16	65.5e3	0.060	0.165	185	30.5	2038	4.5	0.037
17	131e3	0.054	0.141	345	48.6	4485	2.4	0.059
18	262e3	0.050	0.117	694	81.2	9317	1.2	0.098
19	524e3	0.047	0.099	1546	153	21.2e3	0.54	0.183
20	1.05e6	0.045	0.083	4318	358	59.4e3	0.19	0.437
21	2.10e6	0.043	0.070	9274	649	113e3	0.09	0.778
22	4.19e6	0.041	0.059	20487	1209	221e3	0.04	1.475
23	8.39e6	0.041	0.050	41075	2054	375e3	0.02	2.5

When a granular bed filter is used to represent the human lungs, the diameter and length of the void per unit-cell of the granular bed filter should be equal to those of an airway channel in the lung. Internal surface area, cross section and volume in a granular bed filter layer should be equal to those in an airway generation. As the void per unit-cell is compared to an airway channel, the number of airway channels in each generation should be equal to the number of beads in the corresponding layer. Thus, the airway residence time (in case of sedimentation and diffusion) and the airway velocity (in case of impaction and interception) would be equal. Unfortunately, not all these factors can simultaneously be met. There are three possibilities for equal quantities for the simulation of granular beds and human lungs: (1) the diameters and the cross sections are equal, (2) the cross sections and the space volumes are equal, and (3) the surface area and the cross sections are equal. The first equality is suitable for the upper parts of the lung because air flow conditions will be affected by the airway diameters in that area. In the lower parts, however, the space volumes and surface area become the more important parameters for particle deposition. Moreover, in the second and third cases, the cross sections in the two systems are also the same, which results in equal velocities. After calculating these two cases, we found that the height of a bed layer is equal

to the length of an airway generation in the second case. Together with the same velocities, the same length results in equal residence times. Therefore, we use the second case as the criteria of simulation in our study: the total cross section of air spaces and the total void volume in a layer of a granular bed filter are the same as that of the corresponding airway generation.

By equalizing the total cross sections in the two systems, one obtains:

$$S_{layer} = S_z = N_z \frac{\pi D_z^2}{4} + S(alveoli)_z. \tag{3.36}$$

One can also derive the following equations by equating the total void volume per layer and the total lung volume in generation z:

$$V_{vtot} = S_{layer} H_{layer} = V_z = L_z N_z \frac{\pi D_z^2}{4} + V(alveoli)_z. \tag{3.37}$$

From these two equations, the relation between the layer height of a bed and the length of an airway generation can be obtained:

$$(N_z \frac{\pi D_z^2}{4} + S(alveoli)_z) H_{layer} = L_z N_z \frac{\pi D_z^2}{4} + V(alveoli)_z. \tag{3.38}$$

The total cross section of an airway generation is equal to the sum of the cross section of the tubes and the contribution made by alveoli, $S(alveoli)_z$. This contribution is found by dividing the total volume of the alveoli of the generation, $V(alveoli)_z$, by the tube length, L_z (de Jongh, 1995). Thus, the height of the layer, H_{layer}, in Equation 3.38, is equal to the length of the corresponding airway generation, L_z.

In the study of Fayed and Otten (1980), every random packing can be thought of as consisting of parallel layers of identical structure. For any orientation, average values for the distance between sphere centers can be calculated by the following formula:

$$H_{layer} = \sqrt{\frac{2}{3}} \left(\frac{\pi}{3\sqrt{2}(1-\varepsilon)} \right)^{1/3} d_g; \quad d_g = 1.155 L_z, \quad for \ \varepsilon = 0.38. \tag{3.39}$$

The total void volume of beads in a layer can also be calculated by:

$$V_z = V_{vtot} = N_g \frac{\pi}{6} d_g^3 \left(\frac{\varepsilon}{1-\varepsilon} \right). \tag{3.40}$$

Therefore, the total number of beads in a layer is calculated by:

$$N_g = \frac{V_z}{\frac{\pi}{6} d_g^3 \frac{\varepsilon}{1-\varepsilon}}. \tag{3.41}$$

The calculated dimensions of each granular bed filter layer, representing an airway generation z, are shown in Table 3.5. Each airway generation is represented by one layer of beads. The anatomic structure of the lung can thus be represented by a granular bed filter with a circular cross section.

Table 3.5. *Dimensions and average inspiratory flow conditions in a granular bed filter with a tidal volume of 1450 cm³.*

z	N_g	d_g	d_h	H_{layer}	S_{layer}	V_{vtot}	$A_{s,layer}$	U_{layer}	$t_{r,layer}$
(-)	(-)	(cm)	(cm)	(cm)	(cm²)	(cm³)	(cm²)	(cm/s)	(s)
8	34	0.74	0.30	0.64	7.0	4.45	58.5	120	0.005
9	67	0.62	0.25	0.54	9.5	5.15	80.9	87.3	0.006
10	131	0.53	0.22	0.46	13.5	6.25	115.6	61.5	0.0075
11	255	0.45	0.18	0.39	19.1	7.45	162.2	43.5	0.009
12	544	0.38	0.16	0.33	29.1	9.58	246.8	28.7	0.011
13	1221	0.31	0.13	0.27	43.3	11.7	368.6	19.3	0.014
14	2566	0.27	0.11	0.23	70.5	16.2	587.7	11.8	0.019
15	5740	0.23	0.09	0.20	112	22.4	953.9	7.42	0.027
16	13.9e3	0.19	0.08	0.17	185	30.6	1575	4.50	0.037
17	37.0e3	0.16	0.07	0.14	345	48.6	2975	2.4	0.059
18	92.2e3	0.14	0.06	0.12	694	81.2	5678	1.2	0.098
19	358e3	0.11	0.04	0.10	1546	153	13.6e3	0.54	0.183
20	1.12e6	0.10	0.04	0.08	4318	358	35.1e3	0.19	0.437
21	3.95e6	0.08	0.03	0.07	9274	649	79.4e3	0.09	0.778
22	11.0e6	0.07	0.03	0.06	20487	1208	169e3	0.04	1.475
23	29.6e6	0.06	0.02	0.05	41075	2054	335e3	0.02	2.5

The ratios of the parameters of a granular bed filter to that of the human lung are listed in Table 3.6. As the total void volume of a bed layer is equal to the volume of the corresponding airway generation, the hydraulic diameter of the void space and the number of the beads cannot be equal to that of the airway channel. This means that the method of comparing the dimensions of the airspaces in both system by hydraulic diameter has its shortcomings. Because the total cross section in both system are equal and the number of beads is not equal to the number of airway channels, the average cross section per airspace is unequal in both systems. This also means that the average diameter of an airspace in a layer of the granular bed filter is not equal to the diameter of an airway channel in the corresponding generation.

3.5.2 Breathing patterns and fluid dynamics

3.5.2.1 Tidal volume and breathing patterns
Respiratory flow is cyclic: the airflow rate varies from zero to a maximum and back to zero during inhalation and exhalation, and reverses many times per minute. Tidal volume, breathing rate, and breathing period markedly influence deposition. The deeper the air goes, the longer it stays and the greater the extent to which the particles deposit. Increasing inspiratory air velocity enhances impaction deposition, but decreases sedimentation and diffusion by reducing residence time in an airway channel.

Table 3.6. *Dimensions and average inspiratory flow conditions compared in a human lung and in a granular bed with a tidal volume of 1450 cm³.*

z	$N_z/$	$D_z/$	$L_z/$	$S_z/$	$V_z/$	$A_{s,z}/$	$U_z/$	$t_{r,z}/$
(-)	N_g	d_h	H_{laye}	S_{layer}	V_{vtot}	$A_{s,layer}$	U_{layer}	$t_{r,layer}$
8	7.5	0.62	1	1	1	1.64	1	1
9	7.6	0.61	1	1	1	1.65	1	1
10	7.8	0.60	1	1	1	1.66	1	1
11	8.0	0.59	1	1	1	1.69	1	1
12	7.5	0.61	1	1	1	1.63	1	1
13	6.7	0.65	1	1	1	1.54	1	1
14	6.4	0.67	1	1	1	1.49	1	1
15	5.7	0.70	1	1	1	1.42	1	1
16	4.7	0.77	1	1	1	1.29	1	1
17	3.5	0.82	1	1	1	1.51	1	1
18	2.8	0.87	1	1	1	1.64	1	1
19	1.5	1.05	1	1	1	1.56	1	1
20	0.9	1.10	1	1	1	1.69	1	1
21	0.5	1.32	1	1	1	1.42	1	1
22	0.3	1.43	1	1	1	1.31	1	1
23	0.2	1.67	1	1	1	1.12	1	1

The Task Group (1966) adopted three tidal volumes, 750 cm³, 1450 cm³, and 2150 cm³ and a respiratory frequency of 15 cycles per minute as the volumetric basis of its model. The tidal volumes represent light, moderate, and heavy physical activities, respectively. The respiratory cycle with no pause following exhalation for an adult human is described as:

Inhalation:	1.74 seconds
Pause following inhalation:	0.20 seconds
Exhalation:	2.06 seconds
Total cycle:	4.00 seconds

In our study, the deposition of particles during a steady inspiratory flow of 1.74 seconds will be simulated. With a tidal volume of 1450 cm³, the inspiratory breathing rate will be 50 l/min.

3.5.2.2 Flow patterns and distribution of inhaled air in human lungs

There are two key features which must be understood in order to comprehend air flow in a lung: repeated branching of the bronchial tree from the trachea to the alveoli and an increase in total cross section with each airway generation. In order to explain the flow pattern in human lungs, Harris and Fraser (1976) made a number of simplifying assumptions concerning air flow patterns and distribution. In our study, these assumptions have been used for calculating flow conditions and particle deposition.

The lung airways are short tubes. The entry length L_e is the distance needed to establish the parabolic velocity profile for 95%. Airway flow combinations where $L_e/L_z > 5.5$ are considered to have a uniform velocity profile; those where $L_e/L_z < 5.5$ are considered to have parabolic contours. For a tidal volume of 1450 cm^3, the sixth generation is the first one for which $L_e/L_z < 5.5$. Olson et al. (1970) state that it is unlikely that laminar flow is achieved in this bifurcation system with its rough wall surface and short tube lengths. Laminar flow profiles are, however, generally assumed to be a good approximation in the lower air spaces.

Flow is assumed to be distributed to an airway according to the percentage of the total lung volume subtended by that airway. This assumption implies that the airways are uniformly ventilated. In reality, however, the airways are not uniformly ventilated. Bouhuys (1974) found that the lower lobes are better ventilated than the higher ones.

It is assumed that the distribution of aerosols in a cross-section at the beginning of each tube is uniform. At the end of each tube, the distribution of the aerosol particles is no longer uniform because of the loss of particles from the airflow. Moreover, after the bifurcation, the highest concentration of aerosol particles is found at the sides of the tubes of the bifurcation that converge into the carina. In the deeper parts of the lung, the highest concentration remains at one side of the tube (no turbulence). It is assumed that this effect does not affect the mean deposition in a region.

The inspiratory flow varies cyclically with time. However, few data are available for particle deposition under cyclic flow. Particle deposition may increase under cyclic flow conditions for two reasons. These are the enhanced impaction occurring at peak flow and the increased flow instability or turbulence which is likely to disturb the development of a boundary layer. Gurman et al. (1984) measured particle deposition for constant and cyclic flow in a cast of the upper regions of the lung. They observed increased deposition for cyclic over constant flow and a greater increase in deposition efficiency for 3 μm compared to 8 μm particles. This is because the larger particles have sufficient inertia to reach the wall without assistance from turbulent eddies. It is to be expected that deposition by laminar sedimentation and diffusion does not differ very much for steady or cyclical flow because both mechanisms are proportional to the residence time. The effect of cyclical flow will therefore be less pronounced in the lower regions of the lung.

The impaction and interception can be calculated by means of the ideal flow model of a circular bend, which permits precise analytical study of the flow patterns but neglects the geometry of the bifurcating tube. The model of the circular bend lacks many essential features of geometry and fluid dynamics in airways. One may therefore underestimate the deposition efficiency. Flow characteristics in asymmetric bifurcation tubes in the upper lung are highly complex, showing vortex flows near bifurcations and other secondary flows which enhance the particle deposition.

The effect of the larynx is neglected. Particles passing through the larynx are directed towards and impacted against the tracheal wall by the laryngeal jet. This is a high velocity jet of air directed at the back wall of the trachea and is caused by laryngeal constriction. A larynx surrogate is omitted in most of the physical and mathematical models. The developed

49

laryngeal jet and downstream turbulence exerts its influence on the trajectories distant from the larynx. Martonen and Patel (1981) and Lippmann and Altschuler (1976) showed that tracheal deposition may be grossly underestimated unless the influence of the larynx is considered. Particle losses in deeper parts (main bronchi to segmental bronchi), however, are greater when the larynx is omitted from the experimental system.

Most of the assumptions made by Harris and Fraser (1976) do not cause considerable error in calculated deposition in the lower regions. These assumption do, however, cause errors in total deposition calculations in the upper parts of the lung. These errors mean that the concentration and distribution of particles assumed at the entrance of the lower regions are not correct. This error influences the calculation of the total deposition in the lower parts of the lung.

Since air in laminar flow in an airway has a parabolic velocity distribution, the air nearest to the wall has a velocity approaching zero. For this reason, some air which occupies the airway in the process of inhalation will remain in the airway when inhalation is completed. In early generations this quantity may be very small; in late generations it may be a significant fraction of the airway volume.

3.5.2.3 Flow patterns and distribution of the air in a granular bed filter

Air follows a tortuous path in a granular bed filter, as it does through the branching airways in the lung. The geometric structure of a granular bed filter is immensely complicated. In recent years, numerous publications on the flow of fluids through porous media have emphasized the need for geometric models to describe and analyze transport processes in the pores of the media. Characterization of this complex structure with a simple geometric model is essential for the calculation of the flow within the bed.

Generally speaking, There are two models to describe the flow field in the granular bed filter; these were briefly discussed in Chapter 3.2 (see Figure 3.2). Rajagopalan and Tien (1976) showed that the external sphere-in-cell model is highly effective in predicting the collection efficiency and that their predictions parallel those of the constricted tube model proposed by Payatakes et al. (1973). Furthermore, they suggested that this model should be used in combination with the constricted tube model which has been proved to be quite useful in predicting pressure drops. The constricted tube model better reflects the consequences brought about by particle deposition (for instance, change in pressure drop) because of its geometric similarity with the pore structure of the bed. Other authors (Pendse and Tien, 1982) claim that calculations based on the sphere-in-cell model differ substantially from experiments.

The models of flow distribution in the granular bed filter assume that the distribution of flow over the granular bed filter is homogeneous and the aerosol concentration is homogeneously distributed in each plane perpendicular to the flow direction, behind each layer of collectors. Uniform distribution of aerosol throughout the gas entering the cell is, however, questionable. This is so because the motion of particles, particularly in the inertial regime, depends on particle history in preceding cells; consequently deviations may arise from the single sphere efficiencies as the particles proceed along the bed height.
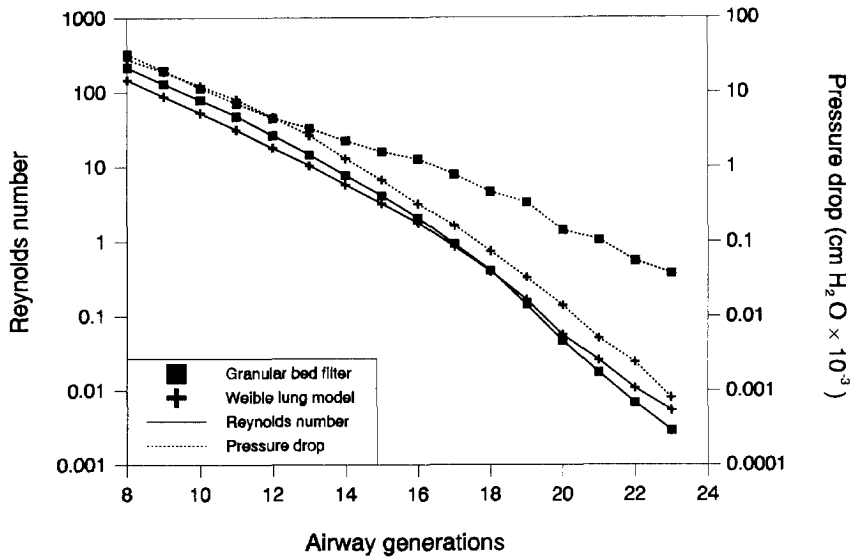
Figure 3.12. *Comparison of the Reynolds number and the pressure drop in the two systems.*

Flow patterns in the human lung and in the granular bed are very complex and certainly not comparable. For both systems, different methods exist to calculate the flow patterns, and no method has as yet been proven to be valid. For this reason, only a superficial comparison can be done. In Figure 3.12 the above-mentioned assumptions were used to compare the Reynolds numbers and the pressure drops in both systems for the different generations. It is seen from Figure 3.12 that the Reynolds numbers are almost equal in the two systems, but pressure drops are different, especially in the deeper parts of the lung.

3.5.3 Deposition comparison

Inhaled particles deposit in the various regions of the respiratory system by the complex action of the same deposition mechanisms as in the granular bed filter. Particle deposition during respiration occurs in three processes: inspiration, expiration, and pause. The relative contributions from these three processes to the total deposition are presented in Figure 3.13 by Gerrity et al., 1979). They assumed that the effective diameter of alveolar duct and alveolar sacs are well approximated by the diameter of the alveolar duct. This figure shows that particle deposition during inspiration is the most significant contribution to total deposition, with the relative importance of inspiration increasing with particle size.

A deposition model or a mathematical deposition model for aerosol particles in the human respiratory tract is mostly composed of a lung structure model, a set of deposition equations for a particle in an airway, and a mathematical computation method for regional and total

51
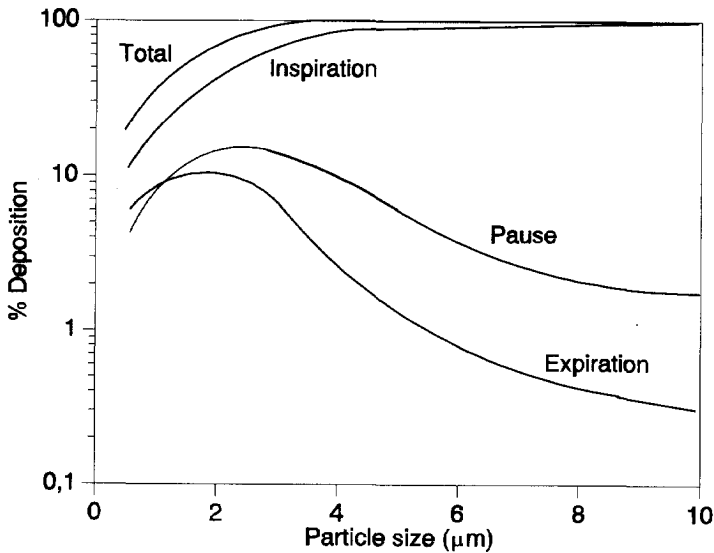
Figure 3.13. *Relative contribution to total deposition from inspiration, breath pause and expiration as a function of particle size (Gerrity et al., 1979).*

deposition. In our study, Weibel's lung structure model was used in two sets of deposition equations, the Landahl (1950) and the Taulbee et al. (1978) models. The first one was developed by Findeisen (1935) and modified by Landahl. This model is the basis of the model used by Task Group on Lung Dynamics (1966) of the ICRP. These equations approximate the deposition by sedimentation and diffusion in an airway. The impaction equation is based on the experimental data of Landahl and Herrmann (1949). The second set uses equations for sedimentation (Thomas, 1958; Pich, 1972) and diffusion (Gormley and Kennedy, 1949) from a parabolic laminar airflow in a tube. The impaction equation is based on experimental data of Johnston et al. (1977) and Schlesinger and Lippmann (1972). In the Landahl and Taulbee et al. models, interception is not included because it is considered to be less important than the first three mechanisms (Hinds, 1982; Ferron et al., 1985). Taulbee et al. included impaction only during inhalation. The deposition of both models in the alveoli is determined by assuming that no air mixing occurs and that all inhaled air is completely exhaled by the following exhalation. This implies that an aerosol particle that does not deposit during respiration is exhaled. These two models (Landahl and Taulbee et al.) were compared with the *granular lung model* described in the previous sections for spherical particle deposition in several generations under the same conditions, as shown in Figure 3.14.

From Figure 3.14 it can be seen that deposition in the granular lung model is greater than the deposition predicted by the above-mentioned two models in the last two generations. This occurs because the granular lung model includes alveoli in the simulation, while the other two models do not. The contribution by diffusion and sedimentation in the granular lung model
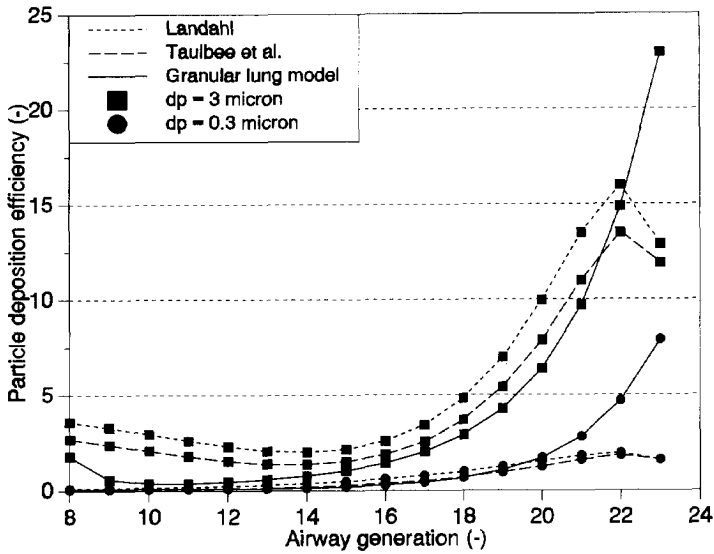
Figure 3.14. *Regional particle deposition predicted by the three models under a tidal volume of 1450 cm³.*

is thus higher in this region than that of other models. However, because we use the granular bed to simulate the human lungs only after the 8th generation, this comparison is not applicable for the region prior to that generation.

Several experimental studies of regional particle deposition in real lungs also exist. The studies of Heyder (1986) and Rudolf et al. (1986) were conducted for mouth-breathing and nose-breathing of monodisperse aerosols of spherical particles with diameters between 0.03 and 15 μm. The experiments were designed to study the dependence of deposition on breathing characteristics and on the properties of the aerosol particles. Based on these experimental data and other theoretical studies in the literature, the ICRP Task Group (1994) developed a particle deposition model which can calculate the particle deposition in various regions of the lung. Figure 3.15 shows the experimental data of particle deposition in the alveolar region (generations 17 to 23) for mouth breathing with a tidal volume of 1000 cm³ compared with the values predicted from the granular lung model and the ICRP model for spheres with a unit density.

From Figures 3.14 and 3.15 it can clearly be seen that the prediction of particle deposition by the granular lung model is in good agreement with both models and experimental data for particle deposition in the lower parts of the lung. This result is very important as it makes credible the use a granular bed filter to represent the lower parts of the human lung.

53
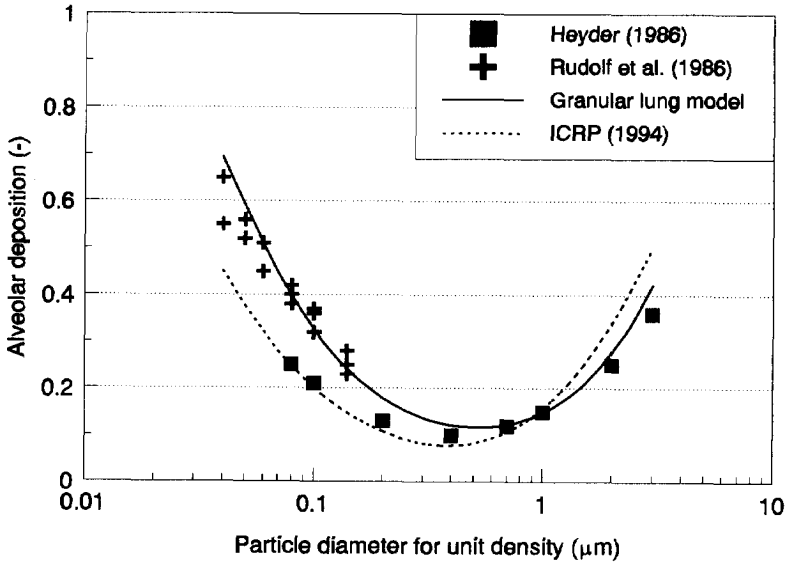
Figure 3.15. *Experimental values for particle deposition found by Heyder (1986) and Rudolf et al. (1986) compared with calculated values based on the new semi-empirical model and ICRP model (1994).*

3.6 Conclusions

This chapter discusses the particle deposition in granular bed filters and compares the granular bed filter with the human respiratory system. Experimental work was done to develop a mathematical particle deposition model. The experimental results showed that this model gives a better fit with the experimental data than the models of Boulaud and Otani et al. In the new model, the equations of the single sphere collection efficiencies for various mechanisms have been obtained by using the expressions in the models of Boulaud and Otani et al.

Since we focus on the particle deposition in the lower parts of the human lung, the alveoli in the alveolar region of the lung have been included in calculating the dimensions of the granular bed filter as a representative model of the human lungs. For the dimensional comparison of the granular bed filter and the human respiratory system, as shown in Tables 3.4 and 3.5, the void volume and total cross section of the bed per layer are equal to that of the corresponding airway generation. This results in the same average velocities of the two systems in every generation, and the layer height of the bed is also equal to the length of the corresponding airway generation. The residence times of the two systems are therefore equal. The hydraulic diameter and the number of beads of the bed per layer, however, cannot be met with the diameter and the number of the lung tubes in each airway generation. This difference affects the pressure drop and Reynolds number in both systems. The surface area, an

important parameter for particle deposition by diffusion, also differs in both systems. This difference influences the diffusion deposition. Fortunately, in the last two generations, which are full of alveoli, the difference in surface area between the two systems is not large.

The flow pattern in a human lung is very complex and cannot be compared with that in a granular bed filter. In the human respiratory system, especially in the lower parts, the flow pattern is influenced by alveoli; moreover, every person has his or her own flow pattern and the differences between individuals are significant. No measurement method for flow patterns has yet been proved to be valid. For this reason, it is difficult to draw definite conclusions about the differences in flow patterns between both systems. Therefore only a superficial comparison of the two systems can presently be carried out.

We can conclude that a granular bed filter is comparable with other models used to describe particle deposition in the lower parts of respiratory system and is also in good agreement with the experimental data of Heyder (1986) and Rudolf et al (1986) in real lungs.

Appendix 3A Experimental data

Table 3A.1 shows the experimental results for particles dispersed by the DeVilbiss 45 nebulizer and the Mollinger nebulizer. The particle size is from 0.094 to 0.82 μm. Table 3A.2 shows the experimental results for particles dispersed by the STAG with the size range of 0.62 to 2.94 μm.

Table 3A.1. *The results for the particles dispersed by nebulizers.*

Q (lpm)	50	50	50	30	30	30	23	23	23
L (cm)	7	7	7	7	7	7	7	7	7
d_g (mm)	1.04	1.28	2.0	1.04	1.28	2.0	1.04	1.28	2.0
d_p (μm)	Overall penetrations, P_T (%)								
0.094	78.1	81.8	89.7	68.3	72.8	87.1	70.5	60.8	87.4
0.101	78.6	81.8	90.4	69.0	73.4	87.0	72.2	61.5	87.5
0.108	78.6	81.8	90.5	69.3	74.1	87.5	72.4	62.0	87.1
0.115	79.4	82.3	91.5	70.1	74.5	87.5	72.4	62.4	87.1
0.122	80.2	83.0	92.0	70.4	74.6	87.8	73.1	63.6	86.7
0.129	80.3	83.1	91.7	71.1	75.5	88.5	73.3	64.8	86.6
0.136	81.0	83.3	91.8	72.0	75.6	88.7	73.3	65.5	86.2
0.143	80.8	84.2	91.8	71.6	76.4	89.1	73.1	66.3	85.7
0.150	80.9	84.3	92.5	72.8	76.4	89.2	73.5	67.0	84.9
0.157	81.2	85.6	92.1	73.1	76.7	90.2	73.7	67.6	84.8
0.164	81.4	85.2	92.5	73.6	76.9	90.1	73.5	69.2	84.4
0.171	81.3	86.5	92.4	74.2	78.1	90.7	73.9	69.8	84.4
0.178	82.0	85.5	92.1	74.0	77.7	91.2	74.1	70.6	83.4
0.185	81.4	86.3	92.5	74.5	78.7	91.8	73.9	71.2	83.1
0.192	81.1	86.8	92.7	75.0	78.6	92.3	73.5	72.2	82.4
0.155	81.0	85.3	93.8	72.5	77.0	89.7	71.0	67.8	82.8
0.165	82.1	85.3	93.8	73.2	77.5	90.5	72.6	68.5	82.3
0.175	82.0	85.3	93.6	74.3	77.9	90.9	73.1	69.5	81.9
0.185	82.1	86.8	93.6	75.0	78.4	91.7	72.9	70.6	81.5
0.195	81.3	86.3	93.6	75.7	79.4	92.2	73.2	72.7	80.5
0.205	80.6	86.5	93.2	76.4	79.6	93.3	72.8	74.3	79.5
0.215	79.5	86.6	91.6	76.8	80.4	94.1	72.5	75.5	79.5
0.225	79.0	87.1	91.2	78.0	80.3	94.6	71.6	77.4	78.5
0.235	78.5	86.6	92.1	78.0	81.4	95.8	70.4	79.8	77.7
0.245	77.4	87.5	91.7	79.2	81.7	96.7	69.5	81.3	76.8
0.255	76.2	88.1	90.5	78.7	82.2	96.6	68.5	82.2	75.9
0.265	76.5	86.9	89.8	80.0	81.4	97.4	68.6	83.1	75.9
0.275	76.0	87.6	88.9	81.1	81.9	97.8	69.2	83.3	75.3
0.285	74.0	88.7	88.8	80.1	81.4	98.0	69.3	86.0	74.8
0.295	77.0	86.6	88.5	80.2	82.1	98.9	68.0	86.3	74.8

Table 3A.1. *continued.*

Q (lpm)	50	50	50	30	30	30	23	23	23
L (cm)	17	17	17	17	17	17	17	17	17
d_g (mm)	1.04	1.28	2.0	1.04	1.28	2.0	1.04	1.28	2.0
d_p (μm)	Overall penetrations, P_T (%)								
0.094	56.2	67.8	79.9	51.3	62.4	72.3	47.0	62.4	68.1
0.101	56.4	68.5	80.3	51.8	63.4	73.1	47.5	62.0	68.7
0.108	57.2	68.8	81.2	52.7	64.3	73.6	48.8	62.7	69.5
0.115	58.1	69.5	81.7	53.6	65.1	74.3	49.9	63.3	70.1
0.122	59.1	70.8	82.0	54.6	66.4	75.2	51.0	64.1	71.3
0.129	60.2	71.3	82.0	55.7	67.2	75.4	52.0	65.4	71.9
0.136	61.3	72.3	83.1	56.5	68.3	76.8	53.6	66.1	72.5
0.143	62.2	72.6	82.6	57.5	69.3	76.5	54.6	67.6	73.5
0.150	63.4	73.1	82.8	58.4	70.2	77.7	55.8	67.8	74.0
0.157	63.9	73.6	83.6	58.9	70.9	78.3	56.8	68.3	74.5
0.164	65.1	74.3	83.2	59.3	71.7	78.9	57.4	69.5	76.0
0.171	65.4	74.2	83.3	60.3	72.1	78.7	58.7	70.3	76.3
0.178	66.3	73.9	83.9	60.3	72.9	79.6	59.3	71.2	76.6
0.185	67.5	74.1	84.6	61.4	73.4	80.0	60.2	71.7	77.6
0.192	67.6	74.4	84.4	62.0	74.2	81.1	60.9	72.4	78.9
0.155	64.7	72.9	81.9	57.7	69.8	77.6	55.4	67.7	74.4
0.165	64.7	73.7	82.7	58.9	70.8	78.3	56.7	68.8	75.2
0.175	65.9	74.6	83.6	60.1	71.4	78.8	58.3	69.4	76.2
0.185	67.1	74.6	83.2	61.0	72.8	79.3	60.1	70.3	77.5
0.195	68.1	75.4	83.5	61.6	73.9	81.0	61.0	71.5	78.4
0.205	69.3	75.1	83.4	62.8	74.4	81.4	62.3	72.6	79.0
0.215	70.2	75.5	82.8	63.2	75.4	82.2	63.3	73.8	80.0
0.225	71.8	74.8	82.6	64.0	76.3	82.9	64.1	74.5	81.1
0.235	72.7	74.8	83.1	64.3	77.1	83.9	65.6	75.8	81.5
0.245	73.0	74.8	83.1	64.6	76.8	84.8	66.0	76.0	82.6
0.255	74.5	75.6	83.3	65.2	78.8	84.9	66.7	76.6	83.9
0.265	74.9	75.2	82.1	65.2	78.8	85.0	67.7	77.2	83.8
0.275	75.9	75.8	82.0	65.5	78.3	86.4	68.2	77.7	84.2
0.285	76.0	74.9	82.6	65.7	80.2	87.2	69.0	78.3	85.1
0.295	76.5	75.2	81.9	66.4	80.8	86.9	68.9	78.9	86.4

Table 3A.1. *continued.*

Q (lpm)	50	50	50	30	30	30	23	23	23
L (cm)	7	7	7	7	7	7	7	7	7
d_g (mm)	1.04	1.28	2.0	1.04	1.28	2.0	1.04	1.28	2.0
d_p (μm)	Overall penetrations, P_T (%)								
0.26	92.8	91.3	92.3	88.4	89.0	92.9	83.7	79.5	92.3
0.30	93.6	91.4	92.5	88.2	89.1	90.9	83.6	79.2	91.8
0.34	92.2	91.3	95.2	90.0	89.2	92.2	83.1	81.2	90.9
0.38	91.8	91.8	90.0	92.3	87.5	93.2	82.7	80.7	92.2
0.42	91.5	90.1	90.0	90.9	87.9	95.2	83.9	84.1	90.9
0.46	91.8	89.9	96.4	92.4	88.1	96.2	84.5	88.2	92.8
0.50	91.5	91.9	93.0	93.3	88.8	95.4	82.7	91.0	90.4
0.54	91.7	89.6	97.0	91.9	88.0	95.7	81.5	93.7	91.3
0.58	89.9	92.7	96.9	89.3	88.7	96.0	82.5	94.0	93.9
0.62	90.9	88.9	94.3	87.1	89.8	95.9	80.3	91.4	86.8
0.66	91.3	90.0	95.2	87.6	88.6	94.0	80.3	87.0	85.7
0.70	88.8	89.0	96.0	87.7	87.6	91.1	80.2	89.9	88.0
0.74	86.0	87.3	93.6	86.4	84.8	91.8	78.6	88.2	85.8
0.78	86.7	85.1	93.5	85.0	86.8	91.5	78.6	89.5	86.0
0.82	85.2	86.6	92.3	84.9	86.1	92.5	77.6	87.1	84.4
Q (lpm)	50	50	50	30	30	30	23	23	23
L (cm)	17	17	17	17	17	17	17	17	17
d_g (mm)	1.04	1.28	2.0	1.04	1.28	2.0	1.04	1.28	2.0
d_p (μm)	Overall penetrations P_T (%)								
0.26	81.0	84.6	88.4	70.7	81.1	86.4	70.3	75.7	84.6
0.30	82.4	85.6	87.5	71.4	82.2	88.7	70.5	75.4	84.4
0.34	81.3	84.3	88.4	73.1	80.9	88.5	69.6	75.8	87.0
0.38	82.4	84.2	89.7	74.7	80.9	87.9	70.0	76.3	86.7
0.42	81.3	82.9	93.4	77.6	79.7	89.5	67.9	76.0	84.5
0.46	77.8	84.0	89.9	78.1	77.9	94.3	67.7	76.5	80.3
0.50	76.5	83.5	91.1	78.4	79.6	94.8	67.2	76.3	79.1
0.54	74.0	83.8	87.4	75.4	76.3	94.4	68.1	77.7	79.3
0.58	71.9	84.7	86.1	72.6	79.4	93.0	69.1	77.1	77.9
0.62	71.3	86.7	85.3	73.5	77.0	93.5	69.3	73.5	77.0
0.66	73.1	84.9	83.7	72.4	75.4	92.0	70.2	71.2	75.0
0.70	73.6	84.6	84.3	70.4	75.4	91.4	69.7	74.5	73.5
0.74	70.2	83.8	84.2	68.9	74.5	91.1	67.0	75.1	72.2
0.78	64.0	82.6	83.8	65.3	76.3	90.5	67.5	72.6	70.4
0.82	64.4	83.5	83.6	68.4	74.7	90.3	64.7	70.6	72.3

Table 3A.2. *The experimental results for aerosols dispersed by STAG with a NaCl concentration of 0.45 vol.%.*

Q,lpm	50	30	23	50	30	23	50	30	23	50	23
L,cm	17	17	17	12	12	12	7	7	7	17	17
d_g, mm	1.04	1.04	1.04	1.04	1.04	1.04	1.04	1.04	1.04	2.0	2.0
d_p, μm	Overall penetrations, P_T (%)										
0.68	69.0	62.9	56.8	77.9	70.8	67.2	85.8	83.4	76.8	86.4	83.6
0.84	67.4	60.2	54.8	75.1	66.5	66.1	83.0	79.8	75.9	83.1	79.5
1.00	62.2	53.4	48.0	71.9	68.1	61.4	82.6	74.7	76.1	78.7	76.3
1.16	59.3	49.3	43.9	68.4	64.9	56.9	82.3	74.1	73.0	77.4	72.8
1.32	61.0	49.2	42.7	68.1	62.5	55.5	78.1	74.9	70.2	78.6	64.0
1.48	57.8	47.5	44.1	64.4	55.6	50.0	79.1	66.5	70.4	75.4	63.0
1.64	53.4	44.7	40.6	63.5	57.3	50.9	77.2	71.6	70.3	68.5	59.5
1.80	50.9	47.4	39.8	60.5	56.8	51.5	77.3	70.8	70.7	71.2	57.1
1.96	49.8	43.2	36.0	59.1	52.9	48.0	71.7	68.4	65.1	64.0	51.3
2.12	42.4	38.6	33.7	57.5	49.9	45.9	68.2	69.4	61.6	62.9	45.9
2.28	39.4	39.4	32.6	47.7	49.3	45.8	65.1	66.8	59.4	58.1	44.7
2.44	34.0	38.4	30.0	47.7	47.3	44.5	60.9	62.6	57.0	56.0	43.2
2.60	30.2	34.8	29.5	39.9	48.6	42.1	58.1	60.2	56.1	47.4	34.7
2.76	30.2	32.0	27.3	37.6	42.8	39.5	51.2	58.4	55.6	39.1	28.5
2.92	24.8	31.1	27.2	34.4	40.4	36.9	43.6	55.7	48.5	30.7	26.4

4

Production, dispersion and measurement of fibrous particles

4.1 Introduction

Fibrous particles have several important properties which make them very different from spherical particles. They are represented as either cylinders or prolate spheroids in the literature. Natural fibers, like asbestos, can have a very irregular shape. The shape of fibers may influence not only the interception mechanism of deposition, which has only small influence on spherical particles, but also the deposition mechanisms of sedimentation, diffusion and impaction. When a fiber moves through the airways, its shape influences the orientation in the stream which can effect the deposition. This will be discussed in the next chapter. Other factors which influence the aerodynamic behaviour, for example, density, electric conductivity and the straightness of the fibers, are important as well. This project focuses the fiber deposition in human lungs, the inhaled fibers which have micron and submicron size are considered. Experiments should be done to investigate the fiber deposition and transportation behaviour in human lungs or in granular bed filters. Thus, the production, dispersion, and measurement of fibrous particles are very important parts of the experiment.

This chapter discusses the production of four kinds of test fibers. Three of them have a uniform size and another is poly-dispersed. The size range is from 0.1 to 20 μm for length and from 0.01 to 1 μm for diameter. Because of unsuitable dispersion for one kind of fibers and insufficiently high concentration for another one, only two kinds of these fibers were used for the experiments for the fiber deposition in granular bed filters because of their suitable concentration and dispersion. Subsequently, the dispersion and measurement methods for these different kinds of fibers are also discussed in this chapter.

4.2 Production of fibrous particles

In order to investigate the fiber deposition behaviour, various sizes of test fibers which cover the diffusional and impactional region are needed in the experiments. Thus, a suitable fiber measurement equipment which can measure fiber size distributions (length and diameter) and concentrations is required. Unfortunately, we have not found this kind of instrument yet. Therefore, we have to use particle sizers or counters which are normally used for spherical particle to measure the fiber concentration. For this reason, different types of monodisperse

61

fibers both in length and diameter are required in our experimental work. This section describes the different kinds of test fibrous particles in our experiments.

4.2.1 Polyamide-6 fibers

The production of monodisperse polyamide-6 fibers is consisted of three processes. The first process is to produce the polyamide-6 fibrils with an average diameter of 1 micron. It was done in help of the Akzo Research Laboratories in Arnhem (ARLA) (van Pinxteren, 1989). The second one is to cut the polyamide-6 fibrils to a specified size with a sharply defined length in the range of 5 to 20 micron. This was done with the use of a microtome of the Interfaculty Reactor Institute (IRI) at Delft (Plaisier, 1991). By cutting bundles of filaments with a sharp microtome knife, thousands of fibrils with a sharply defined length were obtained. The ice-matrix is then removed by melting and the polymer-matrix by dissolving in a suitable solvent. By diluting with water, a suspension of fibers is obtained.

Figure 4.1 illustrates the production process. The production takes place by mixing two polymers in a well defined way with a number of multiflux mixers (mumi), from which a
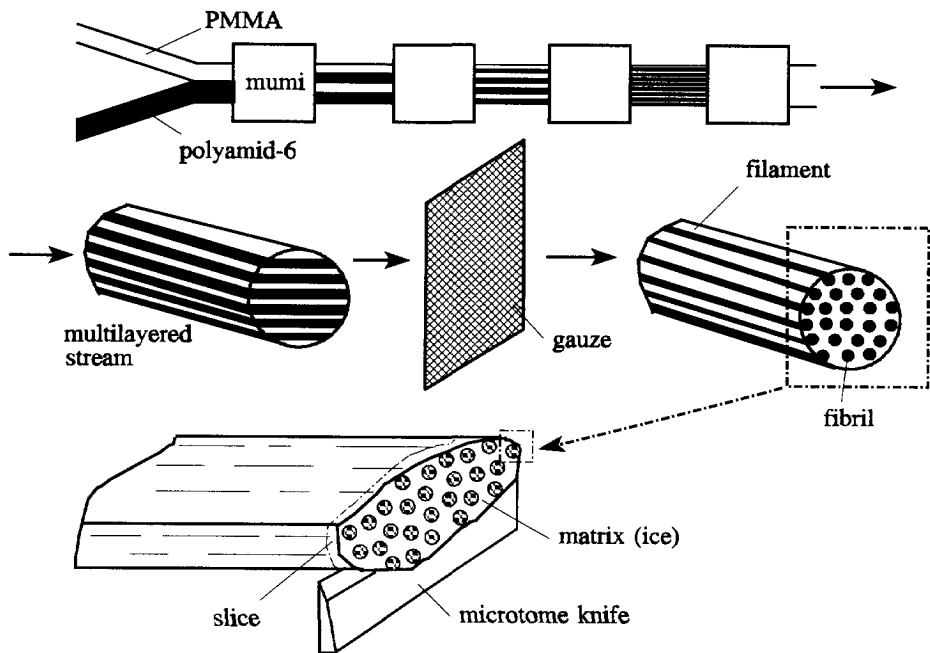

**Figure 4.1**. *Production of well defined polyamide-6 fibers.*

multilayered stream of two polymers is obtained. In our case, these two polymers are polymethyl methacrylate (PMMA) and polyamide-6. The polymer stream is then forced through a fine metallic grid, which causes the layers to split up into fibrils. The PMMA forms a matrix around the polyamide. Like the normal melt spinning process, this polymer stream is forced through a small orifice. After stretching and cooling down, it is wound on a spool. Consequently yarn with polyamide fibrils is obtained. This yarn can be stretched and frozen in a matrix of ice and be cut with a microtome knife to obtain the certain size of fibers.

In principle, one can get monodisperse fibers by cutting the matrixes. In practice, however, it is very difficult to get uniform length with the microtome knife. Thus, the third process, a further separation, should be used to classify the fibers in length. The separation is quite easy since the diameters are uniform. There are several methods to separate the fibers to the same size. This separation could be done by using a centrifuge or a mass spectrometer. Stoelinga (1992) successfully separated some samples at the laboratory of Professor Prodi with the large spectrometer which was developed by Prodi (1982). The length of the fiber is various from 5 to 50 µm and the diameter is approximately 1 µm. Figure 4.2 shows one of the SEM photograph of the separated fibers.

4.2.2 Hydroxyapatite needles

Hydroxyapatite (HA) particles, $Ca_{10}(PO_4)_6(OH)_2$, were developed by the Bio-materials Research Group, Leiden University. It is intended to be used for bone substitute materials because of its close similarity to bone mineral. (Yubao et al., 1994a,b).
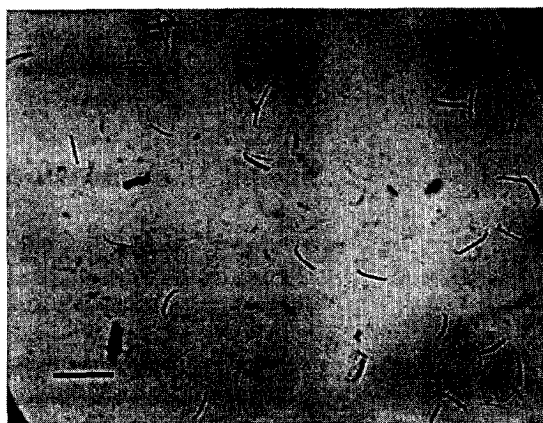
Figure 4.2. *SEM photograph of the polyamide-6 fibers.*

Hydrothermally synthesized nano-apatite (Nap) is a kind of carbonated apatite which has a needle-like shape (Yubao, et al., 1994a,b). It has much more similarity to bone mineral in composition, crystal structure, crystallinity, crystal size, therefore a better osteo-conductivity would be expected.

Particles were prepared by hydrothermal treatment of fully washed as-prepared calcium phosphate precipitates at 140 °C under 0.3 MPa for two hours (Yubao, et al., 1994a,b). The precipitates were synthesized by dropping slowly an $(NH_4)_2HPO_4$ aqueous solution into a stirred $Ca(NO_3)_2$ aqueous solution. The pH value for both solutions was adjusted to 11 with ammonium solution and the reaction was set at room temperature. After hydrothermal treatment, the Nap was kept in aqueous solution for future use. The Ca/P molar ratio of Nap was measured with an atomic absorption spectrometer for calcium and an ultraviolet spectrophotometer for phosphorus.
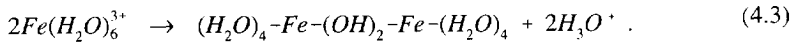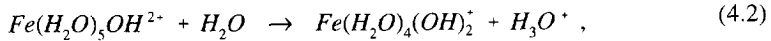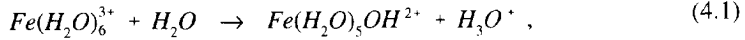
Nap can be used as filler to reinforce polymer. In order to improve the interface of Nap with polymer, polyacrylic acid (PAA) was used as coating (Liu, et al., 1996): 80 gram hydrothermally synthesized Nap was transferred to 1800 ml 2 mM polyacrylic acid sodium salt solution (pH was adjusted to 6 by using 1 M HCl) and stirred for 24 hours. Then the pH of the suspension was brought down to 5 and the sample was washed with ethanol to remove unabsorbed PAA. Finally the Nap was thoroughly washed by acetone. The non-coated Nap underwent the same procedure but omitting PAA from the solution. Figure 4.3 shows the TEM photograph of the PAA coated nano-needles with a length of about 200 nm and a diameter of 20 nm.


Figure 4.3. *TEM photograph of the nano-apatite needles.*

4.2.3 Akaganeite fibers

Akaganeite (β-$FeOOH$) is known as a fibrous crystal. Since the exact mechanism of crystal formation of akaganeite is not known, The first step consists of hydrolysis hydrated ferric ions. Several suggestions have been given by Marijnissen at al. (1991), such as:

$$Fe(H_2O)_6^{3+} + H_2O \rightarrow Fe(H_2O)_5OH^{2+} + H_3O^+ , \qquad (4.1)$$

$$Fe(H_2O)_5OH^{2+} + H_2O \rightarrow Fe(H_2O)_4(OH)_2^+ + H_3O^+ , \qquad (4.2)$$

$$2Fe(H_2O)_6^{3+} \rightarrow (H_2O)_4-Fe-(OH)_2-Fe-(H_2O)_4 + 2H_3O^+ . \qquad (4.3)$$

On continued hydrolysis higher molecular weight species are formed by stepwise condensation polymerisation of the primary hydrolysis products:

$$(3q+2r)H_2O + pFeOH^{2+} \rightleftharpoons [Fe_pO_q(OH)_{p+r}]^{(2p-2q-r)+} + (2q+r)H_3O^+ . \qquad (4.4)$$
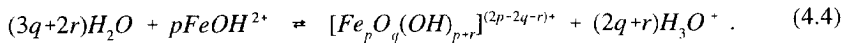
Finally, recrystallization takes place.

In the experiments of producing the fibers described by Marijnissen et al., the reaction parameters, such as pH and ferric ion concentration, were varied in the initial solution. In batch, solutions of analytical grade ferric chloride were prepared and maintained in a thermostated oven. The composition was varied from 0.01 to 1.0 M for $FeCl_3$ and from 0 to 1.0 M for HCl. The reactions took place in Teflon bottles at room temperature, 65 °C, and 100 °C. They carried out a special series to determine the role of silicon as a contaminant in the solution. The reaction time varied from 6 hours to a week. The composition, shape and crystal structure of the crystals were analyzed by corresponding measurements. In our experiments, the fibers was produced, with a length of 600 nm and a diameter of 80 nm. Figure 4.4 shows the SEM photograph of the akaganeite fiber we used in our experiments.

4.2.4 Production of polydisperse glass fibers

Three kinds of glass fibers were used in our experiments as the test fibers for the range from 3 µm to 9 µm of length. They are rather uniform with the count mean diameter (CMD) of 0.92, 0.85, and 0.67 µm and the geometric standard deviations (GSD) are 1.34, 1.18, and 1.36. The samples were made from glass fiber filters, which were kindly supplied by Professor L. Gradon of Warsaw University of Technology. The filters were disintegrated by a ball mill at a speed of about 6,000 rpm for 5 minutes in order to get a wide distribution in length. The SEM photograph of the glass fibers is shown in Figure 4.5. Figure 4.6 shows the fiber diameter distributions counted under the SEM.
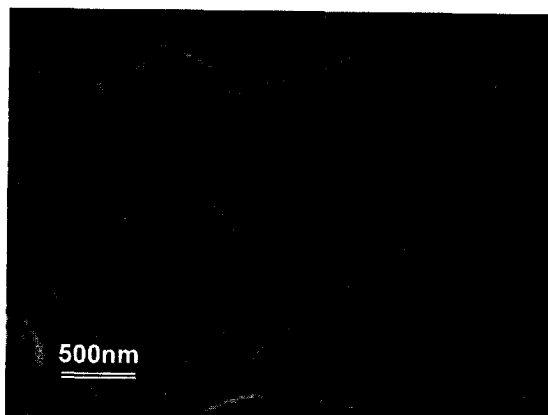
Figure 4.4. *The SEM photograph of the akaganeite fibers.*
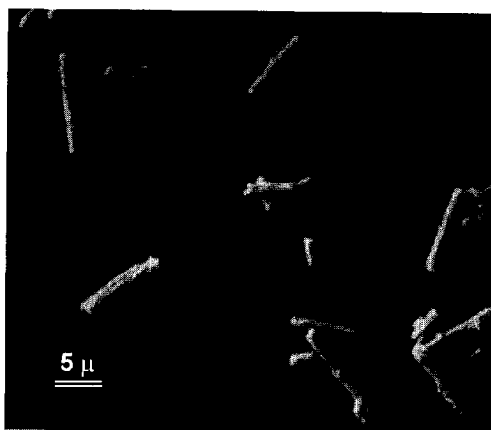
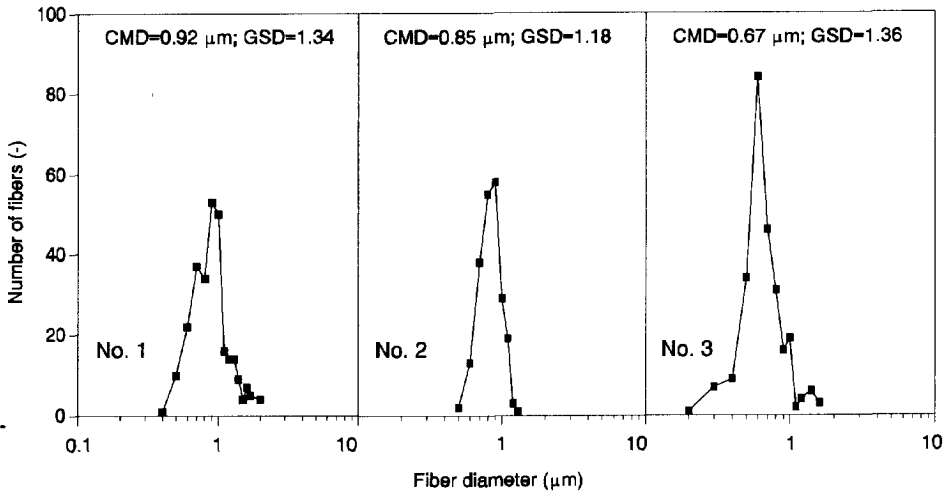**Figure 4.5**. *The SEM photograph of the glass fibers.*

**Figure 4.6.** *Diameter distributions of three test glass fibers.*

4.3 Dispersion of fibrous particles

To date, there is no satisfactory commercial apparatus available which disperses fibrous materials into a suspended state. Generally speaking, like spherical particles, fibers with the length smaller than 1 μm can be dispersed by atomization of a suspensor; a fluidized bed aerosol generator or a vibrating orifice aerosol generator will be used for fibers larger than 1 μm in length. This section will discuss these different types of aerosol generators and the fiber dispersion efficiency in air by these generators.

4.3.1 Fluidized bed aerosol generator

The most widely used method for generating large test aerosols is the pneumatic re-dispersion of a dry powder such as by a fluidized bed aerosol generator. This method which is called dry dispersion can supply a wide range of powdered materials and dust feed rates for various purposes. The basic requirements for these dry-dispersion dust generators are: continuously feeding a powder into the generator at a constant rate and dispersing the powder to form an aerosol. The dispersibility of a powder depends on powder material, particle size and size range, particle shape, and moisture content of the powder.

One of the aerosol generators used in our experiments for dispersing poly-dispersed glass fibers is called **WAG** (van der Wel aerosol generator) which was designed by van der Wel (1986) at the Particle Technology Group of Delft University of Technology as shown in Figure 4.7. A mixture of fibers and glass beads is added to a small glass storage hopper of the generator which can contain about 2.5 kg of material. Through the outlet, the mixture

67
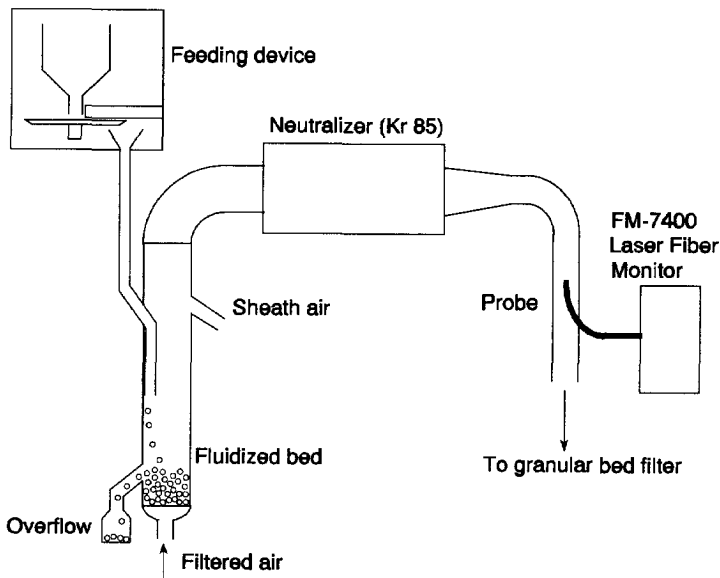
Figure 4.7. *Schematic drawing of the experimental set-up for testing WAG.*

flows on a slowly rotating disk from which it is scraped off by a knife located close to the surface of the disk. The amount of feeding beads is controlled by adjusting the disk speed and the distance between of the hopper outlet and the disk surface. When the mixture is scraped off the disk, it falls through a glass tube to the bottom of the fluidized bed (Zhou et al., 1995b). An overflow tube is located 15 mm above the bottom to balance the total quantity of the mixture in the fluidized bed.

Preparing a dry mixture of fibers with another material is not easy. The best material would be a metal because it would avoid the high charges on the particles. It is, however, hard to find mono-sized metal beads in the range of 300 μm. Also, oxidic film of metals can produce small particles which might cause a high background noise. After trying several sizes of glass beads and sands, it was found that glass beads between 250-320 μm were easy to handle at the conditions of the system. It is, however, not possible to mix the glass fibers with the beads in a dry state. The glass fibers are always agglomerated together in a dry state, which makes it difficult to get a homogeneously dispersed mixture. In our experiments, fibers were suspended in water by using a ultrasonic wave, and then the beads were added with stirring for two minutes. They are mixed in a wet state. Afterwards, the whole mixture was dried in an oven at about 100 °C. In this way, the fibers were dispersed successfully in the beads.

To keep the concentration of the fibers in the air stable, it is important to feed the mixture of beads and fibers to the fluidized bed constant. This can be done by the feeding device of the bed. For dispersing fibers in the air, the minimum fluidization velocity, U_{mf}, can be calculated by means of the Carman-Kozeny equation (Pell, 1990):

$$U_{mf} = \frac{d_g^2(\rho_b - \rho_g)\varepsilon_{mf}^3 \, g}{150(1 - \varepsilon_{mf})\mu} \, ,$$

(4.5)

where ε_{mf} is the bed porosity of minimum fluidization, d_g and ρ_b are the diameter and density of the bead. With the experimental parameters substituted in the formula, a minimum fluidization flow of 3.8 l/min is obtained. Any fluidization flow above 3.8 l/min is applicable as long as the glass beads are not blown through the system. In our experiments, the fluidization flow is 12 l/min which is much larger than the minimum one.

4.3.2 Other methods

A fluidized bed aerosol generator is called a "dry way" generator, because it can directly disperse particles in a dry state. There are also many other ways for dispersing particles in aerosol technology. Many of them, such as nebulizers and spinning top aerosol generators etc. which were discussed in Chapter 3, are "wet way" generators. They can generate various size of particles, but they have the same principle. They all first produce droplets in the system, then the liquid in the droplet should be evaporated by using a heating system, a diffusion dryer or an other kind of dryer. In our experiments, nebulizers were used to disperse fibers less than 1 μm in length. The spinning top aerosol generator was also used a few times trying to disperse the polyamide-6 fibers (Zhou et al., 1994). Figure 4.8 shows the experimental set-up for dispersing and measuring small fibers using "wet way" generators.
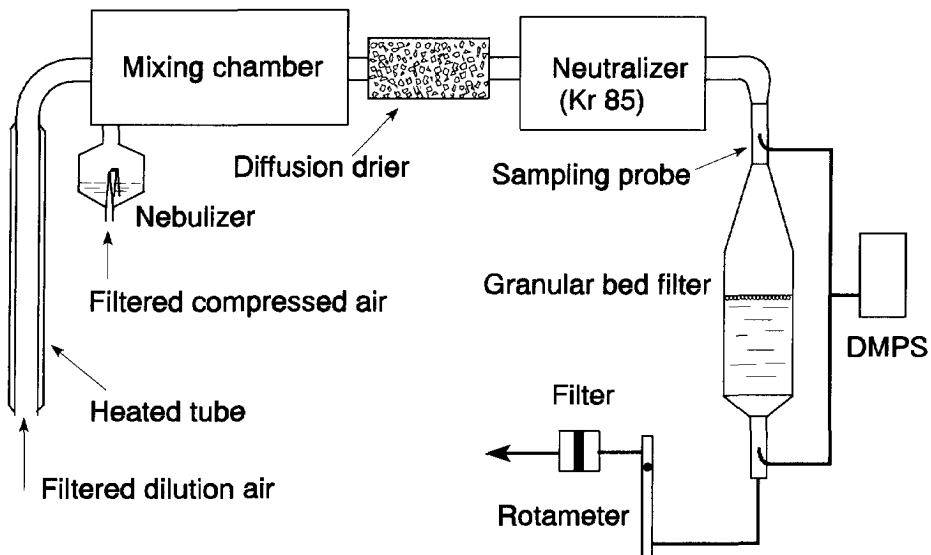

Figure 4.8. *Experimental set-up for dispersion and measurement of small fibers.*

4.4 Measurement of fibrous particles

The fiber concentration can be determined by the number of fibrous particles counted under a microscope. This method, however, has the disadvantage that it requires an appreciable amount of time to obtain results. It is not suitable for real-time monitoring of fibers. This section discusses the measurement of fiber concentration and size distribution for the test fibers discussed in section 4.2.

4.4.1 FM-7400 laser fiber monitor

The FM-7400 Laser Fiber Monitor (MIE Inc., USA) is a real-time electro-optical particle counter operating at a sampling flow rate of 2 lpm. All airborne particles are subjected to a high intensity electric field within a quadrupole geometry as shown in Figure 4.9. The field has a d.c. component which aligns all fibrous particles by induced dipole charge separation, and an a.c. component to oscillate these fibers at 400 Hz within a plane perpendicular to the axis of a He-Ne laser beam. The field-induced periodic oscillation of a fiber passing through the optical sensing region generates light scattering pulses at a photomultiplier detector. Each passing fiber produces a train of pulses whose sharpness (i.e. the ratio of amplitude to area) is proportional to fiber length as shown in Figure 4.10, independently of fiber diameter and index of refraction (Lilienfeld, 1987) for fibers with aspect ratios exceeding 3, approximately. Fibers with a diameter as small as 0.2 µm and 2 µm length can be detected by this instrument.
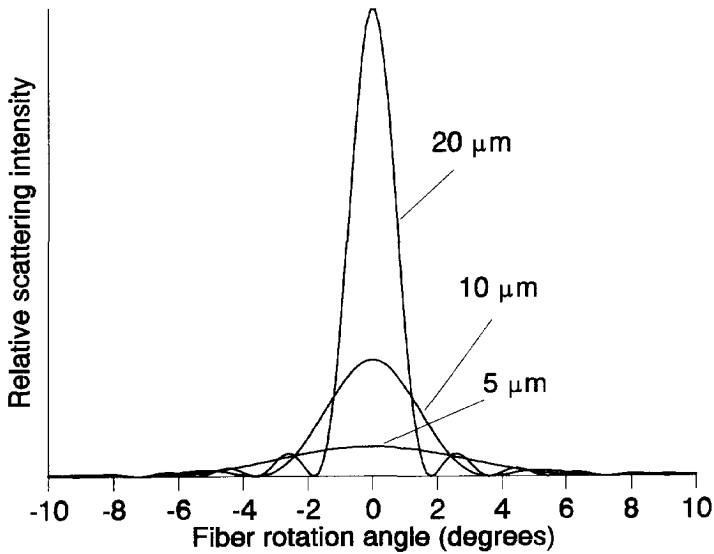
The optical configuration of the monitor is shown schematically in Figure 4.11. A 2 mW HeNe polarized laser operating at a wavelength of 0.6328 µm is used as the source of illumination. The two 45° mirrors are adjustable in three axis to center the beam on the flow tube axis. The beam is vertically polarized and enters the flow/sensing tube through a window at Brewster's angle (reflection angle when the reflected light and the refracted light subtend an angle of 90°), and continues along the tube axis through the sensing/alignment quadrupole section (Lilienfeld, 1985). The beam then reaches a Brewster angle absorption sink at the opposite end of the flow tube. A small portion (< 1/1000 of the beam power) passes through that trap and is sensed by a semiconductor detector which monitors laser output power and proper optical system alignment.

Scattered light from the electrically oscillated fibers is detected by a side-window 9-stage photomultiplier tube with multialkali photocathode. The detector looks through one of the four longitudinal gaps between two adjacent electrode films of the alignment quadrupole (Lilienfeld et al., 1979). The detector field of view in the plane of fiber rotation is approximately 1°, as limited by a laser beam diameter of the order of 0.7 mm.
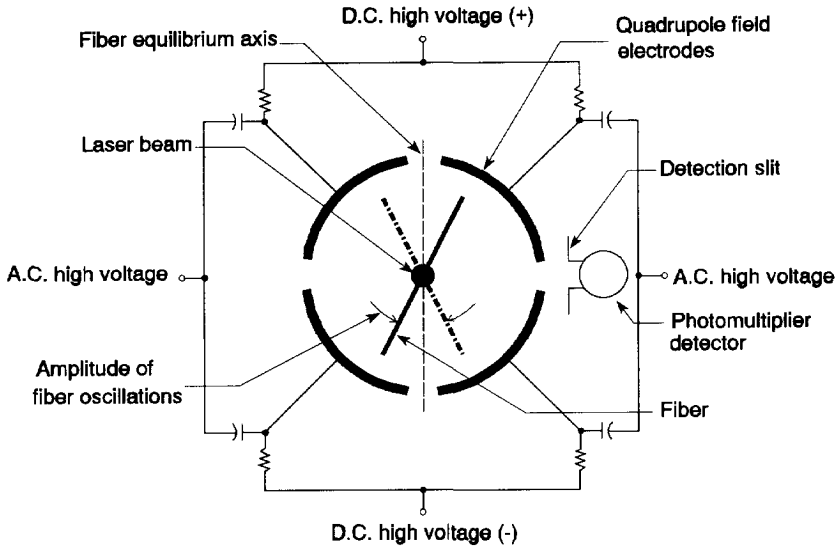
Figure 4.9. *Quadrupole electric field and optical detection configuration of MIE FM-7400 fiber monitor.*

Figure 4.10. *Relative scattering intensity as a function of the fiber rotation angle and the fiber length (Lilienfeld, 1987).*
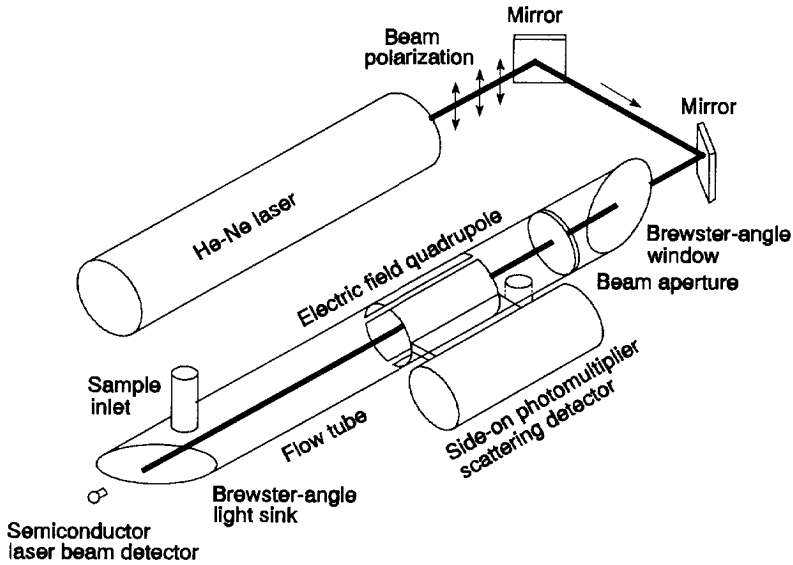
Figure 4.11. *Optical configuration of the FM-7400 Laser Fiber Monitor.*

4.4.2 Differential mobility particle sizer

The DMPS (Differential Mobility Particle Sizer, Model 3932, TSI Inc. USA) is used to measure the size distribution and concentration of submicron range aerosols by detecting the electrical mobility. The aerosols are first classified by an Electrostatic Classifier (EC) which removes a predictable fraction of the particles within a narrow size range, and then, the concentration of these classified aerosols is measured with a condensation nucleus counter. The aerosols which enter the EC passes first through a Kr-85 neutralizer which exposes the particles to high concentrations of both positive and negative ions The particles acquire a charge level described by Boltzmann's equilibrium charge distribution (Keady et al., 1983). The system contains a computer which controls the individual instruments and performs the data reduction as shown in Figure 4.12.

The particle size in the EC can be obtained by selecting the electrical mobility, Z_p, which is defined as the terminal velocity of a particle (V_{TE}) per unit electric field strength (E):

$$Z_p = \frac{V_{TE}}{E} .$$
(4.6)

When the electrical force on the particle (F_E) equals to the fluid drag force (F_D) which resists the movement as shown in Equation 4.7, the particle diameter can be related to the electrical mobility:
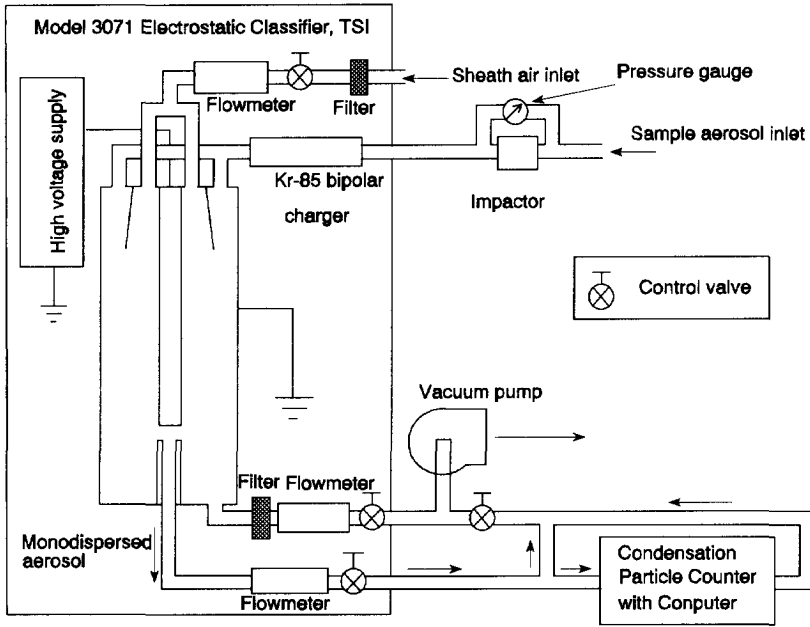
Figure 4.12. *Schematic of the DMPS system (TSI Inc., 1990).*

$$F_E = n_p eE = F_D = \frac{3\pi\mu V_{TE} d_p}{C_f} \ ,$$ (4.7)

where n_p is units of charge, e is the charge on an electron, d_p is particle diameter, and C_f is slip correction factor. One can get the general equation for the electrical mobility of a particle by combining Equations 4.6 and 4.7:

$$Z_p = \frac{n_p e C_f}{3\pi\mu d_p} \ .$$ (4.8)

For a fiber, the drug force is also effected by its orientation in a stream, therefore, the F_D can be obtained:

$$F_D = \frac{3\pi\mu V_{TE} d_e \chi(\phi,\theta,\alpha)}{C_f} \ ,$$ (4.9)

where d_e is the equivalent volume diameter of the fiber, and $\chi(\phi,\theta,\alpha)$ is the shape factor of fibers at the angles of ϕ,θ, and α which will be discussed in Chapter 5. Then the electrical mobility of fibers is:

73

$$Z_p = \frac{n_p e C_f}{3\pi\mu d_e \chi(\phi,\theta,\alpha)} \; .$$ (4.10)

From Equation 4.10, one can calculate the electrical mobility of certain size fibers with a fiber orientation in the fluid. In our experiments, fibers in the submicron size range are mono-dispersed. The DMPS makes it possible to measure the concentration of the test fibers in air.

4.5 Experimental results and discussion

This section discusses the experimental work for dispersing and measuring fibrous particles. Since fibers are their own three dimensions in a stream, they are more difficult to be measured than spherical particles. Several experiments have been done to investigate the possibility of measuring fibers and the stability of the dispersed test fibers.

4.5.1 Dispersing and measurement of large size fibers

There were two kinds of fibers used in our experiments for investigating large fiber deposition behaviour. Mono-disperse polyamide-6 fibers (see 4.2.1) were dispersed successfully in air by a spinning top aerosol generator or a fluidized bed aerosol generator. The Aerodynamic Particle Sizer (APS 33, TSI Inc., 1990) and the FM-7400 fiber monitor were used to measure the fiber concentration in the system. Unfortunately, the concentration measured by both instruments was not high enough to analyze the fiber deposition efficiency in the granular bed. The concentration of the fibers is too small at the outlet of the bed, which causes a large error in the calculation of the deposition efficiencies. Because only very small amounts of these fibers were available and it needs a long time to produce new polyamide-6 fibers, we used glass fibers of various diameters and lengths (see 4.2.5) for our experiments.

The FM-7400 laser fiber monitor makes it possible to measure the concentration and size distribution of poly-disperse fibers in air. Because glass fibers are easy to produce and disperse, they are widely used in experiments for investigating fiber behaviour. In our experiments, the fibers were dispersed by a fluidized bed aerosol generator and measured by the fiber monitor. The experimental set-up was introduced in section 4.3.1 and shown in Figure 4.8. The concentration measured by the fiber monitor was first compared with that measured by a Scanning Electro Microscope (SEM) to make sure that the fiber monitor works well. A filter sample for SEM was taken at the same time as the monitor was measuring. Approximately 300 fibers with various sizes were measured by the SEM. The result is shown in Figure 4.13 where a reasonably good correlation is found between the concentrations obtained by the two methods for different lengths of the fibers (data in the figure with a unit of μm). It can be stated that the FM-7400 fiber monitor is practically equivalent to the conventional SEM measurement for the analysis of the fibers considered (Marijnissen et al., 1996).

After checking the fiber monitor, the fiber concentration stability dispersed by the WAG was checked experimentally. The fluidized bed worked at the required conditions with various
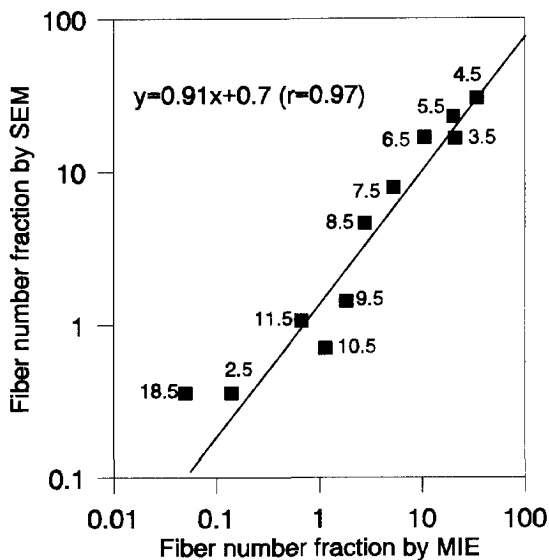
Figure 4.13. *Comparison between the results of fiber measurement by SEM and FM-7400 Laser Fiber Monitor with a fiber diameter of 0.92 μm and various lengths (the data in the figure).*

feeding speeds and fiber concentrations. It was found that one can get a stable distribution when the feeding speed is 0.25 g/s and the concentration of the fibers is 0.5 g per kilo beads. Figure 4.14 and 4.15 show the time history of concentration and length distribution of generated glass fibers after neutralization. This was done by measurement with the fiber monitor. Figure 4.14 shows that the fiber concentration varies in the first 50 minutes. After that, the concentrations are reasonably stable. Thus, the measurement were always made after 60 minutes when the fiber concentration became stable.

4.5.2 Dispersing and measurement of submicron size fibers

The fibers which are dispersed by a nebulizer should be first well dispersed in the liquid. In our experiments, various types of test fibers were checked with the SEM to see if they are well dispersed in the liquid.

HA particles (see 4.2.2) were first tested in our experiments. under the SEM, it can be seen that they are not well dispersed. A possible explanation is that the particles agglomerate during the evaporation of the water in the sample. To check this, the HA fibers were directly measured in the water by an on-line photon correlation spectroscopy (PCS) system which has been developed by Willemse (1996). This technique can measure the size of submicron particles by measuring the fluctuating intensity of scattered light which depends on the particle diffusion coefficient. The particle size measured by the PCS system was much larger
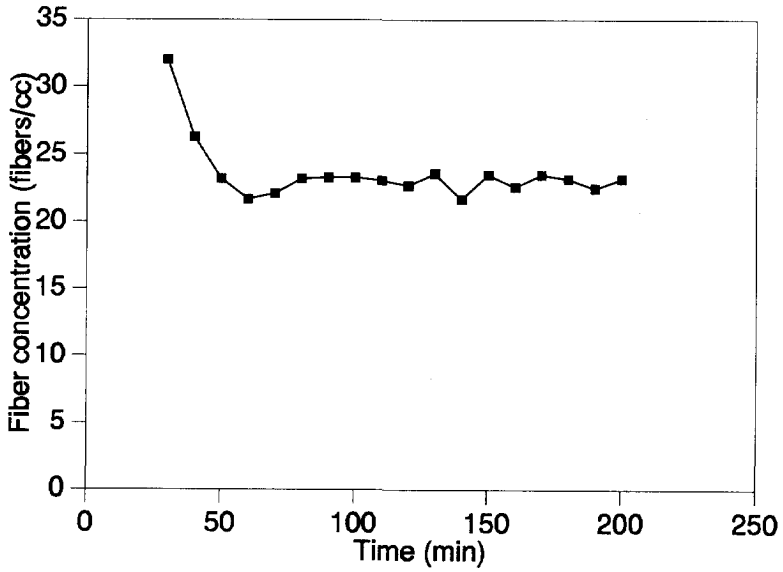
75

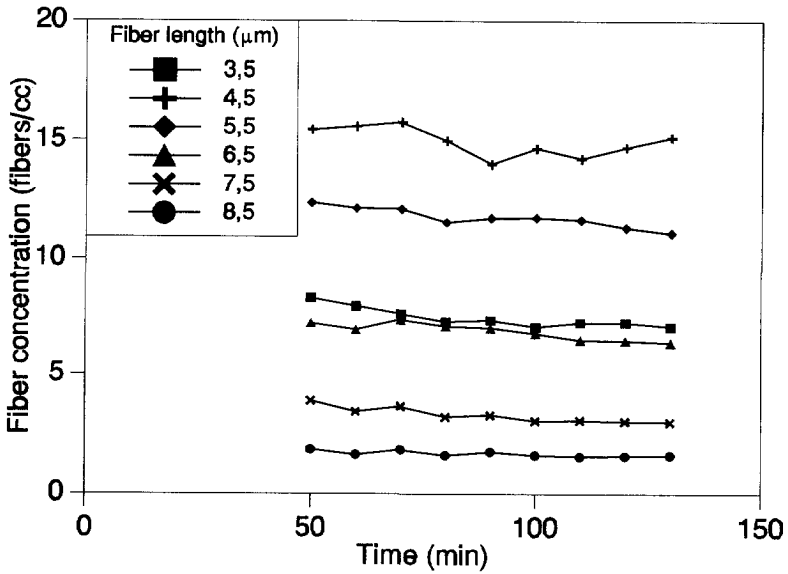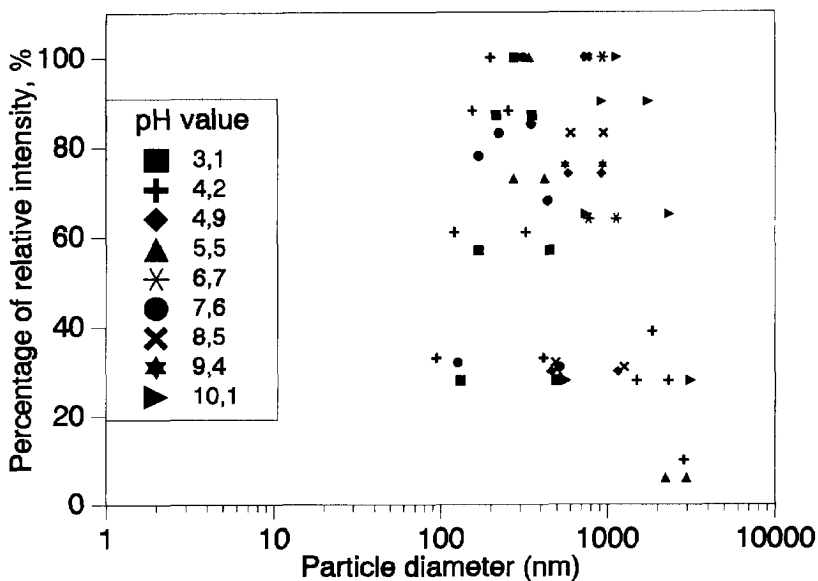**Figure 4.14**. *Time history of the total fiber concentration.*

**Figure 4.15**. *Time history of fiber length distribution.*

76

Figure 4.16. *Particle size distributions in the liquid measured by PCS with various pH.*

than the real size we found from the SEM. Since the particle charge is the main reason for agglomeration, a zero charge point of the particles was expected to get the individual fibers, by changing the pH value of the liquid. After changing the pH value, the PCS system was again used to measure the particle size. Unfortunately, the signals from the PCS system were still much higher than we expected for various pH values. Figure 4.16 shows the PCS measurement for HA particles with pH values from 3 to 10.

Subsequently, the akaganeite particles (see 4.2.3) were used in the experiments. It was proven by SEM investigations that the particles are suspended very well in the water. After being dispersed in air by a nebulizer, separated particles are found on the sampling filter (see Figure 4.17). However, besides the cigar shaped needles, Figure 4.17 also shows monodisperse spheres with a diameter of about 90 nm. The origin of these spheres is not clear. This gives measurement problems since the particle sizers for measuring small particles, such as PMS and DMPS etc., can only measure the concentration and size distribution of particles. It is impossible to distinguish the particle shapes. One should, however, expect two peaks by measuring the particle distribution with the DMPS (see 4.4.2).

The experimental set-up has been shown in Figure 4.8. After nebulizing the liquid which contains fibers, the heated air goes through the chamber for dilution and evaporation of the water droplets. Then, the air which partly contains fibers, flows through silica granules in order to improve the drying of the fibers. Before being measured, the fibers pass a neutralizer to remove the charges on the fibers. There are two sampling probes, one locates at the inlet and one at the outlet of the granular bed filter. The measurements have been done by
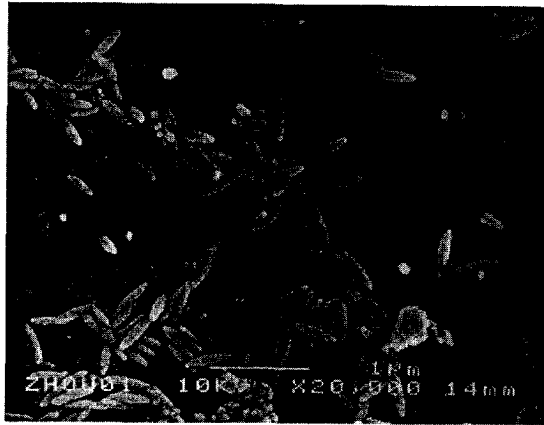
Figure 4.17. *SEM photograph of the akaganeite fibers after dispersion in air.*

isokinetic sampling with the DMPS system by subtracting the background. Figure 4.18 shows the results of a measurement. Clearly two peaks are visible. One peak starts at 90 nm which is just the size of the spheres. Because the computer program of the DMPS has the correction for multi-charged particles, in principle, it should have a narrow peak around 90 nm for the particles with a diameter of 90 nm. In our case, however, the peak is wide, this may be caused by pollutants or even some fibers. Another peak lies between 100 nm and 500 nm approximately. Because the computer correction is for spheres, the program cannot completely correct all multi-charged fibers. From Equation 4.10, we calculated that including double charged fibers with two cases of orientation (parallel and perpendicular to the streamlines), the measurement range for the test fibers is from 90 nm to 220 nm. The minimum point of the two peaks in Figure 4.18 is shown around 100 nm. This indicates that we can consider the particles measured by the DMPS larger than 90 nm as fibers. The rest of the signals are from the spheres and the possible pollutants.

4.6 Conclusions

Dispersion and measurement of various fibers have been discussed in this chapter. Fibers with a length from 3-20 μm were dispersed by the spinning top aerosol generator or by a fluidized bed aerosol generator. A droplet nebulizer cannot be used for fibers in this range, because the droplets produced by nebulizers are too small and not suitable for fibers of such size. In general, polyamide-6 fibers can be used to investigate the fiber deposition behaviour as long as their concentration is high enough for analysis. In this case, however, the concentration of dispersed polyamide-6 fibers was too small to keep it constant. A large amount of glass fibers was successfully dispersed in air by a fluidized bed aerosol generator, but there were also a lot of non-fibrous particles dispersed at the same time. Because the fibers are produced by cutting fibers from a glass filter in a ball mill, there are many particles which have an aspect ratio smaller than 3 in the sample. This makes it difficult to distinguish the fibers with normal
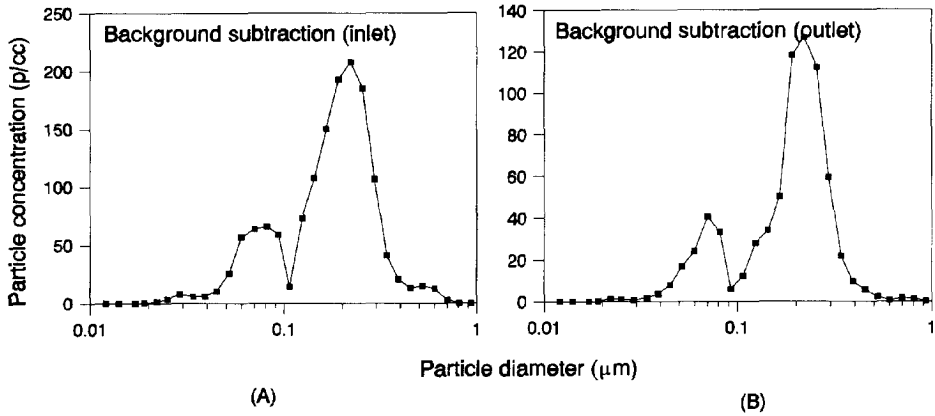
Figure 4.18. *Akaganeite fiber size distribution at inlet (A) and outlet (B) of the granular bed filter measured by DMPS after dispersion.*

aerosol sizers. Therefore, the FM-7400 fiber monitor is used in our experiments. It can only measure fibers with aspect ratio larger than 3. After 50 minutes dispersion by a fluidized bed aerosol generator, the fiber concentration measured by the monitor is constant. This makes it suitable for testing fiber deposition behaviour in a granular bed filter.

Submicron fibers are used to investigate fiber deposition caused by diffusion. Finding well dispersed test fibers is not easy, because fibers of this size are always agglomerated after dispersing them in air, sometimes even in a liquid suspension. Akaganeite particles are well dispersed in the liquid and no agglomeration appears after being dispersed in air by a nebulizer. Because the akaganeite fibers are monodisperse, their concentration can be measured by a particle sizer. In our experiment, the DMPS was used.

5

Fibrous particles deposition in a granular bed filter

5.1 Introduction

Fibrous particle deposition behaviour in a granular bed filter is more complicated than that of spherical particles. Because of the shape of the fibers, three characteristic parameters must be considered: length, diameter and fiber rotation as the fiber moves in a fluid medium. Calculation of fiber deposition in a granular bed is therefore difficult compared with spherical particles, whose dimensions are characterised solely by diameter. Also unlike spheres, fiber orientation in the fluid flow field affects deposition and therefore must also be known.

It is for this reason that this chapter first discusses previous theoretical and experimental research on fiber orientation. On the basis of this literature study, an assumption critically important for our experiments is made, namely that fiber orientation in the fluid flow field is random. From the literature study a new model for calculating fiber deposition in a granular bed filter is also developed. This model is checked using our experimental data. The model is checked further by comparing it with fiber lung deposition models found in the literature.

5.2 Fibrous particle deposition behaviour in tubes

Like deposition of spheres, fiber deposition in lungs is also controlled by the four mechanisms discussed in Chapter 3. The relative importance of these mechanisms depends on fiber mass and shape. Deposition of large fibers results mainly from their relatively high mass. Gravity is thus the most important force effecting deposition in a slow gas flow. For a faster gas flow, inertial effects may become significant. For slow gas flows with small fibers, however, deposition is effected largely by the diffusional mechanism. Depending on fiber orientation in the flow field, the relatively large length to diameter ratio of fibers can cause deposition by interception to play an important role; i.e. fiber deposition by interception occurs most easily when fibers move perpendicularly to the direction of the streamlines.

Because of their great importance to our study, this section first discusses the equivalent Stokes diameter of a fiber and fiber orientation. Then the mathematical expressions of four deposition mechanisms in a horizontal tube with an orientation distribution function developed by Asgharian (1988) are introduced. These expressions are, however, not used further in our

81

study. Because Asgharian's model is compared with our model, it is important to understand the basic idea of his model; this requires that his descriptions of deposition mechanisms be understood.

5.2.1 Calculation of equivalent Stokes diameter of fibers

For fiber deposition occurring in a tube by gravity force or inertial impaction, it is common in the literature that the fiber Stokes equivalent diameter (d_e) is used as the representative parameter. The Stokes equivalent diameter of a fiber is the diameter of a sphere that has the same density and the same settling velocity as the fiber of interest.

From Stokes law, the viscous drag F_s on a particle is given as:

$$F_s = 6\pi\mu r_s u_g . \tag{5.1}$$

where r_s is the radius of a sphere having the same viscous drag as the fiber of interest. When in a gravitational field the fiber is settling at its terminal velocity, the viscous drag force acting on it equals the gravity force F_g:

$$F_g = V\rho_f g . \tag{5.2}$$

From Equations 5.1 and 5.2, the terminal velocity of the particle can be calculated:

$$u_g = \frac{V\rho_f g}{6\pi\mu r_s} . \tag{5.3}$$

Corresponding to this terminal velocity, the Stokes equivalent diameter (d_e) can be presented by using Equations. 5.1 and 5.2:

$$\frac{\pi}{6}d_e^3 \rho_f g = 3\pi d_e \mu u_g . \tag{5.4}$$

The combination of the last two equations finally gives the d_e as:

$$d_e = \sqrt{\frac{3V}{\pi r_s}} . \tag{5.5}$$

The value for r_s for a fiber settling with its length axis parallel to the direction of the flow streamlines can be estimated approximately by the relation of Harris and Fraser (1976):

$$r_{s\parallel} = \frac{d_f \beta}{3(\ln(2\beta)-0.5)} \, , \tag{5.6}$$

where β is the aspect ratio of the fiber (L_f/d_f). Similarly, for the perpendicular orientation, the following relation can be derived:

$$r_{s\perp} = \frac{2d_f \beta}{3(\ln(2\beta)+0.5)} \, . \tag{5.7}$$

When using Equations 5.6 and 5.7 in Equation 5.5, the relations for the Stokes equivalent diameter in the case of parallel and perpendicular movements of the fiber towards its length axis are obtained:

$$d_{e\parallel} = \frac{3}{2}d_f[\ln(2\beta)-0.5]^{\frac{1}{2}} \, , \tag{5.8}$$

$$d_{e\perp} = \frac{3}{2\sqrt{2}}d_f[\ln(2\beta)+0.5]^{\frac{1}{2}} \, . \tag{5.9}$$

Fibers in a fluid flow field, however, are not oriented with their axes only parallel or perpendicular to the direction of the streamlines. Harris and Fraser (1976) suggested that the aerodynamic behaviour of fibers in the human respiratory system could be approximated by the movement of randomly oriented thin straight fibers in the airways. Assuming that fiber volume can be described by a straight cylinder, the Stokes equivalent diameter of a randomly oriented fiber, d_{er}, can be described approximately as:

$$d_{er} = \frac{3}{2}d_f \sqrt{\frac{1}{\dfrac{0.385}{\ln(2\beta)-0.5}+\dfrac{1.23}{\ln(2\beta)+0.5}}} \, . \tag{5.10}$$

A more exact but more complex description of fibers, not used in this study, is to consider them to be prolate ellipsoid. In this case fiber Stokes equivalent diameter can be related to that of truly cylindrical fibers (Gonda et al., 1985),

$$d_{e,\,cylinder} = \sqrt{\frac{3}{2}}\, d_{e,\,prolate} \, . \tag{5.11}$$

In the following discussion, the equivalent diameter is used to represent the equivalent Stokes diameter.

5.2.2 The orientation of the fibers

When a fiber flows through a tube, its orientation in the flow is governed by fiber length and diameter, the flow conditions, and the tube shape. Normally, two mechanisms determine fiber orientation, the velocity shear in the flow and Brownian rotation. In a laminar flow, the velocity at the tube center is higher than that near the tube wall. The velocity of the streamlines decreases from the center to the wall. A fiber can therefore be in contact with streamlines with different speeds and thus rotate. The direction of Brownian motion of a fiber is unpredictable. As fibers becomes smaller (length < 1 μm), Brownian motion becomes increasingly important. Asgharian and Yu (1989a) developed an orientation distribution function $P(\phi,\theta,t)$ to describe fiber orientation. Figure 5.1 shows the orientation of a fiber in a set of axes with the Eulerian angles ϕ and θ. At any time t, the orientation of fibers is governed by the Fokker-Planck equation:

$$\frac{\partial P(\phi,\theta,t)}{\partial t} + \nabla \cdot (\omega P(\phi,\theta,t) - D_r \nabla P(\phi,\theta,t)) = 0 \ , \tag{5.12}$$

where ω is the angular velocity of the particle and D_r is the Brownian diffusion coefficient for rotation. It is clear that the velocity shear influences angular velocity and consequently orientation. All possible orientations at a certain time must satisfy the condition:
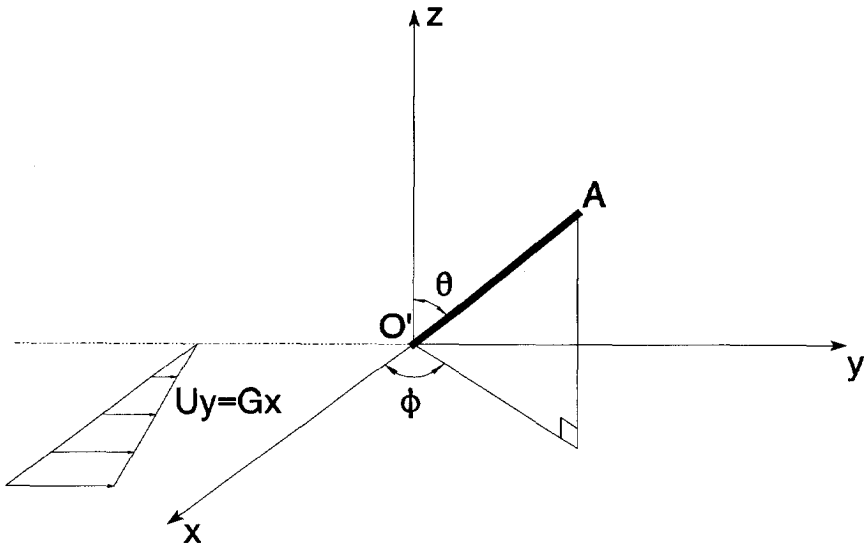

Figure 5.1. *Orientation of a fiber with the Eulerian angles, ϕ and θ.*

84

$$\int_{\phi=0}^{2\pi} \int_{\theta=0}^{\pi/2} P(\phi,\theta,t)\sin\theta \ d\theta d\phi \ = 1 \ . \tag{5.13}$$

The limits of the integration are explained by the fact that all possible combinations of Eulerian angles can be obtained by varying angle θ from 0 to $\pi/2$ when the fiber rotates once around the z axis.

Several publications discuss experiments of the fiber orientation in a laminar flow. After testing four kinds of fibers, glass, amosite, chrysotile and crocidolite, Timbrell (1965) demonstrated in his study of fiber transport in lungs that there is no preferential orientation for fibers which have an aspect ratios less than 5, while fibers definitely tend to align themselves with the direction of the streamlines if their aspect ratio is larger than 5. The tendency is more significant for glass fibers because of their high degree of symmetry. He concluded further that fibers showing a high degree of symmetry must be expected to show the greatest tendency to alignment with air streamlines in the lung. Hirst and his co-workers (1995) described a method by which the angular orientation distribution of fibrous particles in a fluid can be investigated. This method is based on the interpretation of the spatial intensity distribution or scattering profile of laser light scattered by individual fibers. Figure 5.2 shows the alignment angle (the angle between the streamlines and the fiber length axis) distribution of 12 μm long fibers moving in a laminar stream.

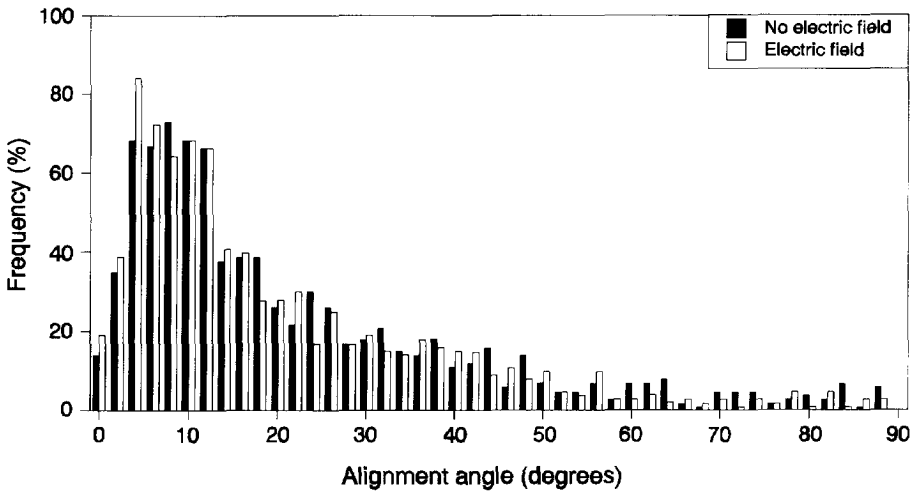**Figure 5.2**. *Histogram showing the alignment angle distribution of 12 μm long silicon dioxide fibers delivered from an aerodynamic focusing nozzle (Hirst et al., 1995).*
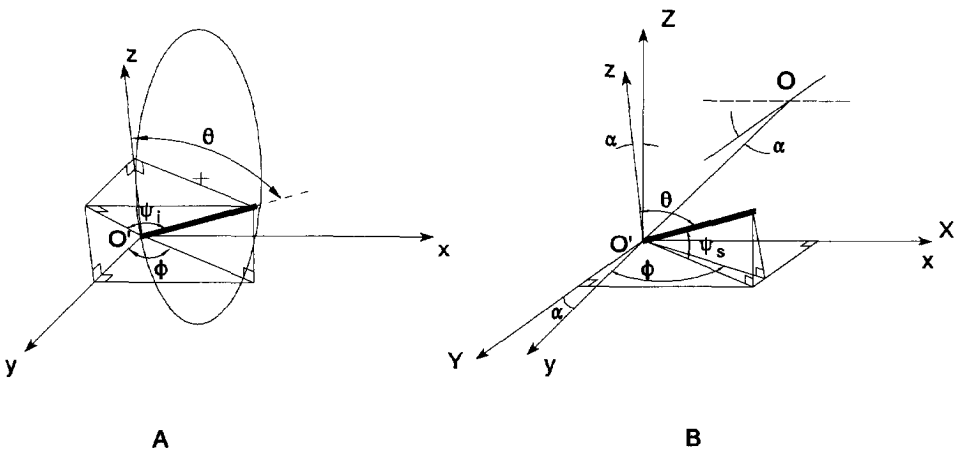
The description of orientation of a fiber in a stream is very complicated and is not clear even in a tube of constant diameter. When a fiber flows into the lungs, its orientation is normally assumed as parallel or random to the streamlines. However, the orientation of fibers depends on the lung region of interest and the fiber size. In the lower parts of a lung, which is the region of our study, the Reynolds number is very low. Fibers moving through the lung tubes can align themselves parallel to the streamlines. At junctures of a generation, however, the flow becomes turbulent and the fiber tends to random orientation.

5.2.3 Impaction and sedimentation

Impaction and sedimentation are only relevant for large fibers. The Cunningham correction or slip correction in the drag force is neglected in our discussion. For the calculation of collection efficiencies occurring by impaction and sedimentation, two particular angles are of importance. This is shown in Figure 5.3 with the flow in x-direction. One of these important angles is the angle between the major axis of the fiber and the cross section of the tube; this is called the impaction angle ψ_i. The second one is the angle between the major axis of the fiber and the horizontal plane; this is called the sedimentation angle ψ_s.

These two angles can be described by the Eulerian angles ϕ, θ and the angle between the line connecting the center of the fiber to the center of the airway cross section and the horizontal α (Yu et al., 1986):

$$\psi_i = \cos^{-1}[(1 - \sin^2\theta \sin^2\phi)^{1/2}] , \tag{5.14}$$

Figure 5.3. *Geometrical description of impaction angle ψ_i (A) and sedimentation angle ψ_s (B).*

$$\psi_s = \cos^{-1}[[(\sin\theta\cos\phi\cos\alpha + \cos\theta\sin\alpha)^2 + (\sin\theta\sin\phi)^2]^{1/2}] \ . \tag{5.15}$$

When a fiber is oriented at angles ψ_i and ψ_s, the drag force per unit velocity on the fiber in the direction of the flow f_i and that in the vertical direction f_s will be presented, respectively (Yu et al., 1986),

$$f_i = 3\pi\mu d_{em}\chi_i \ ; \quad f_s = 3\pi\mu d_{em}\chi_s \ , \tag{5.16}$$

where d_{em} $(= (3\beta/2)^{1/3}d_f)$ is the mass equivalent diameter of the fiber, χ_i and χ_s are the orientation factors at angles ψ_i and ψ_s. The drag force per unit velocity on a fiber can also be expressed (Harris and Fraser, 1976; Asgharian, 1988) as:

$$f_{i,s} = 6\pi\mu(r_{s\parallel}\sin^2\psi_{i,s} + r_{s\perp}\cos^2\psi_{i,s}) \ . \tag{5.17}$$

Combining Equation 5.16 with Equations 5.6, 5.7 and 5.17, the χ_i and χ_s can be obtained:

$$\chi_i = (\frac{2}{3})^{\frac{4}{3}}\beta^{\frac{2}{3}}(\frac{\sin^2\psi_i}{\ln(2\beta)-0.5} + \frac{2\cos^2\psi_i}{\ln(2\beta)+0.5}) \ , \tag{5.18}$$

$$\chi_s = (\frac{2}{3})^{\frac{4}{3}}\beta^{\frac{2}{3}}(\frac{\sin^2\psi_s}{\ln(2\beta)-0.5} + \frac{2\cos^2\psi_s}{\ln(2\beta)+0.5}) \ . \tag{5.19}$$

The fiber deposition efficiency caused by impaction is determined by the Stokes number, which is defined by:

$$Stk = \frac{particle's\ stopping\ distance}{characteristic\ dimension} \ . \tag{5.20}$$

Neglecting the rotational kinetic energy and considering the fibers entering a tube to be randomly oriented, the Stokes number of a fiber system can be determined as:

$$Stk(\theta,\phi) = \frac{\rho_f d_{em}^2 U}{36\mu R_z \chi_i} \ . \tag{5.21}$$

The average Stokes number used to describe the fiber deposition is then given with an orientation distribution $P(r^*,\phi,\theta)$ (Asgharian and Yu, 1989a):

$$\overline{Stk} = \int_{r^*=0}^{1} \int_{\phi=0}^{2\pi} \int_{\theta=0}^{\pi/2} P(r^*,\phi,\theta) \, Stk(\phi,\theta) \sin\theta \, d\theta \, d\phi \, dr^* , \qquad (5.22)$$

where $r^* = r/R_z$ with r being the radial distance from the axis of the airway.

Sedimentation deposition involves the settling by gravity of a collection of aerosol particles on the airway. The deposition pattern for spherical particles and fibrous particles with the same mass differ because of the difference in drag force between the two particles. The Stokes drag force resisting the settling of the spherical particles is always constant. For fibers, however, the drag varies as a result of changes in fiber orientation with respect to the direction of settling. From Stokes law, the settling velocity can be determined by:

$$u_g(\phi,\theta,\alpha) = \frac{\rho_f g d_{em}^2}{18\mu\chi_s} . \qquad (5.23)$$

The average settling velocity for a system of fibers with an orientation distribution is then:

$$\overline{u_g} = \frac{2}{\pi} \int_{\alpha=0}^{\pi/2} \int_{r^*=0}^{1} \int_{\phi=0}^{2\pi} \int_{\theta=0}^{\pi/2} P(r^*,\phi,\theta) u_g(\phi,\theta,\alpha) \sin\theta \, d\theta \, d\phi \, dr^* \, d\alpha . \qquad (5.24)$$

5.2.4 Interception

It is known that fibers can be deposited by combined mechanisms of impaction and interception in airways. If the branching angle at the bifurcation is small and the flow velocity is low, the impaction becomes less important and the site of deposition reduces to a single line which bisects the airway cross section at the exit of the parent tube. Using this simplified model, Asgharian and Yu (1989b) developed a theoretical expression for deposition efficiency of fibers by interception:

$$\eta_i = \frac{1}{2\pi} \int_{\phi=0}^{2\pi} \int_{\theta=0}^{\pi/2} I(\phi,\theta) \sin\theta \, d\theta \, d\phi . \qquad (5.25)$$

The interception function $I(\phi,\theta)$ consists of two parts, one for the rotational Brownian motion, and another for the velocity shear controlled rotation (see Appendix 5B).

5.2.5 Brownian diffusion

Migration of small particles in a gas as a result of collision with gas molecules is referred to as Brownian motion. For spherical particles, the diffusion coefficient, D depends on particle size and gas temperature. Einstein derived the following formula:

$$D = BkT = \frac{kT}{f} ,\qquad\qquad (5.26)$$

where B is the mechanical mobility, k is the Boltzmann constant, T is the absolute temperature, and f is the drag per unit velocity of the particle. When the suspended particles in a gas have a size in the order of the mean free path of gas molecules or smaller, f must be corrected for the velocity slip on the particle surface:

$$f = \frac{f'}{C_f} ,\qquad\qquad (5.27)$$

where C_f is the slip correction factor which is determined only by particle size, and f' is the drag per unit velocity in the continuum regime, which is a function of θ (Asgharian et al., 1988). For a fibrous particle, the continuous impact with gas molecules results in a coupled translational and rotational Brownian motion of the particle. The drag force on a fibrous particle also depends on its orientation with respect to the direction of flow motion. The slip correction factor and the translational diffusion coefficient are therefore direction dependent (Asgharian et al., 1988). The translational diffusion coefficient (D_t) at any orientation θ, can thus be written as:

$$D_t = \frac{kTC_f}{f'(\theta)} .\qquad\qquad (5.28)$$

For a system of fibers with an orientation distribution function, the average translational diffusion coefficient is:

$$\overline{D}_t = kT \int_{r^*=0}^{1} \int_{\phi=0}^{2\pi} \int_{\theta=0}^{\pi/2} \frac{C_f(d_e)P(r^*,\phi,\theta)}{f'(\theta)} \sin\theta \, d\theta \, d\phi \, dr^* .\qquad (5.29)$$

5.3 Fiber deposition models in a granular bed filter

Little experimental and theoretical research on fiber deposition in granular bed filters has yet been carried out. For this reason, two new models for calculating the fiber deposition in a granular bed filter have been developed in this project. One is a theoretical model developed by Podgorski et al. (1996) at Delft University of Technology. This research analyzes the fiber trajectory in the constricted tube model, which is always used in modelling the structure of granular beds. The second model is a semi-empirical model which was developed by modifying the spherical deposition model discussed in Chapter 3. The details of these two models are discussed in the following sections.

5.3.1 The theoretical model

This section presents a formulation of the constricted tube model, determination of the characteristic dimensions of this model for a granular bed filter, description of the fluid flow pattern, and the model's application for analysis of the deposition efficiency of a fibrous particle in a granular bed filter.

5.3.1.1 Geometrical model of a granular bed structure

A geometrical model of a granular bed on an intermediate scale can provide a fundamental basis for analysing the transport phenomena on the microscale. From such a basis the macroscopic characteristics and performance of the system can be calculated. For this analysis, we adopted the idea of a Unit Bed Element (UBE) introduced by Payatakes et al. (1973) and Tien and Payatakes (1979). They assumed that the length of a homogeneous granular bed L may be represented on the intermediate scale as a sequence of unit bed elements of thickness l connected in series. Subsequently, each UBE can be considered as a parallel connection of Unit Cells (UC). The Unit Cells consists of a solid fraction corresponding to one granule or parts of some adjacent ones and a void fraction, as shown in Figure 5.4. The Unit Cells can be generally classified into two groups (Rajagopalan and Tien, 1979): internal and external flow models (see Figure 3.2). As discussed in Chapter 3, the sinusoidal constricted tube model has been chosen as it is coherent with the concept of periodicity which underlies the UBE idea. For the specific sinusoidal tube geometry in the polar cylindrical coordinate system (Figure 5.5), variation of the tube wall radius, r_w, with the axial distance can be generally expressed as:

$$r_w = r_0(1 + a\cos X) , \tag{5.30}$$

where r_0 is the average radius of the tube wall and is equal to the arithmetic mean for the sinusoidal geometry, $r_0 = (d_{min} + d_{max})/4$. In this case, the parameter a is furthermore related to limited diameters of the tube d_{min} and d_{max} by:

$$a = \frac{d_{max} - d_{min}}{4r_0} . \tag{5.31}$$

The dimensionless axial distance, X, in Equation 5.30 is defined as $X = 2\pi x/h$. To complete the quantitative description of the geometrical model of a granular bed, the following parameters have to be specified: l, h, d_{min}, d_{max}, and the number of UCs per UBE, N_{UC}. In the model presented we have chosen both l and h to be equal to the bead diameter, d_g. This is very similar to the suggestion of Payatakes et al. (1973). This is that h is also equal to d_g, but l is a function of the porosity, giving a result very close to d_g while using typical values of the porosity. In our model, three criteria, porosity, interfacial area, and pressure drop, are used to define the geometrical quantities. For a bed with a height of L, cross section area of A, and porosity of ε, the total void volume is $AL\varepsilon$, and the total interfacial area equals $6(1-\varepsilon)AL/d_g$. On the other hand, the surface area and the void volume of one UC are:

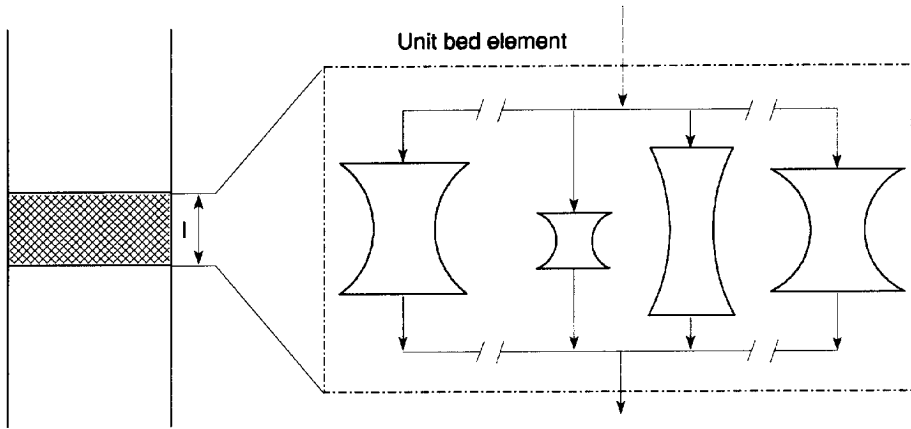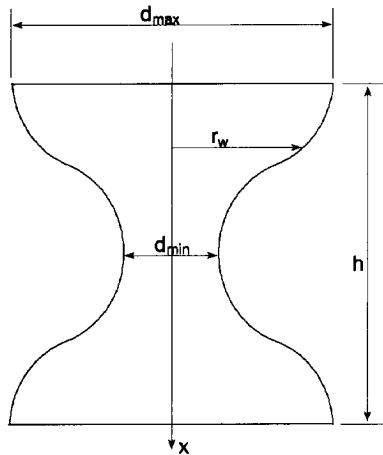**Figure 5.4.** *Schematic representation of a unit bed element.*

Figure 5.5. *Sinusoidal constricted tube model of unit cell.*

$$S_{UC} = 2\pi \int_0^{d_g} r_w(x)dx = 2\pi r_0 d_g \; ; \quad V_{UC} = \pi \int_0^{d_g} r_w^2(x)dx = \pi d_g r_0^2 (1 + \frac{a^2}{2}) \; . \quad (5.32)$$

Thus, to preserve the real bed porosity and interfacial area in the model, the following two conditions must be fulfilled:

91

$$S_{UC}N_{UBE}N_{UC} = 2\pi r_0 d_g (L/d_g)N_{UC} = \frac{6(1-\varepsilon)AL}{d_g} , \qquad (5.33)$$

$$V_{UC}N_{UBE}N_{UC} = \pi r_0^2 d_g (1+\frac{a^2}{2})(L/d_g)N_{UC} = AL\varepsilon . \qquad (5.34)$$

Solving this set of equations we can express N_{UC} and r_0 by means of a, the only unknown parameter:

$$r_0 = \frac{d_g \varepsilon}{3(1-\varepsilon)(1+a^2/2)} , \qquad (5.35)$$

$$N_{UC} = \frac{9A(1-\varepsilon)^2(1+a^2/2)}{\pi d_g^2 \varepsilon} . \qquad (5.36)$$

To determine the value of the constant a, we proceed to consider the third criterion: the pressure drop along the series of UBEs. Solving the Navier-Stokes equation in this geometry should correctly predict the pressure drop through a granular bed. The longitudinal pressure drop per tube length $(\Delta P_1/d_g)$ can be expressed in the form (Chow and Soda, 1972):

$$(\frac{\Delta P_1}{d_g})(\frac{r_0}{\rho u_0^2}) = \frac{8}{Re_0} \int_0^1 \frac{d\xi}{(1+a\cos(2\pi\xi))^4} + 8\pi a\delta \int_0^1 \frac{\sin(2\pi\xi)}{(1+a\cos(2\pi\xi))^5}d\xi , \quad (5.37)$$

where $\xi = x/d_g$, $\delta = r_0/d_g$, the Reynolds number Re_0 is referred to the velocity (u_0) calculated for the radius of the wall r_0. Since $u_0 = u_s(1+a^2/2)/\varepsilon$, one can introduce another definition of Reynolds number based on u_s and d_g: $Re_s = u_s d_g/\nu = 3Re_0(1-\varepsilon)/\varepsilon$. For the case of sinusoidal constricted tube, the second term of the equation on the right side is zero. After integration of Equation 5.37, the pressure drop along the entire bed can be expressed as:

$$(\frac{\Delta P}{L})(\frac{d_g}{\rho u_s^2})\frac{\varepsilon^3}{(1-\varepsilon)^2} = \frac{72}{Re_s} \frac{(2+3a^2)(1+a^2/2)^3}{\sqrt{1-a^2(2-6a^2+6a^4-2a^6)}} . \qquad (5.38)$$

This may be compared with the Carman-Kozeny equation, since the above-mentioned pressure drop was calculated for laminar flow conditions:

$$(\frac{\Delta P}{L})(\frac{d_g}{\rho u_s^2})\frac{\varepsilon^3}{(1-\varepsilon)^2} = \frac{180}{Re_s} . \qquad (5.39)$$

It seems that both formulae predict identical dependence of the pressure drop on porosity,

Reynolds number, bead diameter, and dynamic pressure of the fluid. Comparing Equation 5.38 with 5.39, we get an equation for the constant a:

$$\frac{(2+3a^2)(1+a^2/2)^3}{\sqrt{1-a^2}\,(2-6a^2+6a^4-2a^6)} = \frac{180}{72}, \tag{5.40}$$

which has the unique value of a (= 0.373). After inserting this value into Equations 5.30, 31, 35, and 36, the definition of the geometrical model becomes complete. Using the geometrical model on the intermediate scale defined, one can try to analyze transport processes in a granular bed on the microscale. In most cases, such an analysis would require the knowledge of the fluid flow pattern.

5.3.1.2 Analytical description of laminar flow in a constricted tube model

An analytical solution was obtained by Chow and Soda (1972) for the steady laminar flow of an incompressible Newtonian fluid in a constricted tube. Their expressions of the velocity components were derived with the second-order approximation with respect to δ. This solution was then used in many studies of granular filtration of aerosols. Unfortunately, in the original paper, the final formula for the radial component of the fluid velocity contained two serious errors in the two leading terms. The corrected second order approximation of radial and axial velocity components for the specific sinusoidal geometry described by Equation 5.30 has been described by Podgorski et al (1996):

$$\frac{u_r\eta^2}{u_0\delta\pi aR} = 4(R^2-1)\sin X - \frac{\pi\delta Re_0}{9\eta}[(\eta\cos X + a\sin^2 X)(R^6-6R^4+9R^2-4)$$

$$+a\sin^2 X(8R^6-36R^4+36R^2-8)] - \frac{2\pi^2\delta^2\eta\sin X}{3}\{(R^2-1)[(16a\cos X$$

$$-2)(R^2-1)+2a(10a\sin^2 X+\eta\cos X)(3R^2-1)] \tag{5.41}$$

$$+\frac{Re_0^2 aR^2}{1200\eta^2}[(\cos X + a\sin^2 X/\eta)(32R^8-305R^6+750R^4-713R^2+236)$$

$$+a\sin^2 X(192R^8-1525R^6+3000R^4-2139R^2+472)/2]\} ,$$

$$\frac{u_x\eta^2}{u_0} = 2(1-R^2) + \frac{\pi a\delta Re_0\sin X}{9\eta}(4R^6-18R^4+18R^2-4)$$

$$+\frac{\pi^2\delta^2 a}{3}[(20a\sin^2 X+4\eta\cos X)(R^2-1)(3R^2-1) \tag{5.42}$$

$$+\frac{Re_0^2 R^2 a\sin^2 X}{1200\eta^2}(192R^8-1525R^6+3000R^4-2139R^2+472)] ,$$

where $\eta = 1+a\cos X$ and $R = r/(r_0\eta)$.

93

5.3.1.3 Analysis of deposition of fibrous particles in a granular bed filter

A form of mathematical description of aerosol particle motion in a moving fluid depends significantly on particle shape. In the case of a spherical particle, a set of ordinary differential equations was used for the translation of the particle mass center. A similar procedure is usually adapted for compact non-spherical particles by means of the equivalent aerodynamic diameter. However, such an approach is insufficient for fibrous particles because the rotation of the particles also has to be taken into consideration in addition to the translational motion. The specific form of the equations of the motion for a fibrous particle also depends on mechanical properties of the fiber. For a stiff fiber, it is still the set of ordinary differential equations, as it is enough to trace the translation and rotation of the whole particle. For a flexible fiber, however, displacement of the individual elements of the particle has to be considered, therefore leading to a set of partial differential equations. Two limited cases of a perfectly flexible and a completely stiff fiber were discussed by Podgorski et al. (1996) and the general description valid for any value of the particle elasticity modulus has been presented by Podgorski and Gradon (1997).

For analysis of a fibrous aerosol particle motion in a constricted tube, the Cartesian coordinate system, Ox_i, $i = 1, 2$ and 3, is introduced. This system is fixed at the center of the tube inlet in such a way that the x_1 axis coincides with the main direction of the gas flow. It is also assumed that gravity acts in the same direction. In the absence of forces other than the fluid drag and gravity, translation of the particle mass center is described by Podgorski et al. (1996):

$$\frac{dv_{xi}^{(0)}}{dt} = \frac{4}{\pi d_f^2 L_f \rho_f} \int_0^{L_f} f_{xi}(s)ds + \frac{(\rho_f - \rho)g}{\rho_f}\hat{g}_{xi} , \qquad \frac{dx_i^{(0)}}{dt} = v_{xi}^{(0)} . \tag{5.43}$$

For rotation of the particle around its main axes, they described the following set of equations with the permutation (Levi-Civita) symbol, ε_{ijk}:

$$I_{km}\frac{d\omega_m}{dt} + \varepsilon_{kij}I_{km}\omega_i\omega_m = \varepsilon_{1ik}l_{ij}\int_0^{L_f}(s-L_f/2)f_{xj}(s)ds , \qquad \frac{dx_j'}{dt} = \omega_3 l_{2j} - \omega_2 l_{3j} . \tag{5.44}$$

where L_f, d_f, ρ_f denote the fiber length, diameter and density, $x_i^{(0)}$, $v_{xi}^{(0)}$ are Cartesian elements of the vectors of position and velocity of particle mass-center, $g = 9.81$ m/s^2, $\hat{g}_{xi}$ is the unit vector of the gravity field orientation, s is the distance measured along the longest main axis, ω_m are components of the particle angular velocity, I_{km} are the elements of the tensor of the moments of inertia, and l_{ij} are the elements of the matrix of transformation between the vectors of the local and Cartesian coordinate systems. The vector of fluid drag force per unit length of the fiber was calculated from the theory of Johnson (1980) for a slender-body. The calculations of particle trajectories allow us to find the limiting trajectories and hence the unit cell collection efficiency, E_{UC}:

$$E_{UC} = \frac{\int_{r_{LT}}^{d_{max}/2} u_x(r)2\pi r dr}{\int_0^{d_{max}/2} u_x(r)2\pi r dr}$$

(5.45)

$$= 1 - (\frac{2r_{LT}}{d_{max}})^2[2-(\frac{2r_{LT}}{d_{max}})^2 + \frac{\pi^2 d_{max}(d_{max}-d_{min})}{6d_g^2}(1-(\frac{2r_{LT}}{d_{max}})^2)] \ ,$$

where r_{LT} denotes the distance between the center of the tube inlet and the starting point of the limiting trajectories. Finally, the total efficiency of the filter of height L is calculated according to the formula:

$$E = 1 - (1-E_{UC})^{L/l} \ .$$

(5.46)

By using this model to calculate the fiber deposition in a bed, one has to spend several days of calculation (!) at our work station for only one point in a simple flow condition (very low gas velocity) and large fibers at very low gas velocity. Figure 5.6 shows one calculation of fiber deposition in a bed for parallel and perpendicular orientation at very low gas velocity. From the figure, one can see that the deposition by perpendicular orientation is larger than that by parallel orientation when the fiber length is larger than about 30 µm. This is because the contribution of interception for perpendicular orientation is significant in that case.
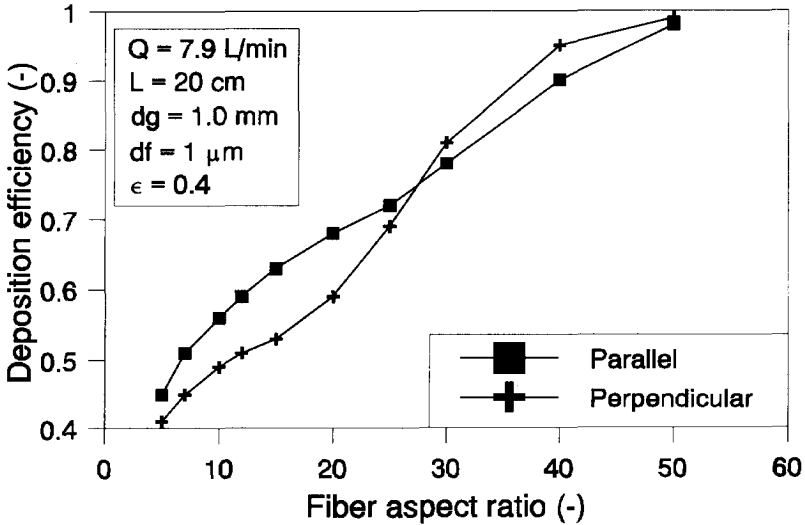

Figure 5.6. *The calculation results of fiber deposition in granular bed filter for parallel and perpendicular orientation.*

5.3.2 Semi-empirical model modified from spheres

Spherical particle deposition in a granular bed filter has been discussed in Chapter 3. The semi-empirical model for spherical particle deposition in a bed is in good agreement with the experimental data. As the first step of our investigation of fiber deposition in a granular bed, this model has been modified for fibers. In order to obtain the overall penetration and single sphere collection efficiency for fibers, the expressions with four deposition mechanisms (see Table 3.4) can be obtained by changing the Stokes number for impaction, gravity number for sedimentation, Peclet number for diffusion, and R_i for interception. Derived expressions for fiber deposition are stated below for every deposition mechanism. The total penetration P_F, and single collection efficiency η_T, can be obtained in a similar way as in Chapter 3:

$$P_F = \exp(-\frac{3(1-\varepsilon)L\eta_T}{2d_g\varepsilon});$$

(5.47)

$$\eta_T = \eta_I(Stk,\ Re,\ \varepsilon) + \eta_S(Grv) + \eta_D(D,\ Re,\ ) + \eta_R(R_i,\ Re,\ \varepsilon).$$

Impaction
Equations 3.21 and 22 show that the single sphere efficiency for impaction is related to the Stokes number, the Reynolds number of the flow, and the bed porosity. The Reynolds number and the bed porosity are only related to the flow conditions and the structure of the bed; only the Stokes number varies with the particle characteristics. For a fibrous particle, the Stokes number is defined by using the equivalent Stokes diameter (Yu et al., 1986):

$$Stk_c = \frac{d_{e,c}^2\rho_f U}{18\mu d_g},$$

(5.48)

where the subscript c is the fiber orientation for parallel, perpendicular, or random movement. The values of d_e can be obtained from Equations 5.8, 5.9, and 5.10 for these three orientations. When the Stokes number in Equation 3.21 is replaced by the one from Equation 5.48, the modified expression for impaction can be obtained.

Sedimentation
The gravity number ($Grv = u_g/U$) in Equation 3.27 is the only parameter that determines particle deposition by sedimentation, in which the settling velocity, u_g, varies with particle size and shape. By using Equations 5.8, 5.9, and 5.10 in Equation 5.4, the fiber settling velocity for three orientations (Gonda and Khalik, 1985) can be obtained:

$$u_{g,c} = \frac{d_{e,c}^2\rho_f g}{18\mu}.$$

(5.49)

Using the fiber settling velocity in the gravity number, the modified expression for

sedimentation can be derived by Equation 3.27.

Brownian diffusion
The single sphere collection efficiency by Brownian diffusion was expressed in Equation 3.28, which is governed by two dimensionless parameters, Reynolds number (*Re*) and Schmidt number (*Sc* = v/*D*). As we have already discussed in Chapter 3, the Reynolds number is not a not a function of particle shape. The diffusion coefficient, *D*, in the Schmidt number is the only parameter affected by particle characteristics. The diffusion coefficient is expressed by Equation 5.26, in which the particle mechanical mobility *B* is given by:

$$B = \frac{\tau}{m} ,$$ (5.50)

where *m* is the mass of the fiber and τ is the particle relaxation time, which is expressed for fibers by its equivalent diameter:

$$\tau = \frac{d_{e,c}^2 \rho_f C_f}{18\mu} .$$ (5.51)

Combining Equations 5.50 and 5.51 with 5.26, the diffusion coefficient for variously orientated fibers is obtained:

$$D_c = \frac{2kTd_{e,c}^2 C_f}{9\pi\mu d_f^3 \beta} .$$ (5.52)

The single collection efficiency of fibrous particle for Brownian diffusion can be calculated by using Equation 3.28 in Chapter 3

Interception
The interception parameter R_i is the characteristic parameter for this mechanism. To estimate the interception deposition efficiency of fibers in a granular bed filter, the expression for R_i can be obtained for various orientations:

$$R_{i\parallel} = \frac{d_f}{d_g} ; \quad R_{i\perp} = R_{i,r} = \frac{L_f}{d_g} .$$ (5.36)

One can obtain the single sphere collection efficiency of fibrous particles for interception by introducing the R_i in Equation 3.24.

Considering all four mechanisms, the modified semi-empirical model for oriented fibers is derived as shown in Table 5.1.

Table 5.1. *Sphere-modified model for fiber deposition in granular bed filters.*

$$P_F = \exp(\frac{-3(1-\varepsilon)L\eta_T}{2d_g\varepsilon}); \quad \eta_T = \eta_S+\eta_D+\eta_I+\eta_R$$

$$\eta_I = \frac{Stk_{eff}^3}{0.014+Stk_{eff}^3}; \quad Stk_{eff} = (1.0+\frac{1.75\,Re\,\varepsilon}{150(1-\varepsilon)})Stk_c$$

$$\eta_S = 0.0375(Grv)^{0.5}+0.21(Grv)^{0.78}; \quad Grv = u_{g,c}/U$$

$$\eta_D = B(Re)(v/D_c)^{f_1(Re)}Re^{f_2(Re)}; \quad f_1(Re) = -\frac{2}{3}+\frac{Re^3}{6(Re^3+2\times10^5)}$$

$$B(Re) = 8; f_2(Re) = -\frac{2}{3} \ (Re<30);$$

$$B(Re) = 40; f_2(Re) = -1.15 \ (30\leq Re<100)$$

$$\eta_R = 6.3\varepsilon^{-2.4}R_i^2; \quad R_i = \frac{L_f}{d_g}$$

This model is called the *"sphere-modified model"*. Experiments have been carried out to investigate the validity of the model for one set of conditions. Results are shown in Figure 5.7 for a flowrate of 30 l/min, a diameter of beads of 2.0 mm, and a bed height of 17 cm. Unfortunately, it can be seen from the figure that this model does not agree well with the experimental data. It can be concluded that an adequate fiber deposition model cannot be derived by just simply modifying a model for spherical particles. Therefore more experiments were done while efforts were made to develop a satisfactory semi-empirical model.

5.4 Experiments, results, and discussion

The experimental work includes the dispersion and measurement of the test fibers. The aim was to investigate fiber deposition behaviour in the granular bed filter, to compare the results with the literature models and to develop a new deposition model based on the results. In order to analyze the experimental results, fiber orientation must be known. Many studies, previously discussed in Section 5.2.2, show that fibers are orientated parallel to the streamlines in laminar flow in a tube. But in the case of human lungs, when air moves from one generation to another, vortex motion occurs at the junction of the two generations. The fiber orientation is controlled by the velocity shear in the flow and by Brownian motion. When passing the junction, the fiber will change its orientation. In the study of Harris and Fraser (1976), fibers were assumed to be in pure periodic rotation in the shear flow when the root mean square of the Brownian rotation angle was less than 10°. Beyond that point, fibers were orientated randomly. In our study, because the direction of streamlines is always changing, the orientation of fibers is assumed to be random to the streamlines.
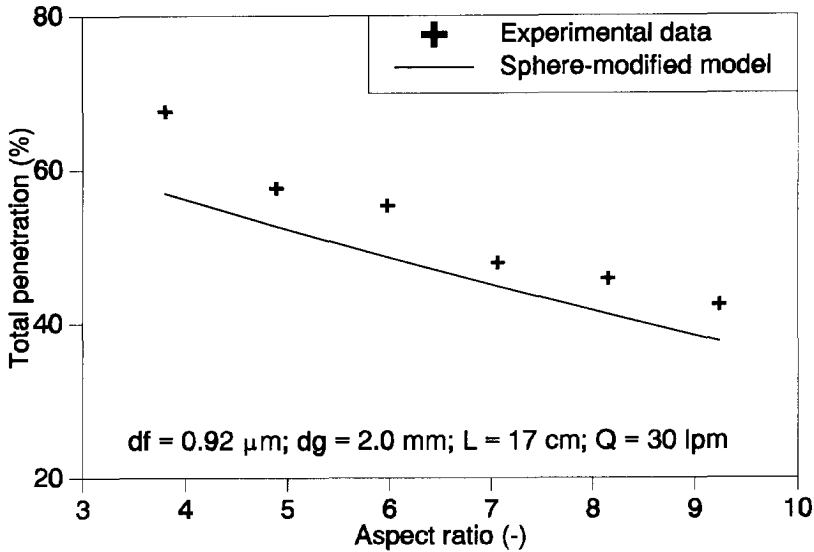
Figure 5.7. *The comparison between the sphere modified model and the experimental data.*

5.4.1 Experimental set-up and conditions

As discussed in Chapter 4, different kinds of fibers of various sizes were tested. From these tests only two kinds of fibers were found suitable for dispersion and measurement; these were glass fibers and akaganeite fibers. A laser fiber monitor and a differential mobility particle sizer were used in the experiments to measure these fibers. The experimental set-up has been shown in Chapter 4 (Figures 4.7 and 4.8), in which fiber dispersion was also discussed. After being dispersed by an aerosol generator, the dried fibers were neutralized by a radioactive source (Kr 85) before introducing them into the granular bed filter; this was done in order to avoid electrostatic effects on particle collection. Two sampling probes, one at the inlet and another at the outlet of the filter, were used to measure the particle concentration. The fiber deposition efficiencies in the granular bed is obtained by measuring the fiber concentrations at the inlet and the outlet using the sampling probes.

In order to study the deposition as a function of the individual deposition mechanism, the flowrate was varied from a small value (for sedimentation and diffusion) to a large one (for impaction). Three regions composed of flowrates and particle sizes were chosen in order to make a given collection mechanism predominant. (1) For large fibers at high velocity, where the effective Stokes number is larger than 0.01, the collection efficiency is governed by impaction (Tardos and Pfeffer, 1985). (2) For large particle at a velocity smaller than 10 cm/s, the predominant mechanism is sedimentation (Otani et al, 1989). (3) For fine particles with equivalent diameter smaller than several tenths of a micrometer, deposition occurs by

Brownian diffusion. Interception deposition always occurs together with the other three mechanisms. However, one can obtain the single collection efficiency for interception by subtracting the impactional, sedimentational, and diffusional efficiencies. The other parameters, such as bead size and bed height, are also varied while investigating the validity of the empirical and theoretical models. The experimental conditions are shown in Table 5.2.

Table 5.2. *The experimental conditions for fiber deposition in the granular bed filter.*

granular medium	glass beads
aerosol particles	glass, akaganeite
aerosol generators	fluidized bed, nebulizer
flow direction	down-flow
analyzing method	Laser Fiber Monitor (MIE Inc. USA), DMPS (TSI Co. USA)
fiber length (μm)	glass: 3 - 10; akaganeite: 0.6
fiber diameter (μm)	glass: 0.85, 0.92, 0.67 ; akaganeite: 0.08
fiber orientation	random
bead diameter (mm)	1.04, 1.28, 2.0
total flowrate (lpm)	9, 23, 30, 50, 60
bed length (cm)	7, 12, 17

5.4.2 Results and comparison with the existing models

Firstly, the experimental results have been compared with predictions of the theoretical model. Unfortunately, the calculation time of the model is too long to get results which correspond to the conditions of the experiments. Normally, it takes one week calculational time on a workstation to calculate only one data point by using conditions which result in a simple trajectory; for example, very low flow velocity and large fibers. For these reasons the calculation was done with a superficial velocity of 2.12 cm/s, a fiber diameter of 1 μm, and a fiber length from 5 to 50 μm. This condition is close (but not identical) to the experimental conditions with a total flowrate of 9 l/min. In our experiments, however, the maximal length of the fiber is only 8.5 μm.

Another way to check the theoretical model is to compare it with the semi-empirical model at the same condition. The advantage of this approach is that conditions can be chosen for which the calculational time required for the theoretical model is relatively low. This type of comparison will be discussed later in this section.

As for spherical particles, Equation 3.32 is used to calculate the single sphere collection efficiencies from total fiber penetration of the bed. For specific experimental conditions, single sphere collection efficiency is dominated by one mechanism. For such conditions we can thus ignore the other three mechanisms. Using the experimental data we performed regression analysis to obtain mathematical expressions to fit the experimental data. In this way

a new model called the "fiber model" was obtained.

When passing through the system with a low velocity fibers whose equivalent diameter is larger than 1 μm are deposited by *sedimentation*. In the experiments a flowrate of 9 lpm was used in the system. The superficial velocity of the bed is thus 2.4 cm/s; this is much less than 10 cm/s, which is considered within the gravity effect area (Otani et al., 1989). Figure 5.8 shows the experimental data compared with the sphere-modified model in this region.

In this figure, the deposition for the sphere-modified model is higher than the experimental data. This occurs because the drag force on fibers is higher than that on spherical particles. From this figure a new equation for fiber deposition by sedimentation in a granular bed filter was obtained by performing regression analysis of the experimental data:

$$\eta_S = 0.022\,Grv^{0.5} + 0.11\,Grv^{0.75} \tag{5.54}$$

Also for the glass fibers, *impaction* becomes the dominant mechanism for deposition when the velocity of the system is high. In this case, a flowrate of 63 lpm is used in the system, assuming that the impaction is the only mechanism effecting fiber deposition. Impaction efficiency is influenced by both Stokes number, *Stk*, and Reynolds number, *Re*. That is why in the calculation of Gal et al. (1985) the effective Stokes number, Stk_{eff}, was proposed (see Equation 3.21). By using the effective Stokes number, the curve predicted by the sphere-modified model is shown in Figure 5.9, in comparison with the experimental data.
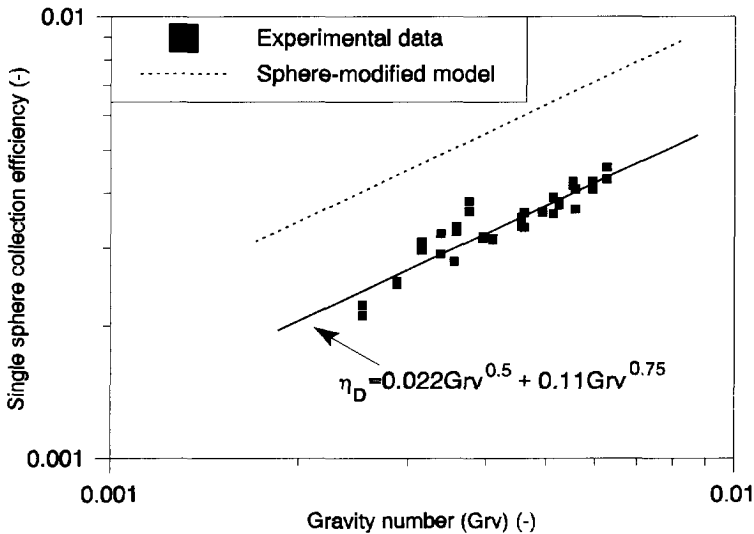

Figure 5.8. *Fiber deposition comparison between experimental data and sphere modified model for sedimentation.*
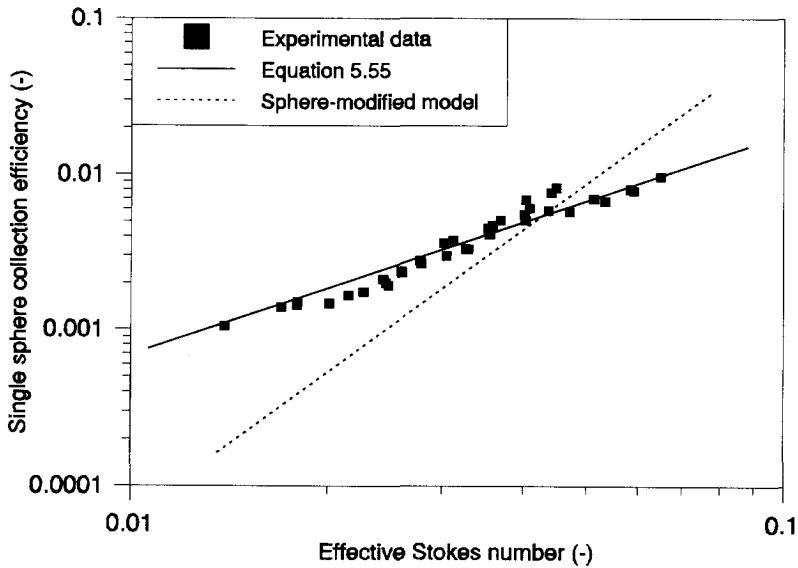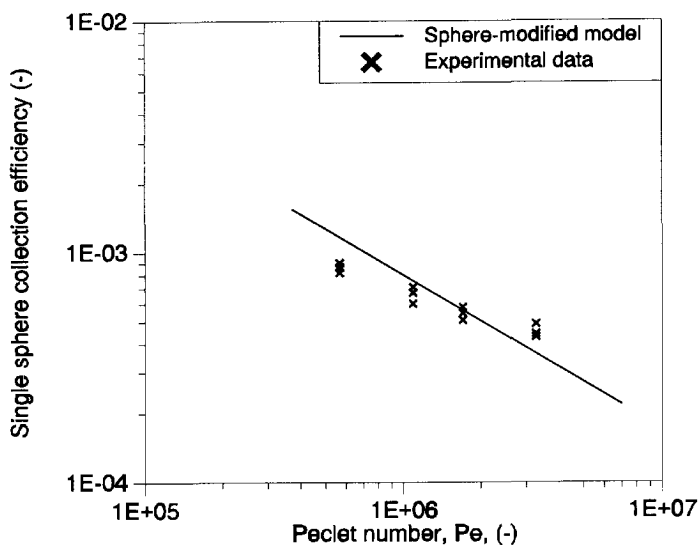
Figure 5.9. *Experimental data compared with the sphere modified model for impaction.*

From this figure it is seen that the present data differ from the model. The cause of this difference is probably fiber orientation. The fluid motion through the bed in this experimental set-up is always laminar. In the case of granular bed filters, however, the directions of the streamlines are changing per layer. The orientation of every fibers regardless of size is therefore assumed to be random in the granular bed filter. Using linear regression the experimental data may be correlated by:

$$\eta_I = \frac{Stk_{eff}^{1.41}}{2.05 + Stk_{eff}^{1.41}} \tag{5.55}$$

Brownian diffusion becomes the dominant collection mechanism when particles are sufficiently small. Since the smaller fibers used in our experiments have a length of only 600 nm and a diameter of only 80 nm, we assumed that the diffusion is the only acting mechanism for fiber deposition. For fibers, the continuous impact with gas molecules will result in a coupled translational and rotational Brownian motion of the particle, giving rise to a translational and rotational diffusion coefficient (Asgharian et al., 1988). Moreover, the drag force on a fiber depends on its orientation with respect to the direction of motion. The translational diffusion coefficient is therefore direction dependent. Since the Reynolds number in the alveolar region of the human lung is very small, the equations for spherical particle deposition discussed in Chapter 3 (Equations 3.28 - 30) can be simplified to the following function of the Peclet number, Pe:

102

Figure 5.10. *Experimental data for small fiber deposition compared with sphere modified model.*

$$\eta_D = 8.0 Pe^{-\frac{2}{3}} \; ; \quad for \quad Re < 30. \qquad (5.56)$$

Experimental collection efficiencies are compared with those predicted by Equation 5.56, taking *Pe* from the abscissa in Figure 5.10.

From this figure it is seen the experimental data differs from predictions of the sphere-modified model. However, for three reasons the sphere-modified model was still used. These are: the equation used in the sphere-modified model is widely used to predict particle deposition in granular bed filter by the diffusion mechanism, experimental data for fine fibers are scarce, and the difference between the equation and our experimental data is not very large. Therefore we use this expression as our new model for diffusion.

As discussed in section 5.2.4, the effect of *interception* mainly depends on the rotation of the fibers. For spherical particles, interception becomes relatively important in the transitional regions of the other collection mechanisms. Thus the interceptional efficiencies were obtained from the data corresponding to a total flow rate of 30 lpm of glass fibers in the transitional regions; interceptional efficiencies were obtained as residues after subtracting the sedimentational, impactional and diffusional efficiencies from the total deposition efficiency. Figure 5.11 shows the experimental results compared with the sphere- modified model. In reality, the deposition efficiency by interception should be related to the Reynolds number. Our experiments are based on the conditions of human lungs, which have a small variation in the Reynolds number. Therefore the effect of Reynolds number can be ignored.

103
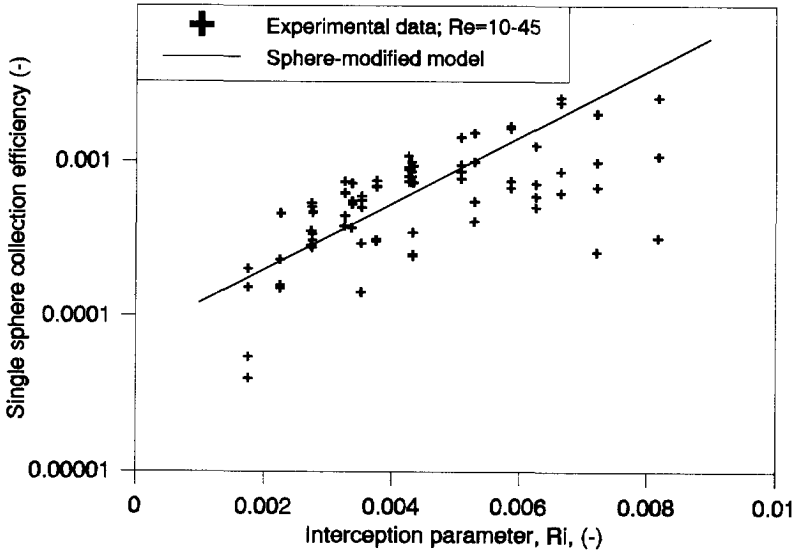
Figure 5.11. *Experimental data for interception as a function of $R_i = L_f/d_g$ compared with the models.*

It can be seen that the experimental data are stochastic and that the sphere-modified model predicts almost the average value of the distribution. In our study, the sphere-modified model is used as the fiber model for interception when the interception parameter R_i is expressed by the fiber length L_f:

$$\eta_R = 6.3\,\varepsilon^{-2.4}R_i^{2}; \quad R_i = \frac{L_f}{d_g}. \tag{5.57}$$

5.4.3 The new semi-empirical model

By using Equation 5.47, the single sphere collection efficiency for fibrous particles can be predicted as a sum of the individual efficiencies. The predicted overall penetration can then be calculated. All expressions of this model are listed in Table 5.3. For the impaction and sedimentation mechanisms, it is found that the difference of the collection efficiency between parallel and random orientation is not large. In our study the orientation of the fibers is therefore assumed to be random in a granular bed filter.

For investigating the total fiber penetration in granular bed filters, a comparison between the predicted penetration and experimental data, which are listed in Appendix 5A, is shown in Figure 5.12 A/B. It can be seen from the figures that the experimental data are in good

Table 5.3. *New semi-empirical model for fiber deposition in a granular bed filter.*

$$P_F = \exp(\frac{-3(1-\varepsilon)L\eta_T}{2d_g\varepsilon}); \quad \eta_T = \eta_S + \eta_D + \eta_I + \eta_R$$

$$\eta_I = \frac{Stk_{eff}^{1.41}}{2.05 + Stk_{eff}^{1.41}}; \quad Stk_{eff} = (1.0 + \frac{1.75\,Re\,\varepsilon}{150(1-\varepsilon)})Stk$$

$$\eta_S = 0.022(Grv)^{0.5} + 0.11(Grv)^{0.75}$$

$$\eta_D = B(Re)Sc^{f_1(Re)}Re^{f_2(Re)}; \quad f_1(Re) = -\frac{2}{3} + \frac{Re^3}{6(Re^3 + 2\times10^5)}$$

$$B(Re) = 8; \, f_2(Re) = -\frac{2}{3} \, (Re<30);$$

$$B(Re) = 40; \, f_2(Re) = -1.15 \, (30\leq Re<100)$$

$$\eta_R = 6.3\varepsilon^{-2.4}R_i^2; \quad R_i = \frac{L_f}{d_g}$$

agreement with the predicted model, especially for a bead diameter of 2 mm. When the bead diameter is 1.04 mm, however, a small difference between the model and data exists. This difference is probably caused by fiber orientation. This is due to the fact that if the fibers move parallel to the streamlines, penetration will be higher than the model predicts, since the model assumes random orientation.

The theoretical model was also tested by using one of the conditions of the experiments to investigate the validity of this fundamental model. The result was also compared with the semi-empirical model and further with experimental data, as shown in Figure 5.13.

From Figure 5.13 it is seen that the experimental data and the prediction of deposition efficiency of the semi-empirical model for all of the three orientations are much higher than that of the theoretical model. For parallel fiber orientation the predicted deposition efficiencies of the semi-empirical model increase very slowly for fiber lengths exceeding 10 μm. This behaviour is not difficult to explain, since increase of fiber length will obviously only slightly increase deposition efficiency for parallel orientation. For perpendicular fiber orientation, the effect of fiber length on interceptional deposition will obviously be much larger. For randomly oriented fibers the effect of fiber length on deposition will also be large. This is due to the rotation of the fibers; as they rotate they will most tend to intercept as they momentarily assume a perpendicular orientation. For shorter fibers, such as those with a length smaller than 10 μm, the semi-empirical model predicts that the difference of fiber deposition does not greatly depend on fiber orientation. Unfortunately, fibers with lengths greater than 10 μm could not be successfully dispersed in air. Therefore no experimental data is available to check the semi-empirical model for fiber length larger than 10 μm.
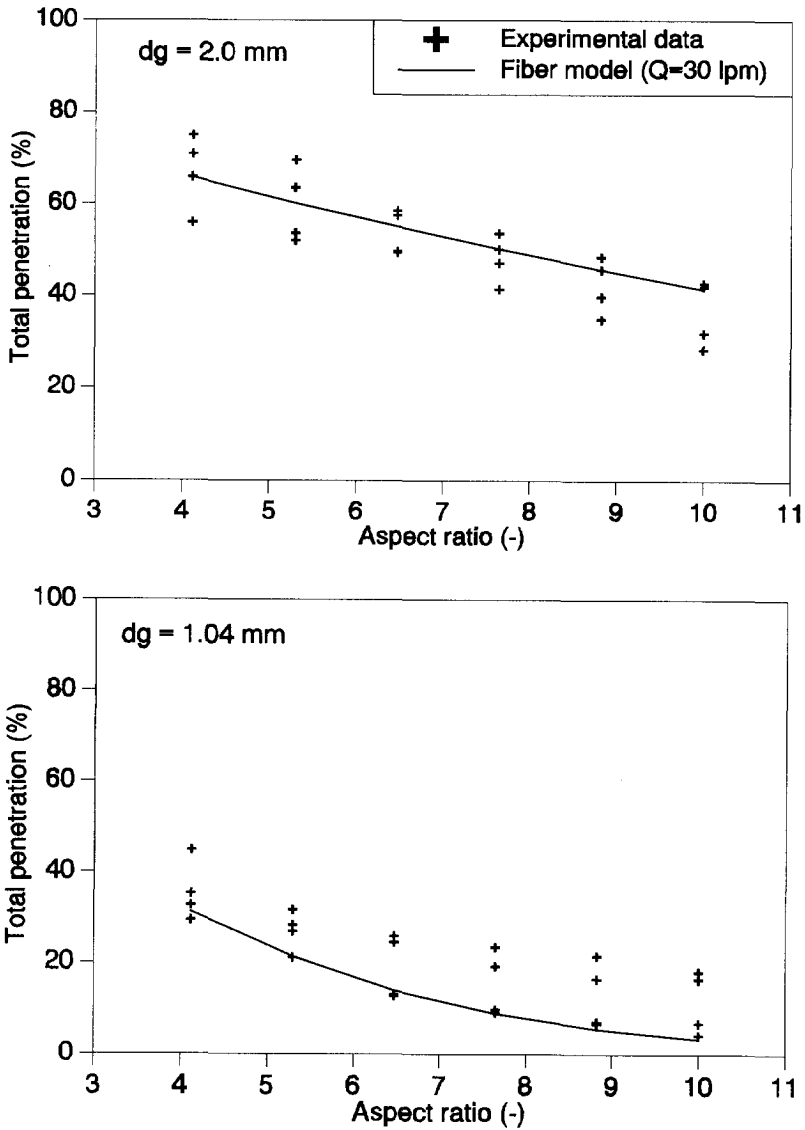
Figure 5.12A. *The total penetration versus fiber aspect ratio with a bed height of 17 cm and the system flowrate from 9 to 63 l/min for the fiber diameter of 0.85 μm.*
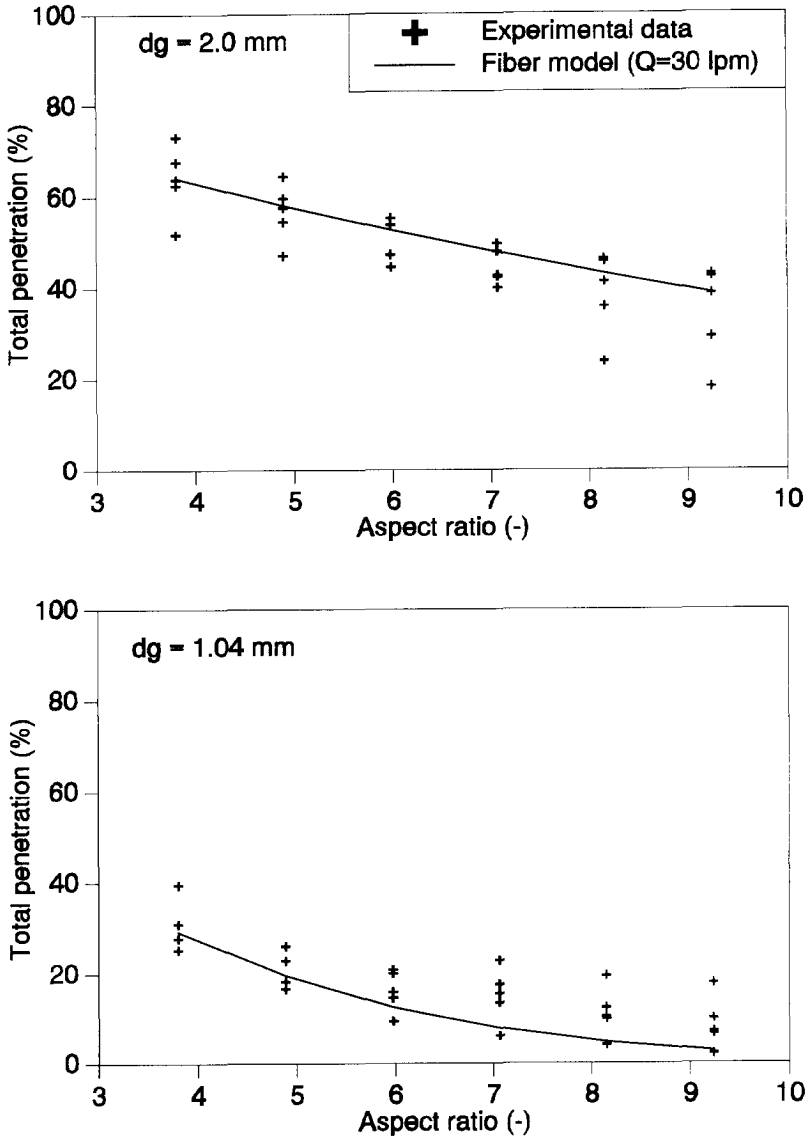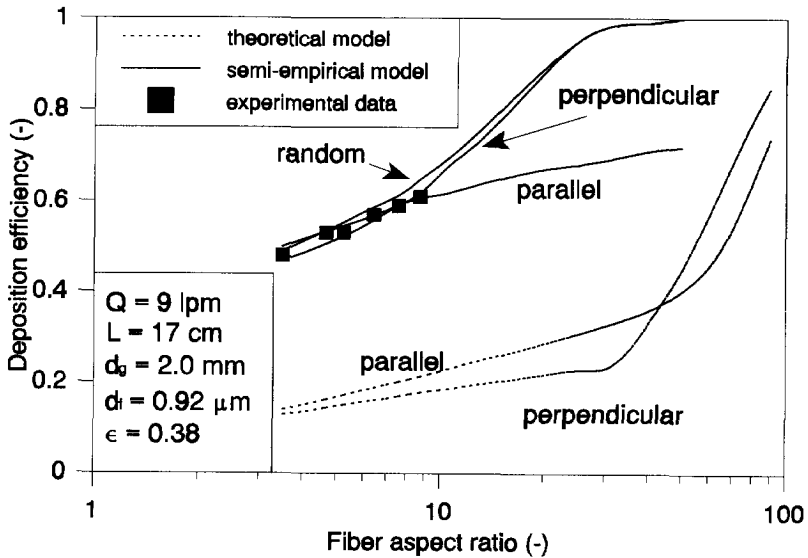
106

Figure 5.12B. *The total penetration versus fiber aspect ratio with a bed height of 17 cm and the system flowrate from 9 to 63 l/min for the fiber diameter of 0.92 μm.*

Figure 5.13. *Comparison of the theoretical model, the semi-empirical model, and the experimental data for fiber deposition in a granular bed filter.*

For the theoretical model, the calculation can only be done at very low bed superficial velocity. As already mentioned, the reason for this is that the calculation at a relatively high superficial velocity is extremely time-consuming. The theoretical model could therefore only be compared with the experimental data at a relatively low velocity, where few data are available. From this comparison, one can see that the theoretical model cannot be used to predict fiber deposition in granular beds.

Velocity in the human respiratory system varies between high and low values. The semi-empirical model can be used to predict deposition at these high and low velocities. As seen from Fig. 5.12 the semi-empirical model also predicts fiber deposition in a granular bed at high velocities well.

The purpose of the project has been to investigate fiber deposition in human lungs. In addition to comparison with experimental deposition data for fibers in a granular bed filter, the deposition model developed should also be compared with other existing lung deposition models for fibrous particles. In the literature the representative models for fiber deposition in lungs are the Asgharian (1988) model and the Harris (1972) model. Details of these two models are discussed in Appendix 5B and 5C. Figures 5.14 and 5.15 show the predictions of fiber deposition as a function of equivalent mass diameter of fibers (diameter of a sphere having the same mass as the fiber of interest) made by these two models in the alveolar region (generation 17 -23), compared with the fiber deposition model in a granular bed filter

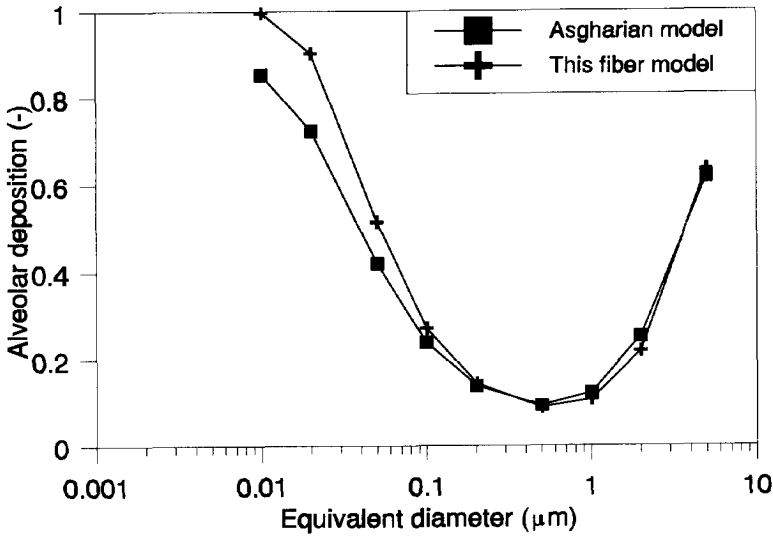**Figure 5.14**. *Alveolar fiber deposition for Asgharian model and granular lung model with a tidal volume of 1450 cm³ and a constant aspect ratio of 10.*
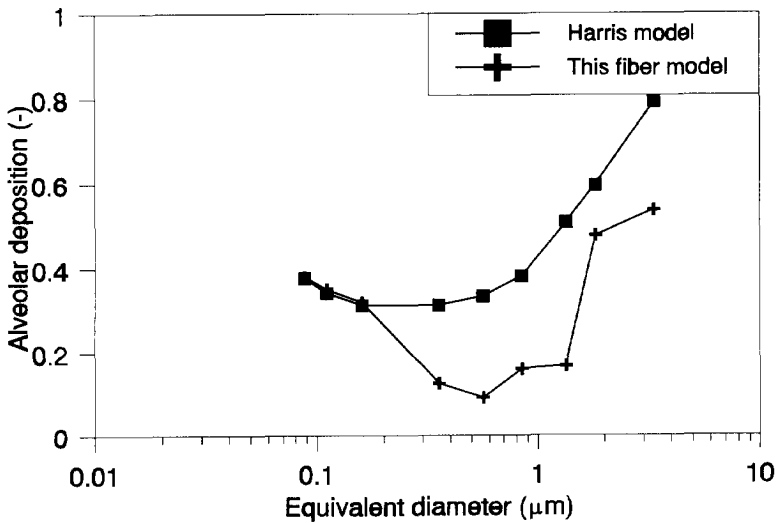

Figure 5.15. *Alveolar deposition for Harris model and granular lung model with a tidal volume of 1450 ml (fiber length varies from 0.5 to 25 µm and diameter from 0.03 to 1 µm in different combinations).*

corresponding to the same region of a human lung (the same fiber parameters as in the models of Asgharian and Harris have been used for the calculation). Note that Asgharian used the equivalent diameter with a constant aspect ratio of 10, and Harris used the equivalent diameter with various fiber lengths and diameters. These two equivalent diameter are therefore not comparable. It is seen from these figures that our fiber deposition model is in good agreement with the Asgharian model but less with the Harris model. We will discuss the reason in next section.

5.4.4 Discussion

The semi-empirical fiber deposition model for fiber deposition in a granular bed filter, based on individual deposition mechanisms, is in good agreement with the experimental data at various conditions. This model can be applied to the lower parts of the human lungs, as discussed in Chapter 3. In Figures 5.14 and 5.15 the semi-empirical model is compared with the existing fiber deposition models in the alveolar region of human lungs. From Figure 5.14, it is seen that our new fiber model applied to a granular bed lung model and the Asgharian model (1988) are comparable, especially when the equivalent diameter is larger than 0.1 μm. For small fibers, however, agreement is slightly less good. This occurs because for such small particles diffusion is the dominant mechanism effecting deposition. In our granular bed lung model, the surface area is larger than in corresponding airways of the human lung while the volumes are equal. The deposition in the granular bed model caused by diffusion mechanism are therefore greater than that in human lungs. In our simulation, however, it is impossible to equalize all dimensions of the two systems. When the granular lung model is compared with the Harris model, as shown in Figure 5.15, a large differences exist. One cannot say which model is better, since no experimental data for fiber deposition in the human lungs exist.

The only method which might be used to test the model is to compare the theoretical model with fiber deposition data from animal experiments. Asgharian (1988) developed his theoretical model for the rat lung structure and compared it with the experimental data of real rat lungs from Morgan et al. (1977); this is shown in Figure 5.16. One can see from the figure that the Asgharian model and this experimental data are in good agreement.

To further test our new semi-empirical model for fiber deposition in a granular bed filter, this model for fiber deposition should be simplified to relate to spherical particles. In principle a model developed for fibers should, upon simplification, also be suitable for sphere. Figure 5.17 shows the comparison of the model and the experimental data for spherical particles. The results are in good agreement. This is gratifying.

5.5 Conclusions

To investigate fiber deposition behaviour in both granular beds and human lungs, fiber transport behaviour in the airstreams must be known. For the fibers themselves, there are three main parameters affecting deposition: fiber length, fiber diameter and fiber orientation in the airstream. This chapter firstly discusses the calculation of the Stokes equivalent
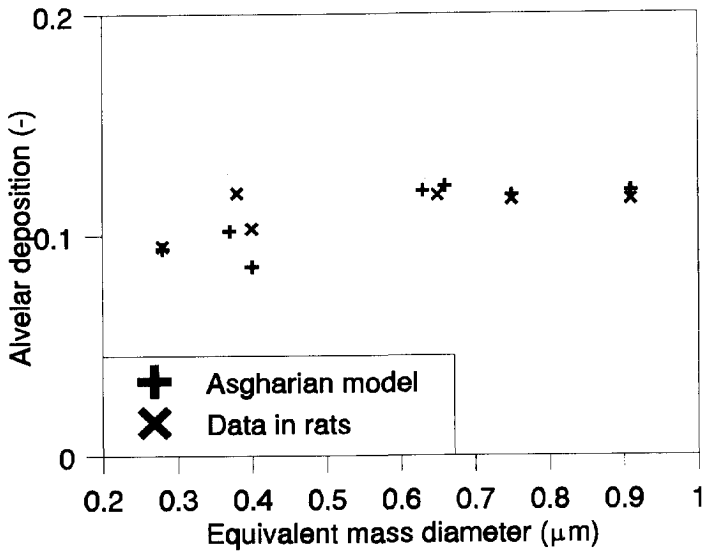
Figure 5.16. *Comparison between the Asgharian model and the experimental data from real rat lung (Asgharian, 1988).*

diameter of fibrous particles, which is used in the later calculation. However, this diameter could not replace fiber length and diameter, because one equivalent diameter represents many sets of the fiber length and diameters. The aspect radio must therefore be introduced. That is why we cannot combine Figures 5.14 and 15 into one figure, even when the fibers have the same equivalent diameter in the x-direction. Fiber orientation is very complicated. Fiber deposition obviously depends on orientation, and in order to solve the fiber deposition problem, orientation must be known. Fiber orientation in the human lung system and in granular bed filters is, however, unknown. Furthermore, the calculation of fiber deposition in a lung at any given orientation is extremely time-consuming. Therefore several assumption must be made to simplify the situation. In our discussion, fibers show the greatest tendency to alignment with air streamlines in a tube when the gas velocity is very low. This is the case in a tube of constant diameter. In the real lung the gas streams become disturbed at the junctures occurring at the different generations; vortexes are the result. In the case of granular bed filters, the direction of the streamlines also change from one generation to the next. For these reasons the orientation of fibers is assumed to be random in the granular bed. Four possible mechanisms by which fiber deposition occurs in human lungs are then introduced.

Because the aim of this project is to simulate the human lung system by using a granular bed filter, we present two models for fiber deposition in granular bed filters: a theoretical model and a semi-empirical model, the latter based on regression analysis of the experimental data. It is very difficult to compare all the experimental data, especially the data at high velocities, with the results of the theoretical model. This problem is due to the extremely long calculation times required by the theoretical model.

111
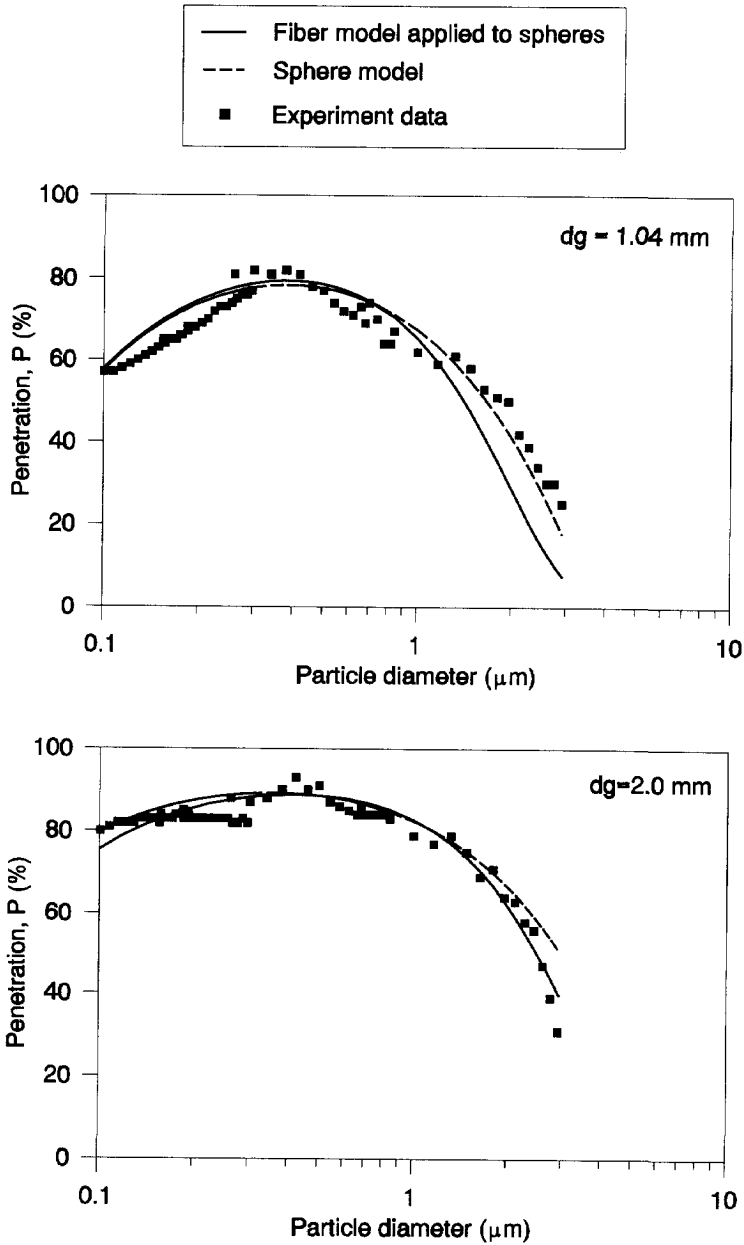
Figure 5.17. *Fiber deposition model used for spheres compared with the corresponding experimental data (Q = 50 lpm, L =17 cm).*

Therefore comparisons were made using experimental data at very low superficial velocities and relatively large fibers. No experimental data exist for larger fibers ($L_f > 10$ μm). It is found that a large difference exists between the models and thus also between the experimental data and theoretical model (see Figure 5.13). It can therefore be concluded that the theoretical model cannot be used for calculating fiber deposition in granular beds. The semi-empirical model is in good agreement not only with the experimental data, but also with the Asgharian lung deposition model at the same breathing conditions. It is unfortunate, however, that no experimental data for large fibers exist with which to check the semi-empirical model.

The Harris model and the semi-empirical model do not agree well. This difference may be caused by the assumptions made in the two models. More work should be done to more clearly investigate the reasons for this difference. It is to be noted that Asgharian et al. (1989a) modified their model for rat lungs and this resulting model agrees very well with the experimental data in rat lungs. It can be therefore concluded that the Asgharian model probably also should be a good model for predicting fiber deposition in human lungs.

As a last check of its validity, the semi-empirical model has been simplified to a spherical particle deposition model. As such it is used to calculate spherical particle deposition in granular bed filters. The agreement between the deposition predicted by this simplified version of the fiber deposition model with the experimental data of spherical particle deposition is good. This agreement further supports our belief that the semi-empirical model can be used for both spherical and fibrous particle deposition in granular bed filters.

Appendix 5A Experimental results for fibrous particles

Table 5A.1 shows the experimental results for glass fibers dispersed by the fluidized bed aerosol generator. Table 5A.2 shows the akaganeite fiber deposition results dispersed by a DeVilbiss 45 nebulizer. The particle concentration at the inlet and outlet of the granular bed filter was measured by a FM-7400 laser fiber monitor (MIE Inc., USA) and the differential mobility particle sizer, DMPS (TSI Inc., USA). The fiber length varies from 3.5 to 8.5 μm, and the diameter varies from 0.67 to 0.92 μm for glass fibers. For the akaganeite fibers there is only one size (i.e. L_f = 0.6 μm; d_f = 0.08 μm).

Table 5A.1. *The overall penetrations for glass fiber particles in the granular bed filter with a bed height of 17 cm.*

Q	d_g	L_f	d_f	P_F	Q	d_g	L_f	d_f	P_F	Q	d_g	L_f	d_f	P_F
lpm	mm	μm	μm	%	lpm	mm	μm	μm	%	lpm	mm	μm	μm	%
63	2.0	3.5	0.92	73.1	9	2.0	6.5	0.92	42.7	50	1.04	0.92	3.5	25.3
63	2.0	4.5	0.92	64.4	9	2.0	7.5	0.92	41.3	50	1.04	0.92	4.5	18.3
63	2.0	5.5	0.92	47.2	9	2.0	8.5	0.92	38.6	50	1.04	0.92	5.5	16.0
63	2.0	6.5	0.92	42.4	50	1.28	3.5	0.92	39.4	50	1.04	0.92	6.5	13.6
63	2.0	7.5	0.92	23.8	50	1.28	4.5	0.92	30.7	50	1.04	0.92	7.5	10.5
63	2.0	8.5	0.92	18.1	50	1.28	5.5	0.92	24.9	50	1.04	0.92	8.5	6.6
50	2.0	3.5	0.92	62.5	50	1.28	6.5	0.92	20.3	30	1.04	0.92	3.5	31.0
50	2.0	4.5	0.92	54.5	50	1.28	7.5	0.92	16.9	30	1.04	0.92	4.5	22.9
50	2.0	5.5	0.92	44.6	50	1.28	8.5	0.92	12.0	30	1.04	0.92	5.5	14.7
50	2.0	6.5	0.92	40.0	30	1.28	3.5	0.92	43.0	30	1.04	0.92	6.5	17.6
50	2.0	7.5	0.92	35.9	30	1.28	4.5	0.92	36.3	30	1.04	0.92	7.5	12.5
50	2.0	8.5	0.92	29.2	30	1.28	5.5	0.92	29.0	30	1.04	0.92	8.5	10.1
30	2.0	3.5	0.92	67.6	30	1.28	6.5	0.92	24.7	23	1.04	0.92	3.5	31.0
30	2.0	4.5	0.92	57.6	30	1.28	7.5	0.92	17.1	23	1.04	0.92	4.5	26.1
30	2.0	5.5	0.92	55.3	30	1.28	8.5	0.92	12.1	23	1.04	0.92	5.5	20.1
30	2.0	6.5	0.92	47.9	23	1.28	3.5	0.92	42.8	23	1.04	0.92	6.5	15.6
30	2.0	7.5	0.92	45.8	23	1.28	4.5	0.92	37.3	23	1.04	0.92	7.5	10.0
30	2.0	8.5	0.92	42.4	23	1.28	5.5	0.92	29.1	23	1.04	0.92	8.5	7.1
23	2.0	3.5	0.92	63.8	23	1.28	6.5	0.92	22.8	9	1.04	0.92	3.5	27.9
23	2.0	4.5	0.92	59.6	23	1.28	7.5	0.92	19.5	9	1.04	0.92	4.5	26.2
23	2.0	5.5	0.92	53.8	23	1.28	8.5	0.92	13.1	9	1.04	0.92	5.5	20.9
23	2.0	6.5	0.92	49.6	63	1.04	3.5	0.92	39.5	9	1.04	0.92	6.5	22.9
23	2.0	7.5	0.92	46.3	63	1.04	4.5	0.92	16.7	9	1.04	0.92	7.5	19.5
23	2.0	8.5	0.92	43.0	63	1.04	5.5	0.92	9.52	9	1.04	0.92	8.5	17.9
9	2.0	3.5	0.92	51.8	63	1.04	6.5	0.92	6.07	63	2.0	0.85	3.5	74.9
9	2.0	4.5	0.92	47.1	63	1.04	7.5	0.92	4.03	63	2.0	0.85	4.5	69.5
9	2.0	5.5	0.92	47.3	63	1.04	8.5	0.92	2.04	63	2.0	0.85	5.5	57.5

Table 5A.1. *Continued*

Q lpm	d_g mm	L_f μm	d_f μm	P_F %	Q lpm	d_g mm	L_f μm	d_f μm	P_F %	Q lpm	d_g mm	L_f μm	d_f μm	P_F %
63	2.0	6.5	0.85	50.1	30	1.28	3.5	0.85	48.9	9	1.04	6.5	0.85	23.4
63	2.0	7.5	0.85	34.9	30	1.28	4.5	0.85	42.7	9	1.04	7.5	0.85	21.6
63	2.0	8.5	0.85	28.4	30	1.28	5.5	0.85	32.1	9	1.04	8.5	0.85	18.2
50	2.0	3.5	0.85	65.8	30	1.28	6.5	0.85	28.9	63	2.0	3.5	0.67	80.4
50	2.0	4.5	0.85	53.6	30	1.28	7.5	0.85	26.2	63	2.0	4.5	0.67	74.3
50	2.0	5.5	0.85	49.3	30	1.28	8.5	0.85	24.6	63	2.0	5.5	0.67	70.8
50	2.0	6.5	0.85	41.4	63	1.04	3.5	0.85	44.9	63	2.0	6.5	0.67	67.0
50	2.0	7.5	0.85	39.8	63	1.04	4.5	0.85	26.8	63	2.0	7.5	0.67	56.0
50	2.0	8.5	0.85	31.9	63	1.04	5.5	0.85	13.2	63	2.0	8.5	0.67	53.8
30	2.0	3.5	0.85	70.8	63	1.04	6.5	0.85	9.95	9	2.0	3.5	0.67	62.8
30	2.0	4.5	0.85	63.5	63	1.04	7.5	0.85	6.77	9	2.0	4.5	0.67	59.6
30	2.0	5.5	0.85	58.5	63	1.04	8.5	0.85	4.24	9	2.0	5.5	0.67	53.9
30	2.0	6.5	0.85	53.6	50	1.04	3.5	0.85	29.3	9	2.0	6.5	0.67	51.0
30	2.0	7.5	0.85	48.5	50	1.04	4.5	0.85	21.1	9	2.0	7.5	0.67	49.7
30	2.0	8.5	0.85	42.7	50	1.04	5.5	0.85	12.9	9	2.0	8.5	0.67	45.0
9	2.0	3.5	0.85	55.9	50	1.04	6.5	0.85	9.2	63	1.04	3.5	0.67	55.4
9	2.0	4.5	0.85	52.0	50	1.04	7.5	0.85	7.2	63	1.04	4.5	0.67	38.7
9	2.0	5.5	0.85	49.6	50	1.04	8.5	0.85	6.9	63	1.04	5.5	0.67	22.2
9	2.0	6.5	0.85	47.1	30	1.04	3.5	0.85	35.2	63	1.04	6.5	0.67	15.2
9	2.0	7.5	0.85	45.7	30	1.04	4.5	0.85	31.6	63	1.04	7.5	0.67	10.9
9	2.0	8.5	0.85	42.0	30	1.04	5.5	0.85	25.8	63	1.04	8.5	0.67	4.65
50	1.28	3.5	0.85	40.9	30	1.04	6.5	0.85	19.3	9	1.04	3.5	0.67	42.9
50	1.28	4.5	0.85	30.1	30	1.04	7.5	0.85	16.7	9	1.04	4.5	0.67	36.4
50	1.28	5.5	0.85	21.7	30	1.04	8.5	0.85	16.6	9	1.04	5.5	0.67	28.9
50	1.28	6.5	0.85	16.4	9	1.04	3.5	0.85	32.6	9	1.04	6.5	0.67	31.2
50	1.28	7.5	0.85	13.8	9	1.04	4.5	0.85	28.2	9	1.04	7.5	0.67	27.0
50	1.28	8.5	0.85	10.4	9	1.04	5.5	0.85	24.4	9	1.04	8.5	0.67	23.3

Table 5A.2. *The overall penetrations for akaganeite fibers in the granular bed filter with a bed height of 17 cm (L_f = 600 nm; d_f = 80 nm).*

Q lpm	d_g mm		P_F (%)		Q lpm	d_g mm		P_F (%)	
10	2.0	81.8	79.9	78.9	10	1.04	57.3	58.9	55.8
30	2.0	86.2	84.9	86.6	30	1.04	68.8	70.5	72.0

115

Appendix 5B Asgharian model

In order to compute the regional and total deposition of fibrous particles in the lungs of humans and animals, Asgharian (1988) developed a mathematical fiber deposition model. This model describes the deposition efficiencies of four basic mechanisms: sedimentation, impaction, interception, and diffusion. The expressions for equivalent diameter of a fiber in each mechanism are also expressed in this model. A breathing cycle of this model consists of four intervals: inhalation, pause, exhalation, and pause. During inhalation, all four deposition mechanisms are active, thus superposition of the individual deposition efficiencies produces the net efficiency:

$$\eta_{net} = \overline{\eta}_S + \overline{\eta}_I + \overline{\eta}_R + \eta_D. \tag{5B.1}$$

The particle orientation in a flow situation is the result of a combined effect of shear flow forces and fluctuating Brownian motion forces acting on the particles. For all mechanisms, a deposition efficiency based on a linear combination of the expressions due to the two effects produces a good approximation. Thus,

$$\overline{\eta}_S = A_1 \overline{\eta}_{S,P} + A_2 \overline{\eta}_{S,R} = \overline{\eta}_{S,R}; \tag{5B.2}$$

$$\overline{\eta}_I = A_1 \overline{\eta}_{I,P} + A_2 \overline{\eta}_{I,R}; \tag{5B.3}$$

$$\overline{\eta}_R = A_1 \overline{\eta}_{R,P} + A_2 \overline{\eta}_{R,R}; \tag{5B.4}$$

$$\eta_D = A_1 \overline{\eta}_{D,P} + A_2 \eta_{D,R} = \eta_{D,R}, \tag{5B.5}$$

where A_1 and A_2 are constant coefficients. They are functions of the Peclet number, Pe, and a constant determined from the limits, A_0:

$$A_1 = \frac{\overline{Pe}}{\overline{Pe} + A_0}; \quad A_2 = \frac{A_0}{\overline{Pe} + A_0}. \tag{5B.6}$$

The subscriptions P and S, for the impaction and sedimentation, represent the deposition in pure shear flow and Brownian motion, and for interception and diffusion, represent the deposition due to periodic rotation and random orientation of particles.

The expressions of the four mechanisms for the fiber deposition in an airway are given below:

Sedimentation
The fiber orientation is random when the sedimentation angle is 38.24°. The sedimentation efficiency can be obtained by:

$$\overline{\eta}_{S,R} = \frac{2}{\pi}(2\varepsilon\sqrt{1-\varepsilon^{2/3}} - \varepsilon^{1/3}\sqrt{1-\varepsilon^{2/3}} + \arcsin\varepsilon^{1/3}),$$ (5B.7)

where

$$\varepsilon = \frac{3\overline{u}_g L C_f}{8UR}.$$ (5B.8)

Impaction

The impaction efficiencies effected by shear flow forces and Brownian motion forces can be expressed by the same equation if the impaction angle is 38.24°:

$$\overline{\eta}_{I,P \ or \ R} = 0.768\,\overline{Stk}\gamma; \quad with \ \gamma = \frac{L_z}{8R_z},$$ (5B.9)

Interception

The interception deposition in shear flow and in Brownian motion can be obtained by using different interception functions, $I(\phi,\theta)$, with the same formula:

$$\overline{\eta}_{R,P \ or \ R} = \frac{1}{2\pi}\int_{\phi=0}^{2\pi}\int_{\theta=0}^{\pi/2} I_{P \ or \ R}(\phi,\theta)\sin\theta\,d\theta d\phi.$$ (5B.10)

Diffusion

The expression for diffusion efficiency due to Brownian motion comes from Ingham (1975):

$$\eta_{D,R} = (1-0.819\exp(-14.63\Lambda)-0.097\exp(-89.22\Lambda)$$
$$-0.0325\exp(-228\Lambda)-0.0509\exp(-125.9\Lambda^{2/3})),$$ (5B.11)

where

$$\Lambda = \frac{L_z \overline{D}_t}{4UR_z^2}.$$ (5B.12)

117

Appendix 5C Harris model

In his PhD study, Harris (1972) developed a fiber deposition model in human lungs. His model identifies four mechanisms of particle deposition in the respiratory system: sedimentation, diffusion, impaction and interception. Fibers are represented by cylindrical rods.

Orientation

Ordered orientation is assumed when the angle of rotation is less than 10° during the time period required for an average particle in an airway to traverse half the length of the airway, e.g. $t_{10°} > t$ where

$$t = \frac{L_z}{2U}; \quad t_{10°} = \frac{3.58 \times 10^7 d_f^3 \beta_e^3}{\ln(2\beta_e) - 0.5},$$ (5C.1)

and

$$\beta_e = 1.07 \beta^{0.87}.$$ (5C.2)

The expressions for the deposition probabilities of the four mechanisms for laminar flow are given below:

Sedimentation laminar flow

$$S_p = \frac{2}{\pi} \left(C_1^{1/3} \sqrt{1 - C_1^{2/3}} - 2C_1 \sqrt{1 - C_1^{2/3}} + \sin^{-1} \sqrt{1 - C_1^{1/3}} \right),$$ (5C.3)

where

$$C_1 = 0.785 \frac{3U_t L_z}{8R_z U},$$ (5C.4)

and

$$U_t = \frac{\rho_f d_f^2 g}{8\mu \left(\dfrac{0.385}{\ln(2\beta) - 0.5} + \dfrac{1.23}{\ln(2\beta) + 0.5} \right)}.$$ (5C.5)

Because the airways are not horizontal, the value of the factor C_1 uses the value 0.785, which is the cosine of the average angle made with the horizontal by randomly oriented airways. A value of 1 or greater for C_1 indicates that all particles deposit.

Diffusion laminar flow

$$D_p = 1 - 4.07C_2^{2/3} + 2.4C_2 + 0.44C_2^{4/3} + \ldots \tag{5C.6}$$

for ordered orientation of the fibers:

$$C_2 = \frac{4.9 \times 10^{11} 2^z L_z (\ln(2\beta) + 0.5)}{V d_f \beta}, \tag{5C.7}$$

and for random orientation of the fibers:

$$C_2 = \frac{9.79 \times 10^{11} 2^z L_z}{V d_f \beta \left(\dfrac{0.385}{\ln(2\beta) - 0.5} + \dfrac{1.23}{\ln(2\beta) + 0.5} \right)}. \tag{5C.8}$$

Impaction laminar flow

$$I_{p,z+1} = 1 - \frac{2}{\pi}(3C_3^3 + C_3 + (1 - 2C_3^2 - 3C_3^4)\tan^{-1}\frac{1}{C_3}), \tag{5C.9}$$

for ordered orientation of the fibers:

$$C_3 = \frac{2R_z \mu}{d_f^2 U \sin\lambda (\ln(2\beta) + 0.5)}, \tag{5C.10}$$

and for random orientation of the fibers:

$$C_3 = \frac{2R_z \mu}{d_f^2 U \sin\lambda} \left(\frac{0.385}{\ln(2\beta) - 0.5} + \frac{1.23}{\ln(2\beta) + 0.5} \right). \tag{5C.11}$$

Very high accuracy and precision are necessary for accurate calculation of deposition with this equation because it involves finding very small differences between large numbers.

Interception laminar flow
For ordered orientation of the fibers:

$$C_d = \frac{1}{\pi R_{z-1}^4}(l_p^2 R_{z-1}^2 (\tan\theta_R - \theta_R) + \frac{l_p^4}{8}(\tan\theta_R - \frac{\tan^3\theta_R}{3} - \frac{\pi}{2}) + R_{z-1}^4(\pi - 2\theta_R)), \tag{5C.12}$$

where

119

$$\theta_R = \frac{\pi}{2} - \sin^{-1}\frac{l_p}{2R_{z-1}}, \tag{5C.13}$$

and

$$l_p = L_f\cos(\tan^{-1}(0.34\beta_e + \frac{0.68L_z}{R_{z-1}})). \tag{5C.14}$$

For "tumbling" particles ($-80° < \phi < 80°$):

$$T_d = \frac{f}{\pi R_{z-1}^4}(\theta_s^2 R_{z-1}^2(L_f^2+l_p^2) - \frac{\theta_s}{8}(L_f^4-l_p^4) - l_p^2(\tan\theta_s)(R_{z-1}^2+\frac{l_p^2}{8}) + \frac{l_p^4}{24}\tan^3\theta_s), \tag{5C.15}$$

where

$$f = \frac{2}{\pi}\tan^{-1}\frac{\tan\phi}{\beta_e}, \tag{5C.16}$$

and

$$\theta_s = \frac{\pi}{2} - \sin^{-1}\frac{l_p}{L_f}. \tag{5C.17}$$

Each of the foregoing expressions yields a probability for deposition by a particular mechanism for a particle which enters an airway. Thus, deposition upon inhalation in a non-alveolate airway may be expressed:

$$De_z = F_z(I_{max}+(1-I_{max})(S_d+D_d-S_dD_d)(1-\frac{V_zF_o}{2(V_T-V_r)})), \tag{5C.18}$$

where F_z is the particle balance for a non-alveolate airway as expressed:

$$F_z = De_z + S_z + F_{z+1}. \tag{5C.19}$$

The fraction of particles deposited upon inhalation in the airway of alveolate generation z may be expressed by:

$$De_z=F_z(I_{max}+(1-I_{max})(S_d+D_d-S_dD_d)(\frac{P_r}{P_a+S_d+D_d-S_dD_d}))(1-\frac{V_zF_o(1-\sum\limits_{i=17}^{z-1}n_i)}{2(V_T-V_r)}). \tag{5C.20}$$

6

Summary and conclusions

This thesis describes experimental and theoretical studies of fiber deposition in the human lung, the latter being modelled using a granular bed filter. The thesis is organized as follows.

A general introduction to fiber deposition and its importance is given in Chapter 1. Chapter 2 discusses particle deposition behaviour and the structure of the human respiratory system, the lung in particular. In discussing particle deposition, deposition mechanisms are very important. Generally speaking, particle deposition in the lung occurs through five mechanisms: inertial impaction, sedimentation, diffusion, interception, and deposition effected by electrostatic forces. Which mechanism is predominant depends on particle composition, particle size and shape, breathing rate, and the region of the lung in question. For large particles, heavy breathing results in deposition occurring predominantly by impaction in the upper regions of the lung. During light breathing, resulting in low air speeds in the lung, larger particles deposit through sedimentation in the lower parts of the lung. On the other hand, for small particles, deposition always tends to occur in the deepest part of the lungs, the alveolar region, and the deposition mechanism is predominantly diffusion (Brownian motion). The fourth mechanism, interception, is actually a kind of impaction occurring when a particle touches a surface. Interception is a more important deposition mechanism for fibers than for spherical particles. This is so because length and particle orientation relative to flow streamlines are meaningless for spherical particles, but of central importance to fibers. The last mechanism is deposition effected by electrostatic forces. However, due to the 100% relative humidity of the human lung, this mechanism is generally considered to be relatively unimportant. For this reason and also to simplify the experiments, deposition caused by electrostatic forces was made negligible by neutralizing fiber charge by means of a radioactive source.

Chapter 3 studies the possibility of using a granular bed filter to simulate the human respiratory system. Firstly, the structure of the granular bed filter is compared with the structure of the human lung. From this discussion it is concluded that it is acceptable to use a granular bed filter as a model for the human lung. A granular bed filter was therefore constructed. Using this filter, experiments were carried out to study the deposition of spherical particles. The results of these experiments were used to check existing models for spherical particle deposition in granular bed filters (models of Boulaud and Otani et al.). Unfortunately, these models were not in good agreement with our experimental data. We therefore developed a new model, based on a combination of various parts of the models of Boulaud and Otani

121

et al. This new model fits our experimental data for deposition in a granular bed filter well.

Since the project is focused on the lower parts of the human lung, the alveoli should also be considered for calculating the dimensions of a granular bed filter which is to model the human lung. For accurate simulation, the void volume and total cross section of the void per layer should therefore be equal to that of the corresponding airway generation. Meeting these criteria result in the same average velocities of the two systems in every generation of the lung. The layer height of the bed is also equal to the length of the corresponding airway generation. Subsequently, the residence times in the two systems are the same. The hydraulic diameter and the bead number of the bed per layer, however, cannot be made to correspond with the diameter and the number of lung tubes in each airway generation. This difference between the human lung and the granular bed filter causes the pressure drop and Reynolds number to be different in both systems. The surface area, another important parameter which affects particle deposition by diffusion, is also not the same in both systems. Fortunately, in the last two generations, which consists almost entirely of alveoli, the difference in the surface areas of the two systems is not large.

Chapter 3 also discusses flow patterns in the human lung. These are very complex. It is therefore difficult to draw hard conclusions concerning possible differences in flow patterns between both systems. For this reason only a superficial comparison of the two systems can presently be carried out. At the end of Chapter 3, the particle deposition model developed earlier for describing deposition in a granular bed filter was checked in a second way. It was now compared with other models (models of Landahl and Taulbee et al.) which are used to describe particle deposition in the human respiratory system. It was found that the calculated deposition in the last two generations of the granular bed lung model is larger than that predicted with the other models. The reason for this difference is that the alveoli are not included in the models of Landahl and Taulbee et al. Thus, the contributions to deposition in the last generations by diffusion and sedimentation mechanisms in the granular bed filter lung model are higher than that of other physical models of the human respiratory system. Finally, particle deposition for the human lung calculated with our model agrees well with the experimental data in real lungs for inhalation (see Figure 3.15).

Chapter 4 describes fiber production, dispersion, and fiber measurements. Four kinds of fibers were originally produced for the experiments: nylon-6 fibers, hydroxyapatite needles, akaganeite cigar-like crystals, and glass fibers. The first three are monodisperse (same diameter and length) while the last has almost the same diameter but varying length. Except for the hydroxy-apatite fibers, all the fibers could be successfully dispersed in air. The nylon-6 fibers, however, could only be dispersed to an insufficiently high concentration, a fact which rendered the sampling accuracy too low. Therefore only two kinds of fibers, glass fibers with lengths from 3.5 to 8.5 μm and diameters of 0.67, 0.85, and 0.92 μm and akaganeite fibers with a length of 600 nm and a diameter of 80 nm, were selected for the experiments for fiber deposition in granular bed filters. The fiber concentration measurements were carried out using a differential mobility particle sizer for akaganeite crystals and a laser fiber monitor for glass fibers.

Chapter 5 has the same structure as Chapter 3, except that in this latter chapter fibers rather

than spherical particles are discussed. Chapter 5 thus studies fiber deposition behaviour, both in granular beds and human lungs. Fiber transport in an airstream is firstly discussed by considering the fiber length and diameter and its orientation in the airstream. Next a fundamental theoretical model developed by Asgharian is introduced to express fiber deposition in the lungs by the various deposition mechanisms. Fiber orientation is explicitly accounted for in this model; indeed, in order to use the model, fiber orientation must be known. In reality, however, fiber orientation in the human lung system and in granular bed filters is unknown. It is therefore assumed in our study that the fibers are oriented randomly.

Chapter 5 also presents two new models developed especially to describe fiber deposition in the granular bed filter. These are a theoretical model, based on fundamental considerations, and a semi-empirical model, based on the experimental data. It is difficult to compare all the experimental data with the theoretical model, especially for high velocities, because the theoretical model requires long calculation times. For both the theoretical and the semi-empirical models, comparisons were obtained using experimental data for small fibers at very low superficial velocities (no experimental data exists for large fibers). Agreement between the theoretical model and the experimental data is poor. It is therefore concluded that the present theoretical model cannot be used for calculating fiber deposition in granular beds. The semi-empirical model, however, is in good agreement with the experimental data. This agreement relates not only to our own experimental data, but also to the Asgharian lung deposition model at the same breathing conditions. This is encouraging, since Asgharian modified his model for rat lungs and compared it to the experimental data; good agreement was found.

Compared with the Harris model, however, the semi-empirical model does not agree well. Only the deposition tendencies of the two models are the same. In the study of Asgharian, the Harris model was also compared; large differences also exist between these two models, especially in the alveolar region. In his thesis Asgharian explained that the differences are due basically to the use of different deposition efficiencies for each mechanism. Because the Asgharian model agrees well with experimental results for rats, it would seem that his model is usable.

In Chapter 5 an additional check was made of the semi-empirical model for fiber deposition. When this model is simplified to the case that the particles are spherical, it should also be capable of describing deposition behaviour of spherical particles in a granular bed. The semi-empirical model was thus modified, and it was indeed found that the model predicted the experimental results accurately. It can therefore be concluded that the semi-empirical model can be used for both spherical and fibrous particle deposition in granular bed filters.

In spite of this present work, more study should be done in the future for fibrous particle deposition in the human lung. For the diffusion mechanism, only one size of submicron fibers has been studied in this thesis. Therefore more studies are necessary using fibers over a range of submicron dimensions. Experiments for the fibers with lengths larger than 10 μm should be also carried out. Another factor which should be studied is the effect of particle composition on deposition. Lastly, the assumption that particle deposition effected by electrostatic forces is negligible should be checked.

123

Samenvatting en conclusies

Een model voor vezeldepositie in longen
Yue Zhou

Dit proefschrift beschrijft de resultaten van een experimenteel en theoretisch onderzoek naar de depositie van vezels in de menselijke longen, waarbij de menselijke long gemodeleerd is met behulp van een korrelbedfilter. Het proefschrift is als volgt ingedeeld.

Hoofdstuk 1 geeft een algemene inleiding van het vezeldepositievraagstuk en het belang hiervan. Hoofdstuk 2 beschrijft de depositie van deeltjes en de struktuur van de menselijke longen. In het algemeen spelen vijf mechanismen een rol bij de depositie van deeltjes in de long: impactie, sedimentatie, diffusie, onderschepping, en depositie onder invloed van electrostatische krachten. Welk mechanisme dominant is hangt af van de deeltjesgrootte, samenstelling en vorm, de ademhalingsfrequentie en het gedeelte van de long dat bestudeerd wordt. Voor grote deeltjes wordt de depositie bij een diepe ademhaling voornamelijk veroorzaakt door impactie in het bovenste gedeelte van de long, terwijl de depositie van deze deeltjes bij een lichte ademhaling, door de lage luchtsnelheden, vooral in een lager gedeelte van de long door sedimentatie optreedt. Voor kleine deeltjes vindt de depositie altijd voornamelijk plaats in het onderste gedeelte van de long, het gebied van de alveoli. Het depositiemechanisme is dan voornamelijk diffusie (Brownse beweging). Het vierde mechanisme, onderschepping is eigenlijk een soort impactie. Dit mechanisme treedt op als het deeltje het oppervlak raakt. Onderschepping is een belangrijker mechanisme voor vezels dan voor bolvormige deeltjes. De reden hiervan is dat de lengte en de deeltjesorientatie relatief ten opzichte van de stroming geen betekenis hebben voor bolvormige deeltjes, maar van groot belang zijn voor vezels. Het laatste mechanisme is depositie, veroorzaakt door electrostatische krachten. Dit mechanisme is echter in het algemeen van minder belang omdat de relatieve luchtvochtigheid in de menselijke long 100 % is. Hierom en om de experimenten eenvoudiger te maken, werden de vezels ontladen met behulp van een radioactieve bron, zodat de electrostatische krachten verwaarloosd kunnen worden.

Hoofdstuk 3 beschrijft het onderzoek naar de mogelijkheid een korrelbedfilter te gebruiken om de werking van het menselijke ademhalingssysteem te simuleren. De struktuur van het korrelbedfilter is vergeleken met de struktuur van de menselijke long. De conclusie is dat het mogelijk is om een korrelbedfilter te gebruiken als model voor de menselijke long. Een korrelbedfilter is gebouwd en gebruikt voor experimenteel onderzoek naar de depositie van bolvormige deeltjes. Met behulp van de resultaten zijn de bestaande modellen die de depositie van deze bolvormige deeltjes in korrelbedfilters beschrijven (Boulaud en Otani e.a.) gecontroleerd. Helaas kwamen experimentele en theoretische resultaten slecht met elkaar overeen. Daarom is er een nieuw model ontwikkeld door het combineren van onderdelen van het Boulaud model met onderdelen van het Otani model. Dit nieuwe model komt wel goed overeen met de experimentele data voor depositie in een korrelbedfilter.

Aangezien het project is gericht op het onderste gedeelte van de menselijke long, zijn de

afmetingen van de alveoli gebruikt voor de berekening van de afmetingen van het korrelbedfilter. Voor een goede simulatie moeten het volume van de lege ruimtes tussen de korrels en het totale oppervlak van de doorsnede van deze lege ruimtes even groot zijn als die van de lege ruimtes in de corresponderende positie in de long. Als aan deze voorwaarden voldaan zijn, dan is de gemiddelde snelheid als functie van de positie in beide systemen gelijk. De hoogte van een laag in het korrelbedfilter is ook even lang als een generatie van de luchtwegen in de menselijke long. Als gevolg hiervan is de verblijftijd in beide systemen aan elkaar gelijk. Echter, de hydraulische diameter en het aantal korrels per laag in het bed komen niet overeen met de diameter en het aantal van de longbuisjes in elke generatie van de luchtwegen. Dit verschil tussen korrelbedfilter en long veroorzaakt een verschil in drukval en een verschil in Reynoldsgetal voor de beide systemen. Ook het wandoppervlak van de lege ruimtes, een belangrijke parameter voor de depositie van deeltjes door middel van diffusie, is niet gelijk voor de beide systemen. In de laaste twee generaties van de luchtwegen, die bijna geheel uit alveoli bestaan, is dit verschil in oppervlak echter niet groot.

Hoofdstuk 3 beschrijft ook de stromingspatronen in de menselijke long. Vanwege de complexiteit van deze stromingspatronen is het moeilijk eenduidige conclusies te trekken over de mogelijke verschillen in stromingspatronen tussen de beide systemen. Daarom kan er nu alleen een oppervlakkige vergelijking tussen de beide systemen gemaakt worden. Het al eerder genoemde model voor de depositie van deeltjes in een korrelbedfilter wordt aan het eind van hoofdstuk 3, nog op een tweede manier gecontroleerd. Dit model wordt vergeleken met andere modellen uit de literatuur voor de depositie in de menselijke long (Landahl en Taulbee e.a.). Er is gevonden dat de depositie in de laatste twee lagen van het korrelbedfilter berekend met het nieuwe model hoger is dan berekend met de andere modellen. De reden van dit verschil is dat de alveoli niet zijn meegenomen in de modellen van Landahl en Taulbee e.a. Daarom zijn de bijdragen van de diffusie en sedimentatie in de onderste lagen van het korrelbedfilterlongmodel hoger dan in andere physische modellen van het menselijke ademhalingsorgaan. Tenslotte, de deeltjesdepositie in de menselijke long berekend met ons model komt goed overeen met experimentele resultaten voor de depositie van deeltjes in een echte long tijdens de ademhaling (zie figuur 3.16).

Hoofdstuk 4 beschrijft de productie, dispersie en meting van vezels. Vier soorten vezels werden oorspronkelijk gebruikt in de experimenten: nylon-6 vezels, hydroxy-apatite naalden, akaganeite sigaarvormige kristallen en glasvezels. De eerste drie waren monodispers zowel in lengte als diameter, terwijl de glasvezels wel ongeveer dezelfde diameters maar variabele lengtes hadden. Behalve de hydroxy-apatite vezels, konden alle vezels gedispergeerd worden in lucht. De maximale nylon-6 concentratie was echter te laag voor een betrouwbare meting. Daarom werden slechts de glasvezels met een lengte tussen 3,5 en 8,5 μm en met diameters van 0,67, 0,85 en 0.92 μm, en de akaganeite vezels met een lengte van 600 nm en een diameter van 80 nm gebruikt voor experimenteel onderzoek naar de depositie van van vezels in korrelbedfilters. De vezelconcentratie metingen zijn uitgevoerd met een 'differential mobility particle sizer' voor de sigaarvormige kristallen en een 'laser fiber monitor' voor de glasvezels.

Hoofdstuk 5 heeft eenzelfde structuur als hoofdstuk 3, met als verschil dat nu de depositie van vezels wordt beschreven in plaats van de depositie van bolvormige deeltjes. Hoofdstuk

5 beschrijft dus de depositie van vezels in zowel het korrelbedfilter als in de menselijke long. Het transport van vezels door een luchtstroom wordt eerst beschreven aan de hand van de lengte, de diameter en de orientatie van de vezel in de luchtstroom. Daarna wordt een fundamenteel theoretisch model van Asgharian geintroduceerd. Dit model wordt gebruikt om te laten zien welke mechanismen een rol spelen bij de depositie van vezels in de long. Waarbij uitdrukkelijk rekening wordt gehouden met de vezelorientatie. Echter de vezelorientatie in de menselijke long en in het korrelbedfilter is niet bekend. Er is daarom in dit onderzoek aangenomen dat de vezelorientatie 'random' is.

Hoofdstuk 5 beschrijft ook twee nieuwe modellen die speciaal ontwikkeld zijn voor de beschrijving van de depositie van vezels in korrelbedfilters. het ene is een theoretisch model gebaseerd op fundamentele overwegingen en het andere een semi-empirisch model gebaseerd op experimentele resultaten. Het is moeilijk om het theoretische model, vooral voor hoge luchtsnelheden, te vergelijken met experimentele resultaten, omdat dit model lange rekentijden met zich meebrengt. Zowel het theoretische als het semi-empirische model zijn vergeleken met experimentele resultaten voor kleine vezels en lage superficiële snelheden. (er bestaan geen resultaten voor grote vezels). De resultaten van het fundamenteel theoretische model komen niet goed overeen met de experimentele resultaten. De conclusie is daarom dat het huidige fundamenteel theoretische model niet gebruikt kan worden voor de berekening van de vezeldepositie in korrelbedfilters. De resultaten van het semi-empirische model komen echter zeer goed overeen met de experimentele resultaten. Dit semi-empirische model komt ook zeer goed overeen met het Asgharian model voor dezelfde ademhaling. Dit is bemoedigend, omdat Asgharian zijn model heeft aangepast voor ratten en de resultaten heeft vergeleken met experimentele resultaten. Hij vond een goede overeenkomst tussen beide.

Het semi-empirisch model wordt ook vergeleken met het Harris model, maar deze modellen komen niet goed overeen. Alleen de depositie trends komen met elkaar overeen. Ook Asgharian vergeleek zijn model met dat van Harris. Hij vond grote verschillen tussen de twee modellen, vooral in het gebied van de alveoli. In zijn proefschrift verklaarde Asgharian de verschillen tussen de beide modellen uit de verschillen in depositie efficiëntie van elk depositie mechanisme afzonderlijk. Daar het Ashgarian model goed overeenkomt met experimentele resultaten voor ratten, lijkt het goed bruikbaar.

In hoofdstuk 5 wordt ook nog een extra controle van het semi-empirisch model voor de depositie van vezels beschreven. Het model wordt vereenvoudigd voor het geval van bolvormige deeltjes. In dat geval zou het dan het gedrag van deze bolvormige deeltjes in een korrelbedfilter moeten beschrijven. Na deze aanpassing bleek het model de experimentele resultaten voor bolvormige deeltjes goed te voorspellen. De conclusie kan daarom worden getrokken dat het semi-empirische model zowel gebruikt kan worden voor de depositie van bolvormige deeltjes als van vezels in korrelbedfilters.

Meer onderzoek is nodig naar de depositie van vezels in de menselijke long. In dit onderzoek is slechts één soort vezel kleiner dan een micrometer gebruikt voor het onderzoek van het diffusie mechanisme. Meer onderzoek is daarom nodig met een reeks van vezels met verschillende afmetingen kleiner dan een micrometer. Ook moeten er experimenten uitgevoerd worden met vezels langer dan tien micrometer. Een ander aspect dat moet worden onderzocht

is het effect van de deeltjes samenstelling. Tenslotte moet de aanname, dat de electrische krachten te verwaarlozen zijn, onderzocht worden.

Symbol list

A	cross section area of a bed [cm^2]
$A_{s,layer\ or\ z}$	internal surface area of a layer or an airway generation [cm^2]
$A, A_1(\varepsilon, Re)$	function of ε and Re [-]
a	constant related to limited diameters of the tube [-]
B	mechanical mobility [s/g]
B(Re)	function of Re [-]
C_d	fraction of fibers leaving generation z which deposit at the bifurcation entering generation z+1 [-]
C_p, C_f	Cunningham slip correction factor for particles and fibers [-]
D	Brownian diffusion coefficient
D_d	probability for deposition by diffusion of a particle in generation z [-]
De_z	fraction of all inhaled particles which deposit in generation z [-]
D_p	fraction of particle entering an airway which escape deposition by diffusion [-]
D_r	Brownian diffusion coefficient for rotation [cm^2/s]
$D_t, \overline{D_t}$	general and average translational Brownian diffusion coefficient [cm^2/s]
D_z	airway diameter [cm]
d_e	size of a spherical void of volume equal to the pore volume of a unit-cell (Ch3) [cm]
d_e	settling velocity equivalent diameter of a fiber (Ch5) [cm]
d_{em}	mass equivalent diameter [cm]
$d_{e\parallel,\perp,r}$	Stokes equivalent diameter of fiber falling with major axis parallel, perpendicular and random to direction of motion [cm]
d_f	fiber diameter [cm]
d_g	bead diameter [cm]
d_h	hydraulic diameter [cm]
$d_{max,min}$	maximum and minimum tube diameters in PCT model [cm]
d_p	diameter of particles [μm]
d_v	diameter of the largest interstitial bead possible [cm]
E	electrical field strength or intensity (Ch3) [stV/cm]
E	the total efficiency of the filter (Ch5) [-]
E_{UC}	unit cell collection efficiency [-]
e	charge on an electron [4.8×10^{-10} stC]
$\mathbf{F}_B$	Basset force vector [dyn]
$\mathbf{F}_D$	drag force vector [dyn]
F_E	electrical force on the particle [dyn]
$\mathbf{F}_e$	external force vector [dyn]
F_g	gravitational force [dyn]
$\mathbf{F}_I$	inertial force vector [dyn]
F_o	fraction of outside air remaining in generation z at the end of inhalation [-]
$\mathbf{F}_P$	pressure gradient force vector [dyn]
$\mathbf{F}_S$	stochastic force vector [dyn]
F_s	viscous drag force [dyn]
$\mathbf{F}_V$	virtual mass force vector [dyn]
F_z	faction of all inhaled particles which enter generation z from generation z-1 or z+1 [-]
f	collision factor (Ch3) [-]
f	drag force per unit velocity on the particle (Ch5) [g/s]

f	fraction of suspended fibers in process of tumbling (App 5C) [-]
f'	drag force per unit velocity in the continuum regime [g/s]
$f_{1,2}(Re)$	functions of Re [-]
$f_{i,s}$	drag force per unit velocity on the fiber in the parallel and vertical direction of the flow [g/s]
Grv	gravity number [-]
g	gravitational acceleration [dyn.cm/s^2]
g_{xi}	unit vector of the gravity field orientation [-]
H_{layer}, h	the height of a layer and the height of a unit cell [cm]
$I(\phi,\theta)$	interception function [-]
I_{max}	the greater of the probabilities for deposition by impaction or interception at the bifurcation at entrance to generation z [-]
k	Boltzmann constant [dyn.cm/K]
K_1	constant for total particle penetration [-]
L	the height of the bed [cm]
L_e	entry length [cm]
L_f	fiber length [cm]
L_z	length of airway [cm]
l	length of periodicity [cm]
l_p	mean length of projection of fibers on plane normal to tube axis [cm]
$I_{p,z+1}$	fraction of particle leaving airway generation z which escape deposition by impaction in airway z+1 [-]
m	mass of the particle [g]
N_g	number of beads in a layer [-]
N_{UBE}	number of unit bed element [-]
N_{UC}	number of unit cell [-]
N_z	number of airways in generation z [-]
n_p	units of charge [-]
n_z	fraction of all alveoli which are in generation z [-]
P, P_1	pressure drop of the bed and of the unit bed element [dyn/cm^2]
$P(\phi,\theta,t,r^*)$	fiber orientation distribution function [-]
P_a	probability that a particle entering generation z and escaping deposition by interception or impaction will reach the entrance to an alveolus of that generation [-]
Pe	Peclet number [-]
P_F, P_S	total penetration for fibers and for spheres [-]
P_r	compound probability of a particle in generation z being deposited by diffusion or sedimentation on reaching the entrance to an alveolus [-]
Q	total flowrate in the experiments [L/min]
R	dimensionless parameter related to the radius of the tube [-]
Re	Reynolds number [-]
$Re_{0,s}$	Reynolds number referred to u_0 and u_s [-]
R_i	interception parameter [-]
$R_{i\parallel,\perp,r}$	interception parameter for parallel, perpendicular, and random oriented fibers [-]
R_z	radius of airway generation z [cm]
r	radial distance from the axis of an airway or a unit cell of beds [cm]
r^*	defined as r/R_z for an airway and r/h for a unit cell [-]
r_0	average radius of the tube [cm]
r_{LT}	distance between the center of the tube inlet and starting point of the limiting trajectories [cm]

130

r_s	radius of spherical particle [cm]
$r_{s\parallel}$, $r_{s\perp}$	equivalent spherical radius of fiber falling with major axis parallel and perpendicular to direction of motion [cm]
r_w	variation of the tube wall radius [cm]
$S(alveoli)_z$	Total cross section of alveoli (cm^2)
Sc	Schmidt number [-]
S_d	probability of deposition by sedimentation of a particle in generation z [-]
S_{layer}	total cross section of air space in a layer [cm^2]
S_p	fraction of particles entering an airway which escape deposition by sedimentation [-]
$Stk, \overline{Stk}, Stk_{eff}$	general, average, and effective Stokes number [-]
S_{UC}	surface area of a unit cell [cm^2]
S_z	total cross section of air space in a airway generation (Ch3) [cm^2]
S_z	fraction of all inhaled particles which remain suspended in generation z at end of inhalation (App 5C) [-]
s	distance measured along the longest main axis [cm]
T	absolute temperature [K]
T_d	fraction of fibers which deposit by interception because of tumbling in airway generation z [-]
t	time [s]
t^*	dimensionless time [-]
$t_{10°}$	the time interval when the angle of rotation is 10° by Brownian motion [s]
$t_{r,layer}$	residence time in a layer [s]
$t_{r,z}$	residence time in a airway generation [s]
U	average velocity of airway or interstitial velocity in bed layer [cm/s]
U_{layer}	average speed of a layer [cm/s]
U_{mf}	minimum fluidization velocity [cm/s]
U_t	average terminal settling velocity for randomly oriented fibers [cm/s]
U_z	average speed of a airway generation [cm/s]
u_0	average velocity at the tube's constriction (Ch3) [cm/s]
u_0	velocity calculated for the radius of the wall r_0 (Ch5) [cm/s]
$u_g, \bar{u}_g$	general and average settling velocity of a particle [cm/s]
$u_r; u_x$	velocities with the r and x directions [cm/s]
$u_r^*; u_x^*$	dimensionless velocities with the r and x directions [-]
u_s	superficial velocity of the bed [cm/s]
V	volume of particle [cm^3]
$V(alveoli)_z$	Total space volume of alveoli [cm^3]
V_b	volume of the beads [cm^3]
V_{gtot}	total void volume of beads in a layer [cm^3]
V_{layer}	total volume of a layer [cm^3]
V_r	volume of outside air retained at the end of inspiration in all airspaces preceding generation z [cm3]
V_T	respiratory tidal volume [cm^3]
V_{TE}	terminal electrostatic velocity [cm/s]
V_{UC}	void volume of a unit cell [cm^3]
V_{vtot}	total void volume per layer [cm^3]
$v_{xi}^{(0)}$	Cartesian elements of the vectors of velocity of particle mass-center [cm/s]
V_z	total volume in generation z [cm^3]
W	total weight of beads [g]
X	dimensionless axial distance defined as $2\pi x/h$

Symbol list

x	axial distance [cm]
x*	dimensionless x, defined as x/h [-]
$x_i^{(0)}$	Cartesian elements of the vectors of position of particle mass-center [cm]
Y	function of Re [-]
Z_p	electrical mobility [cm^2/stV.s]
z	airway generation [-]
α	angle between the line connecting the center of the fiber to the center of the airway cross section and the horizontal [-]
β	aspect ratio of fiber defined as L_f/d_f [-]
$β_e$	empirical equivalent β for cylinder fibers defined as eq. 5C.2 [-]
δ,ξ	defined as r_0/d_g and x/d_g [-]
ε	porosity of the granular bed filter [-]
$ε_{mf}$	bed porosity at U_{mf} [-]
η	defined as 1+acosX [-]
η'	single sphere collection efficiency of a unit cell [-]
$η_T$	single sphere collection efficiency for particles [-]
$η_i$	fiber deposition efficiency by interception in a laminar flow (Ch5) [-]
$η_i ... η_n$	single sphere collection efficiency for various mechanisms (Ch3) [-]
$η_I,η_D,η_S,η_R$	single sphere collection efficiencies for impaction, diffusion, sedimentation, and interception [-]
$η_p$	single sphere collection efficiency for predominant mechanism [-]
θ	Eulerian angle, shown in figure 5.1 [-]
$θ_R$	defined by eq. 5C.13
$θ_s$	defined by eq. 5C.17
λ	angle between initial and final directions of fluid flow at bifurcation [°]
μ	viscosity of fluid [g/cm.s]
$ρ_0$	unit density [g/cm^3]
$ρ_b$	density of the beads [g/cm^3]
$ρ_f$	fiber density [g/cm^3]
$ρ_g$	gas density [g/cm^3]
$ρ_p$	particle density [g/cm^3]
τ	particle relaxation time [s]
φ	Eulerian angle, shown in figure 5.1 [-]
χ	shape factor [-]
$χ_i,χ_s$	dynamic shape factor oriented at angle $ψ_i$ and $ψ_s$ [-]
$ψ_i,ψ_s$	impaction and sedimentation angles [-]
ω	angular velocity of fiber rotation [rps]
∇P	gradient pressure [dyn/cm^2]

Bibliography

Altshuler, B., Palmes, E.D., Yarmus, L., and Nelson, N. (1959a)
> Intrapulmonary mixing of gases studied with aerosols, *J Appl. Physiol.*, 14: 321-327

Altshuler, B. (1959b)
> Calculation of regional deposition of aerosol in the respiratory tract. *Bull. Math. Biophys*, 21: 257-270

Asgharian, B. (1988)
> *The deposition of fibrous particles in the respiratory tract using a mathematical model*, PhD dissertation, Suny, Buffalo N.Y.

Asgharian, B. and Yu, C.P. (1988)
> Deposition of inhaled fibrous particles in the human lung, *J Aerosol Med.*, 1: 37-50

Asgharian, B., Yu, C.P., and Gradon, L. (1988)
> Diffusion of fibers in a tubular flow, *Aerosol Sci. & Technol.*, 9, p213-219

Asgharian, B. and Yu, C.P. (1989a)
> Deposition of fibers in the rat lung, *J Aerosol Sci,* 20: 355-366

Asgharian, B. and Yu, C.P. (1989b)
> A simplified model of interceptional deposition of fibers at airway bifurcations, *Aerosol Sci. & Technol.*, 11, p80-88

Beekmans, J.M. (1970)
> The deposition of asbestos particles in the human respiratory tract, *Int. J Environ. Stud.*, 1: 31-34

Bilius, M. (1989)
> *Lung models*, report, Delft University of Technology

Bouhuys, A. (1974)
> *Breathing*, Grune & Stratton, New York

Boulaud, D. (1991)
> Use of granular beds in the inertial impaction regime for aerosol size distribution measurement, *J. Aerosol Sci.*, 22, 273-287

Brown, J.H. et al., (1950)
> Influence of particle size upon the retention of particulate matter in the human lung, *Am. J Public Health*, 40: 450-458

Bugosh, J. (1959)
> *Fibrous alumina monohydrate and its production*, US Pat. No. 2915475

Buining, P.A., Pathmamanoharan, C., Jansen, J.B.H., and Lekkerkerker, H.N.W. (1991)
> Preparation of colloidal boehmite needles by hydrothermal treatment of aluminum alkoxide precursors, *J. Am. Ceram. Soc.*, 74, p1303-1307

Chow, J.C.F. and Soda, K. (1972)
> Laminar flow in tube with constriction, *Phys. Fluids.*, 16, 1700-1706

Clift, R., Ghadiri, M., and Thambimuthu, K.V. (1981)
> Filtration of gases in fluidized beds, in Progress in *Filtration and separation*, vol. II, Wakeman, R.J. Ed., Elsevier, Amsterdam

Corrsin, S. and Lumley, J. (1956)
> On the equation of motion for a particle in turbulent fluid, *App. Sci. Res.*, 6A, 114-128

Chissick, S.S. and Derricott, R. (1983)
> *Asbestos. Vol. 2. Properties, applications, and hazard*, Wiley, Chichester.

Davies, C.N. (1949)

Inhalation risk and particle size in dust and mist, *Br. J Ind. Med.*, 6: 245-253

Davies, C.N. (1961)

A formalize anatomy of the human respiratory tract, *Inhaled Particles and Vapours,* ed. C.N. Davies, 82-87

D'Ottavio, T. and Goren, S. (1983)

Aerosol capture in granular beds in the impaction dominated regime, *Aerosol Sci. Technol.,* 2, 91-108

Egan, M.J. and Nixon, W. (1985)

A model of aerosol deposition in the lung for use in inhalation dose assessments, *Radiat. Prot. Dosim.*, 11: 5-17

Ergun, S. (1952)

Fluid flow through packed columns, *Chem. Engng Progr.,* 48, 89-94

Fayed, M.E. and Otten, L. (1984)

Handbook of Powder Science and Technology, Van Noster and Reinhold Company, New York

Ferron, G.A. (1976)

On the deposition of aerosols in the human airways, PhD thesis, TU Delft, Delft University Press

Ferron, G.A., Hornik, S., Kreyling, W.G., and Haider, B. (1985)

Comparison of experimental and calculated data for the total and regional deposition in the human lung, *J Aerosol Sci.,* 16: 133-143

Findeisen, W. (1935)

Über das absetzen kleiner, in der Luft suspendierten Teilchen in der Menchlichen Lunge bei der Atmung, *Arch. Ges. Physiol.,* 236, 367-379

Foord, N., Black, A., and Walsh, M. (1978)

Regional deposition of 2.5-7.5 µm diameter inhaled particles in healthy male non-smokers, *J Aerosol Sci.,* 9: 343-357

Gal, E., Tardos, G.I., and Pfeffer, R. (1985)

A study of inertial effects in granular bed filtration, *AIChE J.,* 31, 1093-1104

Gebhart, J. and Heyder, J. (1985)

Removal of aerosol particles from stationary air within porous media, *J. Aerosol Sci.,* 16, 175-187

Gerrity, T.R., Lee, P.S., Haas, F.J., Marinelli, A., Werner, R., and Laurenco, R.V. (1979)

Calculated deposition of inhaled particles in the airway generations of normal subjects, *J. Appl. Physiol.: Respirat. Environ. Exercise Physiol.* 47 (4), 867-873

Gonda, I. and Khalik, A.F. Abd El, (1985)

On the calculation of aerodynamic diameters of fibers, *Aerosol Sci. and Tech.,* 4, p233-238

Gormley, P.G. and Kennedy, M. (1949)

Diffusion form a stream flowing through a cylindrical tube, *Proc. Roy. Irish Acad.* 52A, 163-169

Gradon, L. and Orlicki, D. (1990)

Deposition of inhaled aerosol particles in a generation of the tracheobronchial tree, *J Aerosol Sci.,* 21: 3-19

Gray, W.A. (1968)

Packing of solid particles, Chapman-Hall, London

Gurman, J.L., Lippmann, M., and Schlesinger, R.B. (1984)

Particle deposition in replicate casts of the human upper tracheobronchial tree under constant and cyclic inspiratory flow. I. Experimental, *Aerosol Sci. Technol.,* 3, 245-252

Hammad, Y., Diem, J., Craighead, J., and Weill, H. (1982)
Deposition of inhaled man-made mineral fibers in the lung of rats, *Ann. Occup. Hyg,* 26(suppl): 179-187

Happel, J. (1958)
Viscous flow in multiparticle systems: slow motion of fluids relative to beds of spherical particles, *AIChE J.,* 4, 197-201

Harris, R.L. Jr. (1972)
A model for deposition of microscopic fibers in the human respiratory system, PhD Dissertation, Univ. of North Carolina at Chapel Hill.

Harris, R.L. and Fraser, D.A. (1976)
A model for deposition of fibers in the human respiratory system, *Am. Ind. Hyg. Assoc. J.,* 39, 73-89

Hatch, T. and Hemeon, W.C.L. (1948)
Influence of particle size in dust exposure, *J Ind. Hyg. Toxicol.,* 30: 172-180

Heyder, J., Armbruster, L. Gebhart, J. Grein, E., and Stahlhofen, W. (1975)
Total deposition of aerosol particles in the human respiratory tract for nose and mouth breathing, *J Aerosol Sci.,* 6: 311-328

Heyder, J., Gebhart, J., Roth, C., Stahlhofen, W., Stuck, B., Tarroni, G., de Zaiacomo, T., Formignani, M., Melamdri, C., and Prodi, V. (1978)
Intercomparison of lung deposition data for aerosol particles, *J. Aerosol Sci.,* 9, 147-155

Heyder, J., Gebhart, J., and Stahlhofen, W. (1980)
Inhalation of aerosols: particle deposition and retention, In: Willeke K, ed. *Generation of aerosols and facilities for exposure experiments.* Ann Arbor, MI: Ann Arbor Science Publications, 65-103

Heyder, J., Gebhart, J., Rudolf, G., Schiller, C.F., and Stahlhofen, W. (1986)
Deposition of particles in the human respiratory tract in the size range 0.005-15 µm, *J Aerosol Sci.,* 17: 811-825

Heyder, J. (1986)
Single-particle deposition in human airways, in *Physical and chemical characterization of individual airborne particles,* (Ed. K.R. Spurny) Ellis Horwood Limited, 72-85

Hinds, W. (1982)
Aerosol Technology, John Wiley & Sons, New York

Hinze, J.O. (1975)
Turbulence, 2nd ed., Mcgraw-Hill, New York

Hirst, E., Kaye, P.H., Buckley, K.M., and Saunders, S.J. (1995)
A method for investigating the orientational behaviour of fibrous particles in gaseous flow, *Part. Part. Syst. Charact.,* 12, p3-9

Hofmann, W. and Koblinger, L. (1990)
Monte Carlo modelling of aerosol deposition in human lungs. Part II: Deposition fractions and their sensitivity to parameter variations, *J Aerosol Sci.,* 21: 675-688

Johnson, R.E. (1980)
An improved slender-body theory for Stokes flow, *J. Fluid. Mech.,* 99, 411-431

Johnston, J.R., Isles, K.D., and Muir, C.F. (1977)
Inertial deposition of particles in human branching airways, *Inhaled Particles IV,* Vol. 1, Pergamon Press, Oxford

Jongh, F.H.C., de (1995)
Ventilation modelling of the human lung, PhD thesis, Delft University of Technology

Keady, P.B., Quant, F.R., and Sem, G.J. (1983)
> Differential mobility particle sizer: a new instrument for high-resolution aerosol size distribution measurement below 1 µm, *TSI Quartery,* Vol. IX, Issue 2

Koblinger, L. and Hofmann, W. (1990)
> Monte Carlo modelling of aerosol deposition in human lungs. Part I: Simulation of particle transport in a stochastic lung structure, *J Aerosol Sci.,* 21: 661-674

Landahl, H.D. and Herrmann, R.G. (1948)
> On the retention of air-borne particulate in the human lung. *J Ind. Hyg.,* 30: 181

Landahl, H.D. and Herrmann, R. (1949)
> Sampling of liquid aerosols by wires, cylinders, and slides, and the efficiency of impaction of the droplets, *J. Colloid Sci.,* 4, 103-136

Landahl, H.D. (1950)
> On the removal of airborne droplets by the human respiratory tract: I. The lung, *Bull. Math. Biophys.,* 12 (1950) 43-56

Landahl, H.D., Tracewell, T.N., and Lassen, W.H. (1951)
> On the retention of airborne particulate in the human lung: II. *Arch. Ind. Hyg.,* 3: 359-366

Landahl, H.D., Tracewell, T.N., and Lassen, W.H. (1952)
> Retention of airborne particulate in the human lung: III. *Arch. Ind. Hyg.,* 6: 508-511

Lee, K.W. (1980)
> Maximum penetration of aerosol particles in granular bed filters, *J. Aerosol Sci.,* 12, 79-87

Lilienfeld, P., Elterman, P.B., and Baron, P. (1979)
> Development of a prototype fibrious aerosol monitor, *Am. Ind. Hyg. Ass. J.,* 40, p270-282

Lilienfeld, P. (1985)
> Rotational electrodynamics of airborne fibers, *J. Aerosol Sci.,* 16, p315-322

Lilienfeld, P. (1987)
> Light scattering from oscillating fibers at normal incidence, *J. Aerosol Sci.,* 18, p389-400

Lippmann, M. and Altschuler, B. (1976)
> *Regional deposition of aerosols, Air Pollution and the Lung,* Halsted Press-Wiley, New York

Lippmann, M., Yeates, D.B., and Albert, R.E. (1980)
> Deposition, retention and clearance of inhaled particles, *Br. J Ind. Med.,* 37: 337-362

Lippmann, M. (1990)
> Effects of fiber characteristics on lung deposition, retention, and disease, *Environmental Health Perspectives,* 88, 311-317

Liu, Q., Wijn, J.R. de, and Blitterswijk, C.A. van (1996)
> Nano-apatite / polymer composites I. mechanical and physicochemical characteristics. Trans. *Fifth World Biomaterials Congress,* II-361, Toronto, Canada

Marijnissen, J.C.M., Buwalda, H., Lemkowitz, S.M., and Bibo, B.H. (1991)
> Production of uniform micron and submicron fibers for instrument calibration, *Aerosols: Fifth annual conference and particle shape workshop,* Loughborough University of Technology, p211-216

Marijnissen, J.C.M., Lilienfeld, P., and Zhou, Y. (1996)
> A laser monitor for the fiber deposition in a lung model" *J. of Aerosol Sci.,* 27 (S1), p523-524

Martonen, T.B. and Patel, M. (1981)
> Modeling the dose distribution of H2SO4 aerosols in the human tracheobronchial tree, *Am. Ind. Hyg. Ass. J.,* 42, 453-460

Michaels, L. and Chissick, S.S. (1979)
> Asbestos Vol. 1, Properties, applications, and hazards, Wiley, Chichester.

Morgan, A., Evans, J.C., and Holmes, A. (1977)
>   Deposition and clearance of inhaled fibrous minerals in the rat, Studies using radioactive tracer techniques, In Walton W.H., McGovern B., eds, *Inhaled particles IV*, part 1, Oxford: Pergamon Press, 259-274

McGeary, R.K. (1961)
>   Mechanical packing of spherical particles, *J. Am. Ceram. Soc.*, 44, 513-522

Michaels, L. and Chissick, S.S. (1978)
>   *Asbestos*, John Wiley and Sons, New York

Mollinger, A.M. (1994)
>   *Particle entrainment, measurement of the fluctuating lift force*, PhD thesis, Delft University of Technology

Mori, H., Marijnissen, C.M.J., and Scarlett, B. (1990)
>   Optimal conditions for the generation of monodisperse aerosol particles using the spinning top generator, *J. Aerosol Sci.*, 21, s661-664

Olson, D.E., Dart, G.A., and Filley, G.F. (1970)
>   Pressure drop and fluid flow regime of air inspired into the human lung, *J. Appl. Physiol.*, 28, 482-491

Otani, Y., Kanaoka, C., and Emi, H. (1989)
>   Experimental study of aerosol filtration by the granular bed over a wide range of Reynolds numbers, *Aerosol Sci. Tech.*, 10, 463-474

Paretsky, L.C., Theodore, L., Pfeffer, R., and Squires, A.M. (1971)
>   Panel bed filter for simultaneous removal of fly ash and sulfur dioxide, *J. APCA*, 21, 204-209

Paretsky, L.C. (1972)
>   PhD thesis, City University of New York

Patterson, R.G. and Jackson, M.L. (1977)
>   Shallow multistage fluidized beds for particle collection, *AIChE Symp. Ser.* 161, 73, 64

Pattle, R.E. (1961)
>   The retention of gases and particles in the human nose. In Davies C.N., ed. *Inhaled particles and vapours*, Oxford: Pergamon Press, 302-311

Payatakes, A.C., Tien, C., and Turian, R.M. (1973)
>   A new model for granular porous media, *AIChE J.*, 19, 58-76

Pell, M. (1990)
>   Gas fluidization, series book of *Handbook of powder technology*, Vol. 8, Williams J.C. and Allen, T. ed. Elsevier, Amsterdam

Pendse, H. (1979)
>   *A study of certain problems concerning deep bed filtration*, PhD dissertation, Syracuse University, Syracuse, NY

Pendse, H. and Tien, C. (1982)
>   General correlation of the initial collection efficiency of granular filter beds, *AIChE J.*, 28, 477-686

Pich, J. (1972)
>   Theory of gravitational deposition of particles from laminar flows in channels, *J. Aerosol Sci.*, 3, 351-361

Pinxteren, M. van (1989)
>   *How to produce monodispers polyamide fibers with diameters in the micron-range*, MSc thesis, Faculty of Chemical Technology and Materials Science, TU, Delft

Plaisier, R.B. (1991)
>   *Optimalisate van het snijproces van inhaleerbare vezels*, report of stage at the Delft University of Technology, assigned by the HTS Dordrecht, The Netherlands

Podgorski, A., Zhou, Y., Marijnissen, J.C.M., and Bibo, B.H. (1996)
> Theoretical and experimental study of fibrous aerosol particles deposition in a granular bed, *J. Aerosol Sci.*, 27(S1), 479-480

Podgorski, A. and Gradon, L. (1997)
> *Advances in aerosol filtration science and technology* (Ed K.P. Spurny), Crclewis, NY

Prodi, V., De Zaiacomo, T., Hochrainer, D., and Spurny, K. (1982)
> Fibre collection and measurement with the inertial spectrometer, *J. Aerosol Sci.*, 13, 49-58

Put, S.J. van der (1992)
> *The granular bed filter as a model of the lower parts of the human lung*, Report of Delft University of Technology, The Netherlands

Put, S.J. van der (1991)
> *The granular bed filter as a model of the lower parts of the human lung*, Report of Delft University of Technology, The Netherlands

Rajagopalan, R. and Tien, C. (1976)
> Trajectory analysis of deep-bed filtration with the sphere-in-cell porous media model, *AIChE J.*, 22, 523

Rajagopalan, R. and Tien, C. (1979)
> The theory of deep bed filtration, in Progress in *Filtration and separation,* vol. I, Wakeman, R.J. Ed., Elsevier, New York

Rudolf, G., Gebhart, J., Heyder, J., Scheuch, G., and Stahlhofen, W. (1983)
> Modelling the deposition of aerosol particles in the human respiratory tract, *J Aerosol Sci.*, 14: 188-192

Rudolf, G., Gebhart, J., Heyder, J., Schiller, C.F., and Stahlhofen, W. (1986)
> An empirical formula describing aerosol deposition in man for any particle size, *J. Aerosol Sci.*, 17, 350-355

Scheidegger, A.E. (1957)
> *The physics of flow through porous media*, Macmillan, New York

Scherer, P.W., Shendalman, L.M., and Green, N.M. (1972)
> Simultaneous diffusion and convection in single breath lung washout, *Bull. Math. Biophys.*, 34: 393-412

Schiller, C.F., Gebhart, J., Heyder, J., Rudolf, G., and Stahlhofen, W. (1988)
> Deposition of monodispersed insoluble aerosol particles in the 0.005-0.2 μm size range within the human respiratory tract, *Ann. Occup. Hyg.*, 32(supplement 1): 41-49

Schlesinger, R.B. and Lippmann, M. (1972)
> Particle deposition in casts of the human upper tracheobronchial tree, *Am. Ind. Hyg. Ass. J.*, 33, 237

Schmidt, E.W., Grescke, J.A., Gelfound, P., Lugar, T.W., and Furlung, D.A. (1978)
> Filtration of aerosols in a granular bed, *J. APCA*, 28, 143-

Scott, G.D., Charlesworth, A.M., and Mak, M.K. (1964)
> On the random packing of spheres, *J. Chem. Phys.*, 40, 611-612

Sherrington, P.J. and Oliver, R. (1981)
> *Granulation*, Heyden & Son Ltd., London

Snaddon, R.W. and Dietz, P.W. (1980)
> *Interstitial flow intensification within racked granular bed filters*, General Electric Co., Internal Rpt. No. 80CRD290

Soo, S.L. (1967)
> *Fluid dynamics of Multiphase systems*, Blaisdell, Waltham, MA

Spurny, K.R. (1980)
    Fiber generation and length classification, in *Generation of Aerosols: Methods*, ed. Willeke K., AASP, Ann Arbor

Stahlhofen, W., Gebhart, J., and Heyder, J. (1980)
    Experimental determination of the regional deposition of aerosol particles in the human respiratory tract, *Am. Ind. Hyg. Assoc. J*, 41: 385-398

Stöber, W., McClellan, R.O., and Morrow, P.E. (1993)
    Approaches to modelling disposition of inhaled particles and fibers in the lung, In: Gardner D.E. et al., ed. *Toxicology of the lung*, Raven press, Ltd., New York

Stoelinga, M. (1992)
    Dispersion, humidification and deposition of uniform fibers in a lung model, MSc thesis, TU, Delft

Tardos, G.I., Gutfinger C., and Abuaf, N.C. (1974)
    Deposition of dust particles in a fluidized bed filter, *Israel J. Tech.*, 12, 184-

Tardos, G.I., Abuaf, N., and Gutfinger, C. (1978)
    Dust deposition in granular bed filters -- theories and experiments, *J. APCA*, 28, 354-

Task Group on Lung Dynamics (1966)
    Deposition and retention models for internal dosimetry of the human respiratory tract. *Health Phys.*, 12: 173-207

Task Group of ICRP (1994)
    Human respiratory tract model for radiological protection, *Annals of the ICRP*, Pergamon, New York

Taulbee, D.B. and Yu, C.P. (1975)
    A theory of aerosol deposition in the human respiratory tract, *J Appl. Physiol.*, 38: 77-85

Taulbee, D.B., Yu, C.P., and Heyder, J. (1978)
    Aerosol transport in the human lung from analysis of single breaths, *J. Appl. Physiol.*, 44, 803-810

Tchen, C.M. (1947)
    Mean value and correlation problems connected with the motion of small particles suspended in a turbulent fluid, Dissertation, Delft, Martinus Nijhoff, The Hague

Thomas, J.W. (1958)
    Gravity settling of particles in a horizontal tube, *J. Air Pollut. Contr. Ass.*, 8, 32-34

Tien, C. (1989)
    Granular filtration of aerosols and hydrosols, Butterworth, MA

Tien, C. and Payatakes, A.C. (1979)
    Advances in deep bed filtration, *AIChE J.*, 25, 737-759

Timbrell, V. (1965)
    The inhalation of fibrous dusts, *Ann. N.Y. Acad. Sci.*, 132, 255-273

Timbrell, V. (1982)
    Deposition and retention of fibers in the human lung, *Ann. Occup. Hyg.*, 26(suppl): 347-369

TSI Inc. (1990)
    Model 3932 DMPS/C differential mobility particle sizer, Instruction manual.

Weibel, E.R. (1963)
    Morphometry of the human lung, New York

Wel, P.J.G. van der (1986)
    De dispersie van deeltjes in een turbulente stroming, Report of Delft University of Technology

Willemse, A.W., Marijnissen, J.C.M., Roos, R., Wuyckhuyse, A. van, and Scarlet, B. (1996)
    Photon correlation spectroscopy for analysis of low concentration submicrometer samples, *J. Aerosol Sci.*, 27(S), S535-S536

Yeh, H.C. (1980)
>   *Respiratory tract deposition models,* Final Report, LF-72, UC-48, March 1980, Albuquerque, NM: Inhalation Toxicology Research Institute, Lovelace Biomedical and Environmental Research Institute, Albuquerque, NM

Yeh, H. and Schum, G.M. (1980)
>   Models of human lung airways and their application to inhaled particle deposition, *Bull. Math. Biol.,* 24, 42, 461-480

Yu, C.P., Asgharian, B., and Yen, B.M. (1986)
>   Impaction and sedimentation deposition of fibers in airways, *Am. Ind. Hyg. Assoc. J.,* 47, p72-77

Yu, C.P. and Taulbee, D.B. (1977)
>   A theory of predicting respiratory tract deposition of inhaled particles in man, In: Walton W.H., McGovern B., eds. *Inhaled particles IV,* part 1. Oxford: Pergamon Press, 35-47

Yu, C.P. (1978a)
>   A two component theory of aerosol deposition in human lung airways, *Bull. Math. Biophys.,* 40: 693-706

Yu, C.P. (1978b)
>   Exact analysis of aerosol deposition during steady breathing, *Powder Technol.,* 21: 55-62

Yu, C.P. and Diu C.K. (1982)
>   A comparative study of aerosol deposition in different lung models, *Am. Ind. Hyg. Assoc. J.,* 43, 54-64

Yu, C.P. and Diu, C.K. (1983)
>   Total and regional deposition of inhaled aerosols in humans, *J Aerosol Sci.,* 14: 599-609

Yubao, L., Wijn, J. de, Klein, C.P.A.T., Meer, S. van der, and Groot, K. de (1994a)
>   Preparation and characterization of nano-grade osteoapatite-like rod crystals, *J. Mater. Sci.: Mater in Med.,* 5, 252-255

Yubao, L., Klein, C.P.A.T., Wijn, J. de, Meer, S. van der, and Groot, K. de (1994b)
>   Shape change and phase transition of needle-like non-stoichiometric apatite crystals, *J. Mater. Sci.: Mater. in Med.,* 5, 263-268

Zechendorf, A. (1991)
>   *Het ontwerp van een longmodel voor het bestuderen van het transport en depositiegedrag van vezels,* MSc thesis, TU, Delft

Zhou, Y., Marijnissen, J.C.M., Put, S.J. van der, Lemkowitz, S.M., and Bibo, B.H. (1993)
>   A physical and mathematical model for fiber deposition in the lower parts of the lung, *J Aerosol Sci.,* 24(S1), 469-470

Zhou, Y., Marijnissen, J.C.M., Lemkowitz, S.M., and Bibo, B.H. (1994)
>   The granular bed as a model of the lower parts of the lung, Presented at *Fourth International Aerosol Conference,* Los Angeles, USA, Sep. 1994, 882-883

Zhou, Y., Marijnissen, J.C.M., Lemkowitz, S.M., and Bibo, B.H. (1995a)
>   The deposition of fibrous particles in the lower parts of respiratory system using a mathematical model, Presented at *3rd European Symposium Separation of Particles from Gases,* Nurnburg, Germany Mar. 1995, 223-231

Zhou, Y., Marijnissen, J.C.M., Lemkowitz, S.M., and Bibo B.H. (1995b)
>   A physical and mathematical modelling of fiber deposition in the lower parts of the lung, *J. of Aerosol Sci.,* 26(S1), 619-620

Zhou, Y., Marijnissen, J.C.M., Lemkowitz, S.M., and Bibo, B.H. (1996)
>   A deposition model for fibers in the deep parts of the lung based on similarities of bead beds and human lungs, in *Aerosol Inhalation: Recent Research Frontiers,* (Ed. J. Marijnissen and L.Gradon) Kluwer Academic Publisher, 127-142

Acknowledgements

Curriculum Vitae

Zhou Yue was born in Hangzhou, Zhejiang provence, P.R. China, on 30 April, 1961.

1974-1979:   Secondary and high school study in Beijing, China.

1979-1983:   Study at Refrigeration and Air Conditioning Section, Department of Power Mechanical Engineering, Jiao Tong University, Shanghai, China, and obtained B.Sc. degree.

1983-1986:   Assistant Engineer at Dong Guang Electronic Company, Beijing, China

1986-1989:   Study at Institute of Environmental Health and Engineering, Chinese Academy of Preventive Medicine, Beijing, China, and obtained M.Sc. degree with a thesis titled "Development of a new PM-10 cyclone sampler".

1989-1993:   Worked at Institute of Environmental Health and Engineering, Chinese Academy of Preventive Medicine, Beijing, China as a research assistant.

1993-1997:   Worked at Faculty of Chemical Technology and Materials Science, Delft University of Technology, Delft, The Netherlands, as a research assistant (AIO); the work results in the present dissertation.